ELECTROCHEMICAL AND TRIBOLOGICAL BEHAVIOR OF NOVEL TITANIUM BASED ALLOYS FOR HUMAN BODY IMPLANTS

By

Animesh Choubey

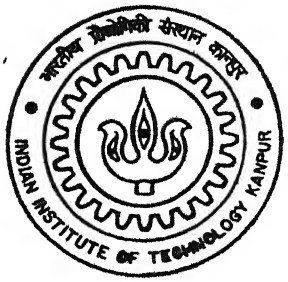

DEPARTMENT OF MATERIALS AND METALLURGICAL ENGINEERING

INDIAN INSTITUTE OF TECHNOLOGY KANPUR

SEPTEMBER, 2003

ELECTROCHEMICAL AND TRIBOLOGICAL BEHAVIOR OF NOVEL TITANIUM BASED ALLOYS FOR HUMAN BODY IMPLANTS

A Thesis Submitted

in Partial fulfillment of the Requirements
for the Degree of

MASTER OF TECHNOLOGY

by

Animesh Choubey
(Y120602)

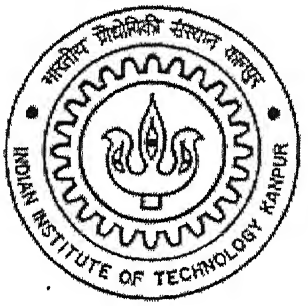

to the

DEPARTMENT OF MATERIALS AND METALLURGICAL ENGINEERING

**INDIAN INSTITUTE OF TECHNOLOGY KANPUR
INDIA**

September 2003

Dedicated to .....
my Grandmother

CERTIFICATE

This is to certify that the thesis entitled **ELECTROCHEMICAL AND TRIBOLOGICAL BEHAVIOR OF NOVEL TITANIUM BASED ALLOYS FOR HUMAN BODY IMPLANTS** by Animesh Choubey (Y-120602) has been carried out under my supervision and has not been submitted elsewhere for the award of a degree.

9 Sep 03

Dr. R. Balasubramaniam
Professor
Materials and Metallurgical Engg.
Indian Institute of Technology
Kanpur, INDIA.

9/9/03

Dr. Bikramjit Basu
Assistant Professor
Materials and Metallurgical Engg.
Indian Institute of Technology
Kanpur, INDIA.

TABLE OF CONTENTS

ABSTRACT

Corrosion and wear of metallic implant materials is of major concern as that limits the life of the body implant. In this research, the electrochemical and wear behavior of several Ti-based alloys like CP Titanium, Ti-15Al, Ti-5Al-2.5Fe, Ti-6Al-4V, Ti-6Al-4Fe, Ti-6Al-4Nb, Ti-13.4Al-29Nb, Ti-13Nb-13Zr and 316L stainless steel was studied. The Hank's solution (pH-7.4) used in this study for simulating body fluid conditions and the experiments were conducted at 37°C. The electrochemical behavior of these Ti alloys was compared with that of 316L steel. Specific attention was focused on the breakdown potentials, pitting/crevice corrosion resistance, and the ability to form protective oxide scales. The corrosion rates of the materials were compared in the simulated human body fluid conditions using Tafel extrapolation method. Ti-13Nb-13Zr exhibited the least corrosion rate of 0.0045 mils per year (0.0001 mm/year) and 316L stainless steel the maximum of 0.16 mils per year (0.004 mm/year). Maximum breakdown potential was shown by Ti-6Al-4V (1290 mV vs. SCE) and minimum of 37 mV (vs. SCE) by 316L stainless steel. Commercial pure titanium and 316L stainless steel exhibited maximum and minimum passive range of 1898 mV (vs. SCE) and 319 mV (vs. SCE) respectively. Least value of i_{pass} (passive current density) was exhibited by Ti-5Al-2.5Fe (1.2 $\mu A/cm^2$).

Microstructural analysis revealed a maximum volume fraction of beta phase in Ti-13Nb-13Zr alloy. This alloy also exhibited a fibrous structure, which resembles with that of bone. Absence of grain boundaries and maximum volume fraction of beta phase could dictate the corrosion behavior of this alloy. Niobium addition caused a considerable increase in grain size and hence a decreased corrosion rate. Although addition of alloying elements like aluminum, niobium, iron, zirconium and vanadium lowered passive current density, Al enrichment was found to be detrimental to the passivity of the alloy. As the passive layer can be broken down in certain circumstances by wear, it is important to study the corrosive wear behavior of these alloys. Hence tribological investigation was conducted on selected material combinations (CP Titanium, Ti-13Nb-13Zr,

Ti-6Al-4V and Ti-5Al-2.5Fe) and the selection was based on the critical analysis of the electrochemical data (corrosion rate, passive range and break down potential).

The wear experiments were carried out in Hank's solution under extreme testing conditions (load of 10N) to investigate the severe wear behavior. The measured COF is found to be lowest for Ti-5Al-2.5Fe (COF-0.3), whereas for other alloys the COF varies between 0.46-0.50. The detailed microstructural investigation of the worn surfaces was carried out using SEM. The major wear mechanism was identified as the abrasion, cracking and the formation of tribochemical oxides. The occurrence of cracking is found to be less severe for Ti-5Al-2.5Fe and Ti-13Nb-13Zr.

LIST OF FIGURES

LIST OF TABLES

Chapter 1

INTRODUCTION

1.1 Biomaterial

The definition of biomaterials covers a broad area. In fact, any natural or synthetic material that interfaces with living tissues and/or biological fluids may be defined as a biomaterial [1]. Several common materials have shown some usefulness in some biomedical applications. However, certain physical and mechanical characteristics render some materials more desirable than the others for biomedical applications. To complicate things further, the determination of these desirable traits depends on the materials intended for use in the human body. For example, the material for a bone implant must exhibit greater compressive strength, while the material for a ligament replacement must exhibit far more flexibility and tensile strength [2]. In all cases, however, the biomaterial must be compatible with the body. In other words, the biocompatibility and in some cases, bioactivity, of the material are the key factors in determining the performance of a biomaterial.

Typically a biocompatible material disrupts normal body function as little as possible. For a material to be deemed biocompatible, any adverse reactions, which may ensue at the blood/material interface, must be minimal, while resistance to biodegeneration must be high. This requires a biomaterial to interact as a natural material in the presence of blood and tissues [3]. A biocompatible material, should ***not*** exhibit following characteristics:

- Cause thrombus formation (The possible effect of biomaterials on the living environment due to a lack of blood compatibility is known as thrombogenicity).
- Destroy or sensitize the cellular blood elements.

- Alter plasma proteins (including enzymes) so as to trigger undesirable reactions.
- Cause adverse immune responses (Immunogenic).
- Cause cancer (Carcenogenic).
- Cause teratological effects.
- Deplete electrolytes.
- Be affected by sterilization.

Bioactive materials play a more aggressive role in the body. While a biocompatible material typically affects the equilibrium function of the body as little as possible, a bioactive material introduces specific interactions between the material and surrounding tissue. For example, a bioactive material can encourage, tissue integration to aid in the fixation of the implant in the body. Many total hip implant operations today rely partially on a porous coating of hydroxyapatite (HA), a normal component of bone, to help permanently stabilize the stem of the implant in the bone. The coating encourages growth from the surrounding tissue that interlocks within the pores [4].

1.2 Historical Perspective

Metallic devices have been used to repair and replace parts of the human body for centuries. Archaeological evidence clearly indicates that surgical procedures were performed in several ancient civilizations. The use of surgical metal implants in humans was first recorded in 1562 when a gold prosthesis was used to close a defect in a cleft plate [5].

Progress in surgery, however, was slow and mixed liberally with superstition until the latter part of the nineteenth century. Pasteur's and Lister's aseptic surgical techniques, developed around 1883, and shortly thereafter Roentgen's discovery of X-rays in 1895, added a new dimension to orthopedic surgery [6]. As the occurrence of the infection was brought under control, the relationship between material properties and success of implant surgery became more clearly apparent. Tissue compatibility, corrosion resistance and strength were critical characteristics found to be necessary.

The noble materials like gold and silver met the first two criteria but lacked strength for applications with high stress. Metals such as brass, copper and steel possessed adequate strength for many applications but exhibited poor corrosion behavior and tissue compatibility.

In the beginning of the twentieth century, surgical techniques were developed for the fixation of bone fractures with a plate and screw combination. Sherman-type bone plates were fabricated from the best available alloy at that time, vanadium steel. By 1920s the use of vanadium steel became questionable due to poor tissue compatibility. At that time however, no other alloy was available with high strength and good corrosion resistant properties. During 1930s, stainless steel containing 18% chromium and 8% nickel were first used for surgical implants. This material had far superior corrosion resistant properties than anything that had been available up to that time and immediately attracted the interest of orthopedic surgeons. Bone plates, screws and other fixation devices were fabricated and used as surgical implants. Although the material performed better than anything else available, it still showed some susceptibility to attack in the saline environment of the human body. In 1926 when Strauss patented the 18-8 molybedenum stainless steel, containing 2 to 4% molybdenum and a reduced carbon content of 0.08%, a material was created which promised improved resistance to acid and chloride containing environments. This material formed the basis for the type 316L alloy in common use today. Also, in the 1930s, a cobalt-chromium-molybdenum casting alloy previously used for dental appliances began to be used for surgical implants.

When titanium became commercially developed in the late 1940s it was very soon evaluated as a suitable surgical implant material. The metal possessed a good combination of mechanical and corrosion resistance properties and also demonstrated outstanding tissue compatibility characteristics. Although a few internal fixation devices were also used in United States in 1950s and 1960s,the most extensive clinical use of titanium

alloys was in England. Interest in the Ti-6Al-4V alloy and Extra Low Interstitial (ELI) versions of this alloy for total joint prostheses spurted in United States in late 1970s. This alloy now finds wide scale application in orthopedic surgery [7].

1.3 Aim of Study

The aim of study is to understand the electrochemical behavior of different Ti-based alloys by focusing specific attention on the breakdown potentials, pitting/crevice corrosion resistance, and the ability to form protective passive films. The major attention was on:

- Evaluation of corrosion rates in simulated body fluid environment.
- Study of the electrochemical behavior of the Ti-based alloys and understanding of the influence of the alloying element addition and the corrosion behavior of these alloys.
- Study of the effect of replacing vanadium in Ti-6Al-4V by Fe and Nb.
- Study the effect of beta phase distribution in Ti alloys on the electrochemical behavior.
- Tribological behavior of selected alloy combinations.

When considering titanium alloys for orthopedic applications it is important to examine their corrosion behavior. Therefore, electrochemical experiments were planned to evaluate candidate Ti-based implant materials.

1.4 Work Plan

The strategy for experimental work was as per the following sequence:

1. Procurement of materials to be tested from DMRL, Hyderabad and Salem Steel plant.
2. Preparation of as received samples for electrochemical, microstructural and tribological characterization.
3. Design and installation of experimental set up for simulating human body conditions in laboratory.
4. Experimental Program.
5. Analysis of results including materials characterization.

Current research aims in studying the behavior of all potential biomaterial combinations in simulated human body body environment. Chapter 2 deals with literature survey. Experimental procedures are discussed in Chapter 3. Chapter 4 presents the results and discussion. Conclusions and suggestions for future work are listed in Chapter 5, followed by glossary of medical terms, Bibliography and Appendix.

Chapter 2

LITERATURE SURVEY

Over the recent decades, quantitative analysis of basic biomaterial properties have been utilized to better optimize biocompatibility profile for surgical implant devices [8]. In this regard, relevant correlations between results from pre-clinical and clinical investigations have provided intercomparisons of cause-effect relationships between the synthetic material properties and longer-term device function. Significant relationship exists between biomaterial/biomechanical properties and the complex aspects of force transfer/motion (fretting and wear) and that is now recognized as critical to many types of biodegradation or corrosion. While ASTM G5 is still the governing standard for corrosion testing of materials [9], it is imperative that the environment in which the tests are conducted and examples of data used to explain the analytical process be representative of the end application [10]. The focus of this chapter is to summarize the corrosion and wear behavior of Ti-based alloys.

2.1 Fundamental Aspects of Corrosion of Metallic Implants

The corrosion of metals in aqueous environment of the body fluids involves the setting up of electrochemical corrosion cells. The corrosion produced by these cells is controlled by thermodynamic and kinetic factors. The thermodynamic factors determine the corrosion tendencies; the kinetic factors determine the rate. Galvanic corrosion is affected by both thermodynamic and kinetic factors and occurs when two metals with widely differing potentials are placed in contact with each other. Other forms of corrosion depend more directly on factors controlling the rate of corrosion. For most alloys used in implants the corrosion rate is mainly dependent on

the protective properties of the thin passive films that exists on the surface of these alloys. The quality of protection afforded by passive films is related to their ability to resist chemical breakdown by damaging species and, once broken down, their ability to reform rapidly (repassivate). The interplay between breakdown and repassivation is important in determining the susceptibility of metallic implants to pitting, crevice corrosion, stress corrosion, corrosion fatigue, intergranular corrosion and fretting corrosion. [11].

Corrosion, the gradual degradation of materials by electrochemical attack, is a concern particularly when a metallic implant is placed in the hostile electrolytic environment provided by the human body [12]. Even though the freely corroding implant materials used in the past have been replaced with modern corrosion resistant superalloys, deleterious corrosion processes have been observed in certain clinical settings [13].

Two characteristics determine implant corrosion. First, thermodynamic forces, which cause corrosion (oxidation and reduction) reactions. These forces correspond to the energy required or released during a reaction [13]. The electrochemical series links the normal electrode potentials of metals, usually in relation to hydrogen. Unfortunately, this series does not take into account the oxide film forming capability of these metals in any given electrolyte and it is more useful from the engineer's point of view to refer to the galvanic series in which metals are ranked in order of their relative reactivity in saline solutions [14]. Secondly, kinetic barriers to corrosion, that are related to factors that physically impede or prevent corrosion reactions from taking place [13]. Only those metals, which have the capacity to form a protective oxide layer against corrosion, can be used in orthopedic implants. In order to limit oxidation, passive films must have certain characteristics. They must be non-porous and must fully cover the metal surface; they must have an atomic structure that limits the migration of ions and electrons across the metal oxide-solution interface; and they must be able to remain on the surface of the material even with mechanical stressing or abrasion, which can be expected in association with orthopedic devices [13].

2.1.1 Human Body Environment

It is widely appreciated that the deterioration of metal and plastic implant materials within the body is one of the most important aspects of implant surgery. This particular application of materials places an almost unique demand on the resistance to deterioration. The reasons are basically two fold, for not only may the environmental effects alter the structure and properties of the material, which may itself affect the function of implant and hence the well being of the patient, but also the by-products of any structural change may have harmful effects on the patient [15].

Ideally a metallic implant should be completely inert in the body. However, that is rarely the case. The body environment is extremely hostile to all foreign materials and therefore, the effect of the environment on the implant and the effect of implant on its host tissue are of primary concern. The adapted potential-pH chart in Figure 1 illustrates the range and complexity of conditions that could be experienced by an implant alloy used for different applications. A surgical implant is constantly bathed in extra cellular tissue fluid. Basically water, this fluid contains electrolytes, complex compounds, oxygen and carbon dioxide. Electrolytes present in largest amounts are sodium (Na^+) and chloride (Cl^-) ion. Most of the fluids existing in the body (such as blood, plasma and lymph) have chloride content (and pH) somewhat similar to sea water (about 5 to 20 g/l and pH about 8) [16].

A 0.9% salt solution in considered to be isotonic with blood. Other electrolytes present include bicarbonate ions (HCO_3^-) and small amounts of potassium, calcium, magnesium, phosphate, sulphate and organic acid ions. Included among the complex compounds and present in smaller amounts are phospholipids, cholesterols, natural fats, proteins, glucose and amino acids. Under normal conditions the extra cellular body fluid is slightly alkaline with a pH of 7.4 [17].

In 1965, Zapffe [18] found that after fracture trauma, local pH values decreased to 5.3-5.6. As healing took place, the pH increased gradually to

normal (pH-7.4). Another source of low pH *in vivo* is the presence of crevices between components of fixation device. A restriction of the oxygen supply to these locations can lead to pH values of about unity [19]. When an implant is surgically inserted into the human body, the internal environment is greatly disturbed. Haematomas are likely to collect around the implant, resulting in a lowered pH. Laing [24] observed pH values as low as 4.0 in healing wounds. The low pH usually persists until the haematomas are reabsorbed after several weeks [17]. From what has been said it is quite obvious that the environmental conditions within the human body are quite hostile and vary according to the degree of interaction with the body and the implant and the degree of trauma and infection associated with implantation procedure.

With internal fixation, the disturbance of the blood supply to the bones is often accompanied by severe pathological changes that may effect healing and variation in the equilibrium state electrochemically [20,21]. The ionic species also perform numerous functions, which include maintenance of the body pH and participation in oxidation-reduction reactions [22]. Normal imbalance occurs in the fluid compartment and different transport of ions and non-uniform changes normally accompany disease state. For example, during intensive care, after accidents or surgical operation, the fluid compartments are often disturbed. From an electrochemical viewpoint, the acceleration of corrosion can be due to differential conditions existing along the implant interface. These conditions may be responsible for the formation of electrochemical cells accompanied by active metal dissolution at favored localized spots at the implant-body fluid interface [23].

Reaction of the host tissue to the metallic implants affected by many factors including shape and size of the implant, movement between the implant and the tissue, extent of corrosion attack, general degradation of the implant, and the biological activity of the resulting by-products of corrosion or degradation.

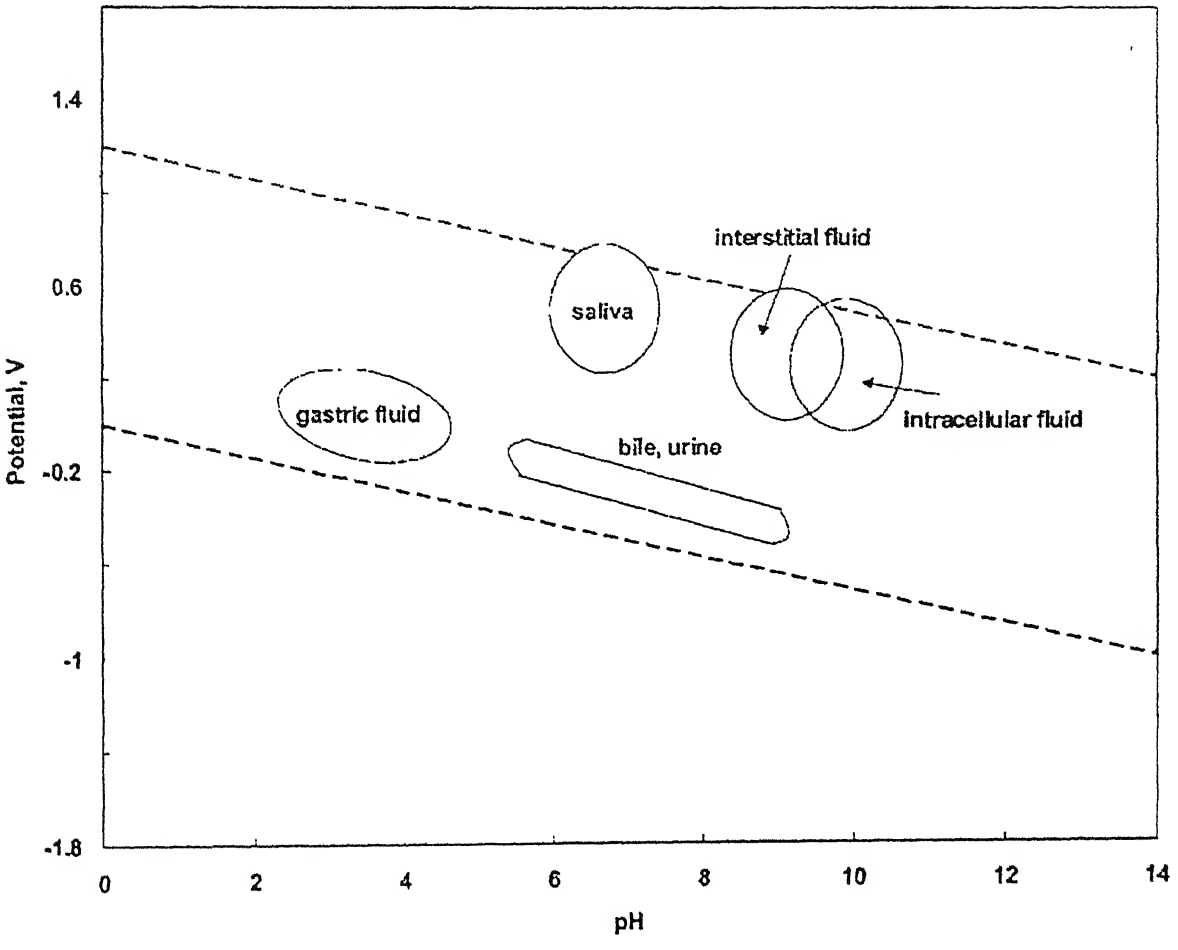

Figure 1: Potential-pH schematic illustrating complexity of environmental conditions that may be experienced by the implant alloy in the body [138].

2.1.2 Clinical Importance of the Process of Corrosion

Corrosion can severely limit the fatigue life and ultimate strength of the material, leading to the mechanical failure of implant. There is a low but finite prevalence of corrosion-related fracture of the implant [13]. The release of corrosion products may elicit an adverse biological reaction in the host, and several authors have reported increased concentrations of local and systemic trace metals in association with metal implants [25,26]. Although there is no specific histological evidence of the slow release of metal species that is thought to occur in association with all metal implants, accelerated corrosion and a tissue response (e.g., discoloration, foreign body response) that can be related directly to identifiable corrosion products have been demonstrated in the tissues surrounding multiple-part devices [27].

Corrosion products have been implicated in causing local pain and swelling in the region of the implant, in the absence of infection [28]. The presence of particulate corrosion and wear products in the tissue surrounding the implant may ultimately result in a cascade of events leading to periprosthetic bone loss [27], excretion of excess metal ions (especially chromium, cobalt and nickel) and their suspected role in induction of tumors e.g. malignant fibrous histiocytoma [29]. It remains to be proven whether the reports of tumors developing in the vicinity of metal implants are coincidental or otherwise. When the litany of documented toxicities (metabolic, bacteriological, immunological or carcinogenic) of these elements is considered, it should be emphasized that they generally apply to soluble forms of the elements and may not apply to the degradation products of prosthetic implants [13].

A number of studies have been carried out on the difficult task of measuring corrosion parameters *in-vivo*. These have involved measurement of corrosion potential [30-32] or corrosion rate using the polarization methods [33-36]. Only one on these studies has involved a functional loading situation. Brown and Simpson [37] measured corrosion potential versus time for a 316L stainless steel bone screw/plate combination in a sheep tibia

in-vivo. Potential shift towards more active potentials was observed as the sheep increased the loading of the device by walking on the treadmill. Thull *et al.* [38] have performed corrosion experiments in dogs using telemetric methods. Corrosion potential versus time measurements were made fro various implant alloys. The results were interpreted in terms of a situation where implant/tissue relative movement established a fretting corrosion situation. No information on stress levels or corrosion rates were obtained in either of these studies.

In-vitro fretting corrosion potential experiments have been performed using weight loss [37], polarization [35] and corrosion potential measurements. Thull and Schaldach [38] have performed corrosion potential versus time measurements *in-vitro* in a joint simulator with different values of applied load. Brown and Simpson [37] have performed similar studies with screw/plate fretting. Both studies found larger shifts towards active potentials with larger loads [39]. One of the main problems of corrosion testing *in-vivo* and the interpretation of the mechanism of corrosion, which have taken place *in-vivo* after the implant has been removed from the patient, is well illustrated in Figure 2 used by Semlitsch and Willet [40] to illustrate the types of corrosion, which are associated with a total hip joint replacement. This figure shows that many corrosion mechanisms could be taking place simultaneously in a system of this nature. To understand each of the corrosion mechanisms that could take place *in-vivo* and because of the difficulties of conducting in-vivo experiments most of the experimental work has been carried out in-vitro under somewhat simplified experimental conditions.

An Anodic polarization curves for the basic materials used for implants (e.g. stainless steel type 316 S12, Ti-6Al-4V and Co-28Cr-6Mo casting alloy) have been obtained under varying conditions of surface finish, environment, chloride ion concentration, pH, aerated and deaerated in the literature [41-43]. Typical results are shown in Tables 1 and 2.

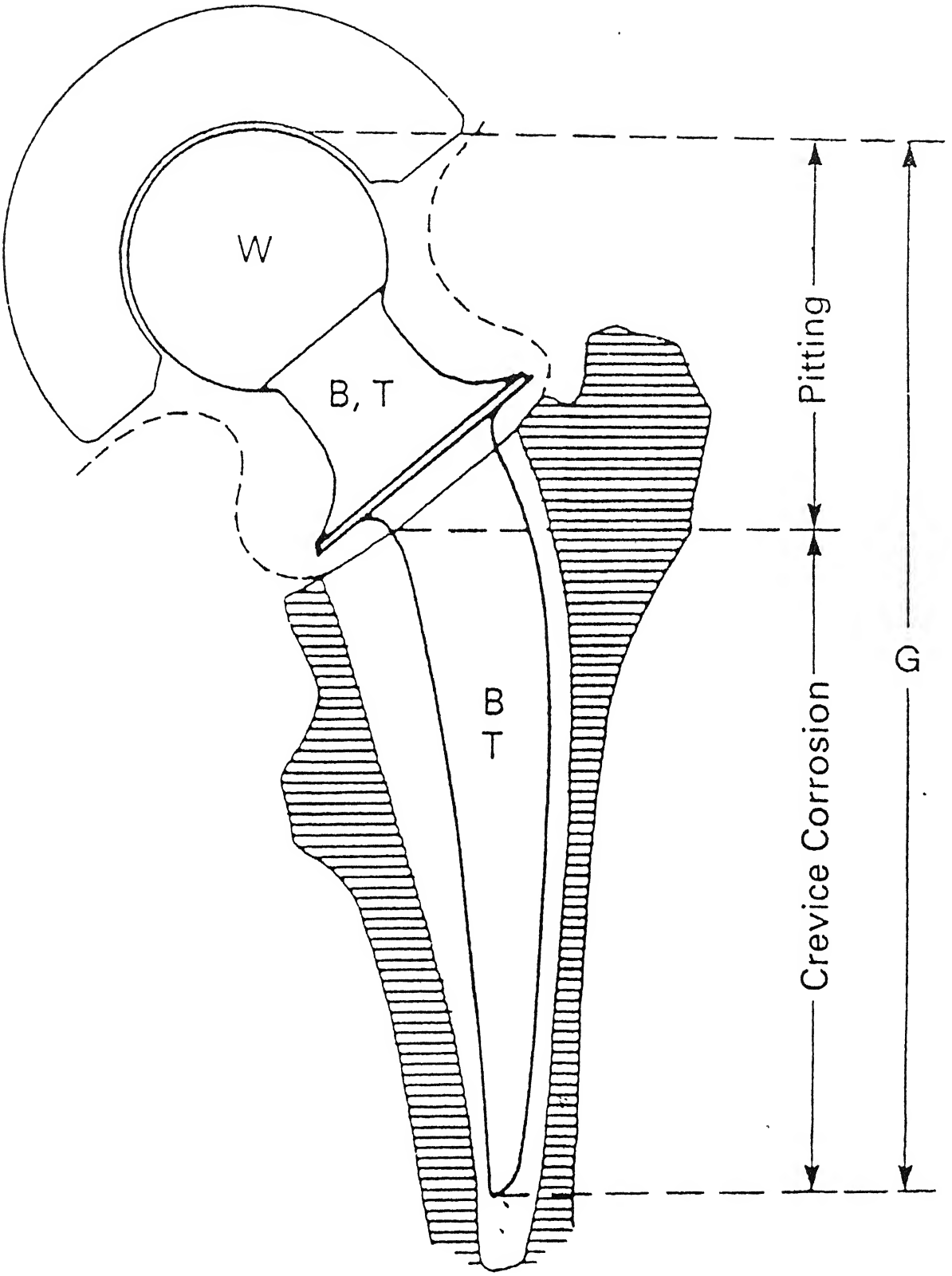

Figure 2: Mechanical stresses and corrosive effects to which a joint endoprosthesis is exposed in the human body; W-wear (mechanical and/or depassivation), B-bending (corrosion fatigue), T-torsion, G-general and localized attack [64].

Table 1:

Breakdown potentials (mV) for 316 stainless steel, titanium and cobalt-chromium-molybdenum alloy in oxygen-free 0.17 M NaCl solution at 37 °C. using silver/silver chloride reference electrode.

Material	E_b (mV vs. Ag-AgCl)	
	Hank's solution [92]	Ringer's Solution [43]
316 Stainless steel	400-800	160-650
Titanium	9000	800
Co-Cr-Mo	870	790

Table 2:

Breakdown potentials (mV) for 316S12 stainless steel (cold worked), high nitrogen stainless steel (cold worked), Ti-6Al-4V and cast Co-Cr-Mo alloy in continuously aerated aqueous acidified chloride solution 0.23 M (Cl^-) pH 1.5 at 25 °C (results provided by De Puy international Ltd. Leeds).

Material	British standard	Condition	Breakdown potential (mV vs SCE)	Free Corrosion potential (mV vs SCE)
316 S12 Stainless steel	BS7252/1 Comp. D	Cold worked	180	-100
High nitrogen stainless steel	BS7252/9	Cold worked	850	300
Ti-6Al-4V	BS7252/3	Annealed	1700	150
Co-Cr-Mo	BS7252/4	Cast	850	155

These results show that the basic material used for implantation exhibit good corrosion resistant properties in simulated body fluid environments (Hank's physiological solution) and in much more aggressive solutions such as 0.23 M (Cl^-) acidified to pH 1.5, which simulate deep crevice and infection conditions. The material's free corrosion potential is well below their respective breakdown potentials and are therefore stable under these conditions. These results only provide an indication of how materials behave under non-stressed, non-crevice and non-fretting conditions [44].

Ogundele and White [44] carried out a series of polarization studies on surgical grade stainless steel in Hank's physiological solution. Under varying conditions of temperature, (Cl^-), (HCO_3^-) and pH. Their results are summarized as follows:

1. Increasing concentrations of chloride ions adversely affected corrosion resistance in lowering passivation breakdown potentials, marginally lowering corrosion potentials, lowering passivation potentials and generally increasing the propensity to pitting attack as evidenced by the increase in size of hysteresis loops from potentiodynamic cycling tests.

2. Increasing concentration of bicarbonate tended to raise the break down potentials but also increased the corrosion potentials. This, in combination with high chloride concentration, high bicarbonate concentrations may raise the corrosion potentials such that they border on passivation breakdown. The increase in hysteresis loop size on potentiodynamic cycles with increasing bicarbonate concentration shows a lowered resistance to pitting attack and crevice corrosion.

3. Variations in pH promoted increases in corrosion potentials from acid pH levels to neutral pH; thereafter, however, corrosion potentials were lowered in alkaline solutions to

more active values. Decreasing pH caused a lowering of breakdown potentials in the presence of Cl^- and an increase in the current densities for passivation.

4. Increasing temperature tended to raise corrosion potentials, lower breakdown potentials, thereby generally lowering corrosion resistance. Ogundele and White [44] re-emphasized that 316L type stainless steels are generally corrosion resistant in biological fluids and are suited to application in orthopedic implants. They support their argument by the fact that there is a low incidence of implant failures (<5% from corrosion and corrosion related mechanisms or both) [45].

2.1.3 Corrosion Susceptibility of Orthopaedic Implants

Typical implant materials commercially in use are 316L stainless steel (for femoral stem and as a temporary implant device), Ti-6Al-4V (for femoral stem) and Co-28Cr-6Mo (for femoral head). Different types of corrosion attack to which these implant materials are susceptible is (seen in Figure 2) is elaborated below:

a) Uniform Attack

This refers to the inevitable corrosion to which all metals immersed in electrolytic solutions are condemned [46]. Titanium-base alloys have lower overall corrosion rates compared to stainless steel and cobalt chromium alloys. However, serum proteins can complex with chromium and nickel, increasing uniform attack by 2-to 10-fold [46].

b) Galvanic Corrosion

It is defined as dissolution of metals driven by macroscopic differences in electrochemical potentials, usually as a result of dissimilar metals in proximity [13]. It is caused by inappropriate use of metals, e.g., a stainless steel cerclage wire in contact with a cobalt or titanium–alloy femoral stem, a

cobalt-alloy femoral head in contact with a titanium-alloy femoral stem, and a titanium– alloy screw in contact with a stainless-steel plate [47].

Due to cold-welding between instrument and implants using radioactive tracer techniques, Bowden and coworkers (1955) have shown that significant amounts of metal were transferred from screwdrivers to screw heads and from drill bits to plates. Work hardening and surface-finishing processes that produce plastic deformation generally make the deformed metal basic with respect to undeformed material of the same composition [46]. Compositional differences, either between parts because of manufacture from different master ingots within the same specification limits or because of deliberate mixing of metals, is the most likely cause of such effects [46].

c) Pitting and Crevice Corrosion

Pitting is a form of localized, symmetric corrosion in which pits form on the metal surface [46]. Stainless steel is particularly predisposed to pitting corrosion due to inclusions of a dissimilar material trapped in the metal during a manufacturing process. These impurities may initiate pitting corrosion in relation to a grain boundary and thus can lead to component failure [28]. It can also be initiated by scratches or handling damage [46]. Pitting was frequently observed in older stainless steel fracture fixation hardware, e.g., on the underside of screw heads [46]. It also occurs infrequently on the neck or the underside of the flange of proximal femoral endoprostheses [46].

The literature contains a number of studies on the susceptibility of the cobalt-based alloys to pitting corrosion. In-vitro studies conducted by Muller and Greener [43], involving static conditions, revealed no evidence of pitting having occurred. Syrett and Wing [48], utilizing cyclic polarization analyses, observed that neither as-cast nor annealed Co-Cr-Mo alloy demonstrated hysteresis loops in their cyclic polarization curves. They concluded that this substantiated the fact that neither should be susceptible to pitting or crevice

corrosion. Other investigators [49-55], studying the susceptibility of the cobalt alloy to pitting corrosion under in-vitro static conditions has shown the alloy not to be susceptible. However, when the alloy is either severely cold worked or subjected to fretting or cyclic loading [56-57] conditions, pitting corrosion has been observed *in-vitro* [58].

The addition of a minimum of 2% of molybdenum content in type 316 stainless steel has been shown to reduce the tendency for pitting-type corrosion in chloride environments. Hoar and Mears [30] postulated that chloride ions accelerate the corrosion of stainless steel by penetrating the oxide film. The chloride-contaminated film then loses its passivating quality and a local attack on the metal follows, creating a pit. The exact mechanism by which molybdenum strengthens the oxide film is not clearly understood [17].

Crevice is a form of local corrosion due to differences in oxygen tension or concentration of electrolytes or changes in pH in a confined space, such as in the crevices between a screw and a plate [59]. The narrower and deeper the crack is, the more likely crevice corrosion is to start [46]. Recent retrieval studies have shown that 16 to 35% of modular total hip implants demonstrated moderate to severe corrosion in the conical head-neck taper connections [60]. Studies of retrieved stainless steel multipart internal fixation devices show visible corrosion at the junction between screw head and the plate in 50-75% of all devices [46]. Other typical crevices are scratches on the surface of an implant, the interface between bone and an implant, the cement-metal interface, and any other sharp interface likely to be depleted of oxygen relative to another oxygenated area [61].

d) Stress Corrosion Cracking

It is a phenomenon in which a metal in a certain environment, especially those rich in chlorides, is subjected to stress and falls at a much lower level than usual as a result of corrosion [62]. Pitting and stress corrosion cracking, although usually associated with stainless steel in chloride media, have not been observed on recovered surgical implants. Implants

often exhibit cracks and surface pitting, but these are most likely the result of improper manufacture rather than corrosion [63-64].

Sheehan *et al.* [65] studied stress corrosion cracking (SCC) of type 316L stainless steel *in-vitro*. Tests were conducted using specimens with electropolished surface in slow strain rate tension tests and Schneider intramedullary nails in static bend tests. They concluded, as previous investigators had done, that SCC is not a mode of failure of 316L stainless steel implants *in-vitro* and found no indication that SCC of this material would occur *in-vivo*. Bundy and Desai [66] studied SCC of type 316L stainless steel and ELI (extra low interstitial) Ti-6Al-4V using fracture mechanics and measuring crack propagation velocity versus stress intensity in environments of $MgCl_2$, HCl and Ringer's solution. Crack propagation occurred in precracked type 316L stainless steel in Ringer's solution held at a potential that disrupted the passive film. The conclusion from this investigation was that SCC of type 316L could occur *in-vivo* if these conditions existed. A straight fracture plate, when flexed, will experience a tensile stress on its convex surface and a compressive stress on its concave surface. This produces a difference in electrochemical potential, which renders, the convex surface anodic with respect to the rest of the plate. Corrosion, as an acceleration of uniform attack, or perhaps secondary tensile rupture of the passive film, will then attack the convex surface preferentially [46]. The same process will occur at stress risers in loaded devices, such as screw holes in fracture fixation plates or kinks in cerclage wire. In this case, the regions of higher stress, in the immediate vicinity of the stress risers, will corrode at the expense of the surrounding less stressed material [46].

e) Corrosion Fatigue

The corrosion fatigue failure of total joint prostheses has been widely studied. It can be concluded from an extensive literature survey carried out by Leclerc [67] that provided the alloy used in the manufacture of the joint prosthesis conforms to the current national and international standards and that it is in the correct metallurgical condition the contribution of corrosion in the corrosion fatigue failures of joint prostheses is marginal. The corrosion

contribution increases with the time that the prosthesis is present in the patient. It has also been shown by various testing laboratories that the *in-vivo* failures can be simulated using *in-vitro* simulators without the presence of a corrosive medium and provided that a torsional component of load is applied to the prosthesis. Bechtol [68] in reviewing his clinical experience with 1087 cemented Charnley and Bechtol total hip replacements conclude that prosthetic stem failure is actually the final sequence of previous failures of bony and cement support. His suggested sequence of prosthetic stem failure has been substantiated in the literature and are as follows:

1. Poor blood supply in the area of the medical femoral neck (as the consequence of a pre-existing pathological condition or excessive early weight bearing) leads to initial loosening of the cement bond;

2. Resorption of the bone in the medial neck places the forces of continued weight bearing on the bone cement in that area and may lead to medial and/ or distal migration of the femoral cement and prosthetic component;

3. Fracture of cement transversely near the distal end of the prosthetic stem or in the area of the medial neck results in slight downward or medial shift of stem position and further increase the forces upon the stem;

4. Repeated fixing of the proximal stem in a fatigue mode over a period of months or years results in a widening of the separation between the metal and cement laterally and ultimately in an actual deformity or fracture of the metal stem.

Hughes et al. [19] reported some corrosion fatigue tests that carried out on an Amsler Vibrophone with specimens immersed in saline environments with a pH range 2 to 7.4. They found that titanium showed

slight decrease in fatigue properties over the pH range whereas stainless steel showed a drastic decline in fatigue strength at pH 4 and below this level became inferior to the titanium. Rollins et al. [70] tested steels in chloride solutions of varying pH and found that corrosion in the range pH 4-10 was independent of pH since the process was controlled by oxygen diffusion to cathodic areas, i.e. it depended on the solubility of oxygen in the solution. Below pH 4 there was an increase in corrosion rate associated with cathodic hydrogen evolution. Although there was insufficient data to analyze fully the effects of changes of pH, it is clear that the increased corrosion rate reported below pH 4 was making a contribution to the reduction of the fatigue strength of the stainless steel. Piehler et al. [71] reported on corrosion fatigue of hip nails and emphasized the importance of materials selection and design. Large plate designs had superior corrosion-fatigue performance over small plates.

2.2 Titanium as an Implant Material

The high strength, low weight, outstanding corrosion resistance possessed by titanium and titanium alloys have led to a wide and diversified range of successful applications which demand high levels of reliable performance in surgery and medicine as well as in aerospace, automotive, chemical plant, power generation, oil and gas extraction, sports, and other major industries [72]. More than 1000 tonnes (2.2 million pounds) of titanium devices of every description and function are implanted in patients worldwide every year. Requirements for joint replacement continue to grow as people live longer or damage themselves more in by hard sports play or jogging, or are seriously injured in road traffic and other accidents. Light, strong and totally biocompatible, titanium is one of few materials that naturally match the requirements for implantation in the human body [24].

Medical grade titanium alloys have a significantly higher strength to weight ratio than competing stainless steels. The range of available titanium alloys enables medical specialist's designers to select materials and forms closely tailored to the needs of the application. The full range of alloys

reaches from high ductility commercially pure titanium used where extreme formability is essential, to fully heat treatable alloys with strength above 1300 MPa, (190ksi) [73]. Shape-memory alloys based on titanium further extend the range of useful properties and applications. A combination of forging or casting, machining and fabrication are the process routes used for medical products. Surface engineering frequently plays a significant role, extending the performance of titanium several times beyond its natural capability.

'Fit and forget', is an essential requirement where equipment in critical applications, once installed, cannot readily be maintained or replaced. There is no more challenging use in this respect than implants in the human body. The effectiveness and reliability of implants, and medical and surgical instruments and devices is an essential factor in saving lives and in the long-term relief of suffering and pain. Implantation represents a potential assault on the chemical, physiological and mechanical structure of the human body. There is nothing comparable to a metallic implant in living tissue. Most metals in body fluids and tissue are found in stable organic complexes. Corrosion of implanted metal by body fluids, results in the release of unwanted metallic ions, with likely interference in the processes of life. Corrosion resistance is not sufficient of itself to suppress the body's reaction to cell toxic metals or allergenic elements such as nickel, and even in very small concentrations from a minimum level of corrosion, these may initiate rejection reactions. Titanium is judged to be completely inert and immune to corrosion by all body fluids and tissue, and is thus wholly biocompatible [36].

The natural selection of titanium for implantation is determined by a combination of most favorable characteristics including immunity to corrosion, biocompatibility, strength, low modulus and density and the capacity for joining with bone and other tissue (osseointegration) [74]. The mechanical and physical properties of titanium alloys combine to provide implants, which are highly damage tolerant. The human anatomy naturally limits the shape and allowable volume of implants. The lower modulus of titanium alloys compared to steel is a positive factor in reducing bone

resorption [75]. Two further parameters define the usefulness of the implantable alloy, the notch sensitivity, the ratio of tensile strength in the notched vs. un-notched condition, and the resistance to crack propagation, or fracture toughness. Titanium scores well in both cases. Typical NS/TS ratios for titanium and its alloys are 1.4 - 1.7 (1.1 is a minimum for an acceptable implant material). Fracture toughness of all high strength implantable alloys is above 50 MPa $m^{-1/2}$ with critical crack lengths well above the minimum for detection by standard methods of non-destructive testing [76].

Forms and material specifications are detailed in a number of international and domestic specifications, including ASTM and BS7252/ ISO 5832 examples, which are listed below:

Table 3:

Titanium Medical Specifications [77].

ASTM	BS/ISO	Alloy designation	
F67	Part 2	Unalloyed titanium - CP Grades 1- 4	(ASTM F1341 specifies wire)
F136	Part 3	Ti-6Al-4V ELI wrought	(ASTM F620 specifies ELI forgings)
F1472	Part 3	Ti-6Al-4V standard grade (SG) wrought	(F1108 specifies SG castings)
F1295	Part 11	Ti-6Al-7Nb wrought	
-	Part 10	Ti-5Al-2.5Fe wrought	
F1580	-	CP and Ti6Al-4V SG powders for coating implants	
F1713	-	Ti-13Nb-13Zr Wrought	
F1813	-	Ti-12Mo-6Zr-2Fe Wrought	

2.2.1 Applications of Titanium in Human Body [78]

Some specific bio-medical applications of Titanium and its alloys are listed below.

- **Bone and Joint Replacement**: About one million patients worldwide are treated annually for total replacement of arthritic hips and knee

joints. The prostheses come in many shapes and sizes. Hip joints normally have a metallic femoral stem and head which locates into an ultrahigh molecular weight low friction polyethylene socket, both secured in position with polymethyl methacrylate bone cement (Figure 3) Some designs, including cementless joints, use roughened bioactive surfaces (including hydroxyapatite) to stimulate osseointegration, limit resorption and thus increase the implant lifetime for younger recipients. Internal and external bone-fracture fixation provides a further major application for titanium as spinal fusion devices, pins, bone-plates, screws, intramedullary nails, and external fixators.

- **Dental Implants**: A major change in restorative dental practice worldwide has been possible through the use of titanium implants. Titanium 'root' is introduced into the jawbone with time subsequently allowed for osseointegration. The superstructure of the tooth is then built onto the implant to give an effective replacement.

- **Maxillo and Cranio/facial treatments**: Surgery to repair facial damage using the patients own tissue cannot always obtain the desired results. Artificial parts may be required to restore the ability to speak or eat as well as for cosmetic appearance, to replace facial features lost through damage or disease. Osseointegrated titanium implants meeting all the requirements of biocompatibility and strength have made possible unprecedented advances in surgery, for the successful treatment of patients with large defects and hitherto highly problematic conditions.

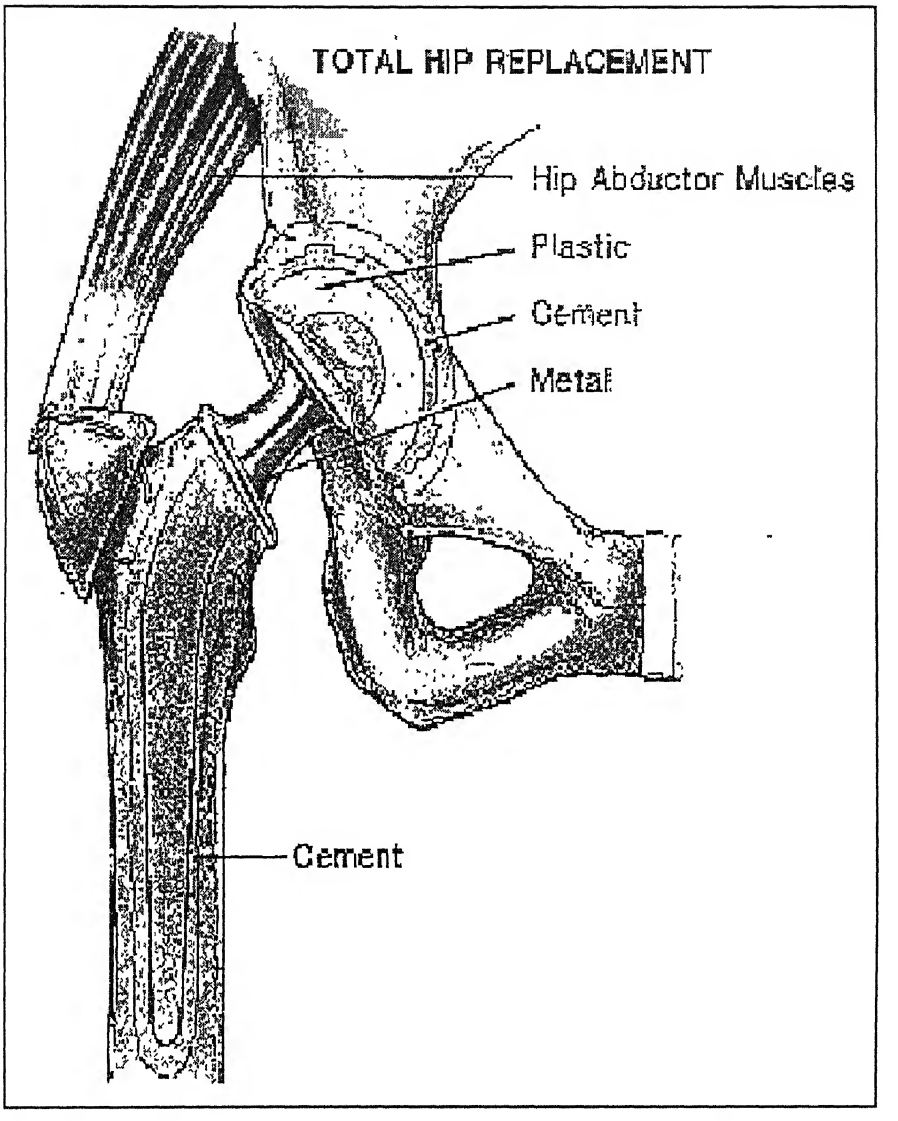

Figure 3: A schematic drawing of a hip prosthesis.

- **Cardiovascular devices**: Titanium is regularly used for pacemaker cases and defibrillators, as the carrier structure for replacement heart valves, and for intra-vascular stents.

- **External Prostheses**: Titanium is suitable for both temporary and long term external fixations and devices as well as for orthotic calipers and artificial limbs, both of which use titanium extensively for its light weight, toughness and corrosion resistance.

- **Surgical Instruments**: Wide ranges of surgical instruments are made in titanium. The metal's lightness is a positive aid to reducing any fatigue of the surgeon. Instruments are frequently anodized to provide a non-reflecting surface, essential in microsurgical operations, for example in eye surgery. Titanium instruments withstand repeat sterilization without compromise to edge or surface quality, corrosion resistance or strength. Titanium is non magnetic, and there is therefore no threat of damage to small and sensitive implanted electronic devices.

Titanium also tends to seize when in sliding contact with itself or other metal. Titanium-based alloys having high co-efficient of friction can cause problems. Wear particles are formed in a piece of bone if a piece of bone rubs against the implant, or if two parts of an implant rub against one another. Therefore, implants of self-mated titanium generally are not used as joint surfaces. Titanium derives its corrosion resistance due to the formation of a surface oxide film. Under *in vivo* conditions, the oxide is the only stable reaction product [79].

Most common alloy used for implants is Ti-6Al-4V. It contains titanium, aluminum, and vanadium. Aluminum increases transformation temperature between alpha and beta phases. Vanadium decreases the transformation temperature between the alpha and beta phases. Alpha alloys have, good weldability, high strength, oxidation resistance at high temperatures [80]. Beta alloys are stronger than alpha phased alloy.

Alpha-beta alloys formed by heat-treating beta solutions are stronger than annealed alpha-beta alloys. Although this alloy has an excellent corrosion resistance and biocompatibility, considerable controversy has developed over the biocompatibility of the alloy [81].

There are two main points to consider in this controversy.

a. Firstly although titanium has an excellent corrosion resistance, if titanium is released into the tissue even by the way of passive dissolution or perhaps another process involving wear, the tissue reaction may vary. This reaction could be anything ranging from a mild response (e.g. a discoloration of the surrounding tissue) to a more severe one (e.g. inflammatory reaction causing pain and even leading to loosening owing to osteolysis) [82].

b. Secondly, if deposits of titanium alloy particles are present in the tissue, then concentrations of aluminium and vanadium (which themselves have different biological properties than titanium) will also be present. It has thus been proposed that better performance in terms of corrosion resistance and biocompatibility would be achieved through the use of alloys of different composition. However, even though several such alloys have been investigated there is still very little data to support this view [83].

2.2.2 Corrosion behavior of Ti and its alloys under simulated Physiological conditions

Corrosion of metal implants is critical because it can adversely affect biocompatibility and mechanical integrity. The material used must not cause any adverse biological reaction in the body, and it must be stable and retain its functional properties. Corrosion and surface film dissolution are two mechanisms for introducing additional ions in the body. Extensive release of metal ions from prosthesis can result in adverse biological reactions and can lead to mechanical failure of the device. The passive films formed on titanium and its alloys consist mainly of amorphous titanium dioxide [84-86]. The

physico-chemical and electrochemical properties of the oxide film and its long-term stability in biological environments play a decisive role for the biocompatibility of titanium implants [87]. Electrochemical impedance spectroscopy study regarding the influence of alloying elements and the potential on the corrosion resistance of Ti and other Ti-based biomedical implant alloys under simulated physiological conditions (Ringer's solution Table 4) has proved to be very successful [89]. Deaerated Hank's Solution also simulates human body environment at pH of 7.4 (Table 5). Table 6 illustrates the corrosion rate and break down potentials of different materials as compared to Ti-6Al-4V in de-aerated Hank's Solution at 37 °C. and 7.4 pH.

Table 4: Composition of Ringer's [88-89] solution.

Compound	Composition g/lt.
NaCl	6.80
KCl	0.40
CaCl2	0.20
MgSo4.7H2O	0.20
NaH2Po4.H2O	0.14
NaHCo3	2.20
Glucose	1.00

The other material being considered is Ti–13Nb–13Zr, which once again relies on niobium as a beta phase stabilizer. The other alloying element, zirconium, is one that is unique in that it is isomorphous with both the alpha and beta phases of titanium [90]. A combination of these two alloying elements has made it possible to develop a structure that is a 'near' beta phase supposedly possessing a superior corrosion resistance over the alpha–beta phase alloys mentioned earlier, but one that still has enough alpha phase present in the final structure to provide the necessary mechanical strength. It has been proposed that Ti–13Nb–13Zr alloy is more

favorable for orthopaedic implants than Ti–6Al–4V alloy because of its superior corrosion resistance and biocompatibility [91]. Reasons for this superiority have included the fact that less metal ion release is likely to occur during spontaneous passivation of Ti–13Nb–13Zr alloy because the corrosion products of the minor alloying elements, niobium and zirconium, are less

Table 5: Composition of Hank's solution [92].

Compound	Composition g/lt.
NaCl	8.0
KCl	0.40
$CaCl_2$	0.14
$MgSO_4.7H_2O$	0.06
$NaH_2PO_4.2H_2O$	0.06
$NaHCO_3$	0.35
Glucose	1.00
KH_2PO_4	0.60
$MgCl_2.6H_2O$	0.10

soluble than those of aluminium and vanadium. Also, that the passive oxide layer on the surface of the alloy is more inert consisting of a dense rutile structure providing greater protection to the underlying alloy [93].

It is well known that proteins affect the corrosion behavior of some metals, and that there presence can either inhibit or accelerate the corrosion phenomena. They are known to behave differently with different metals, since their role in a corrosive environment is governed by many factors such as the surface chemistry of the metal, protein adsorption characteristics, interaction of protein molecules with other ions present in the electrolyte solution to produce organic complexes, and the transport of anionic and cationic charges around and away from the local environment [94].

Table 6:

Breakdown Potentials and Corrosion rates of different materials in de-aerated Hank's solution at 37 °C. [95].

Material	Breakdown Potential (mV vs SCE)	Corrosion rate (mils/year)
316L stainless steel	280	0.17
Cobalt alloy	600	0.056
Ti-6Al-4V	1900	0.007

The corrosion resistance of the alloys was studied using cyclic anodic polarization techniques to break down the passive layer and then allow repassivation to occur. The value of the breakdown potential for Ti alloys is difficult to assess owing to the instability of the aqueous electrolytes at the high potentials required. The ability of the surfaces to repassivate in the environment, as measured by the hysteresis in the cyclic polarization curve, is a better measure of the corrosion behavior of these materials. For these reasons the corrosion resistance of these alloys was estimated by recording the difference between the breakdown potential (E_b) and the repassivation potential (E_p) [96]. This study showed that in different environments (i.e. at different pHs or in the presence of proteins) the ability of the alloys to repassivate is affected. Hardness measurements was done to evaluate the surface oxide formed during repassivation and to determine that it is different from the original surface oxide [97]. Figures 4 and 5 present the corrosion resistance data for the three alloys in different environments. From Figure 4 the corrosion resistance of the alloys (i.e. E_b–E_p values) at three different pH levels (i.e. 5, 7.4 and 9) can be evaluated. Generally, it was noticed that as the pH level increased in Phosphate buffered saline solution,

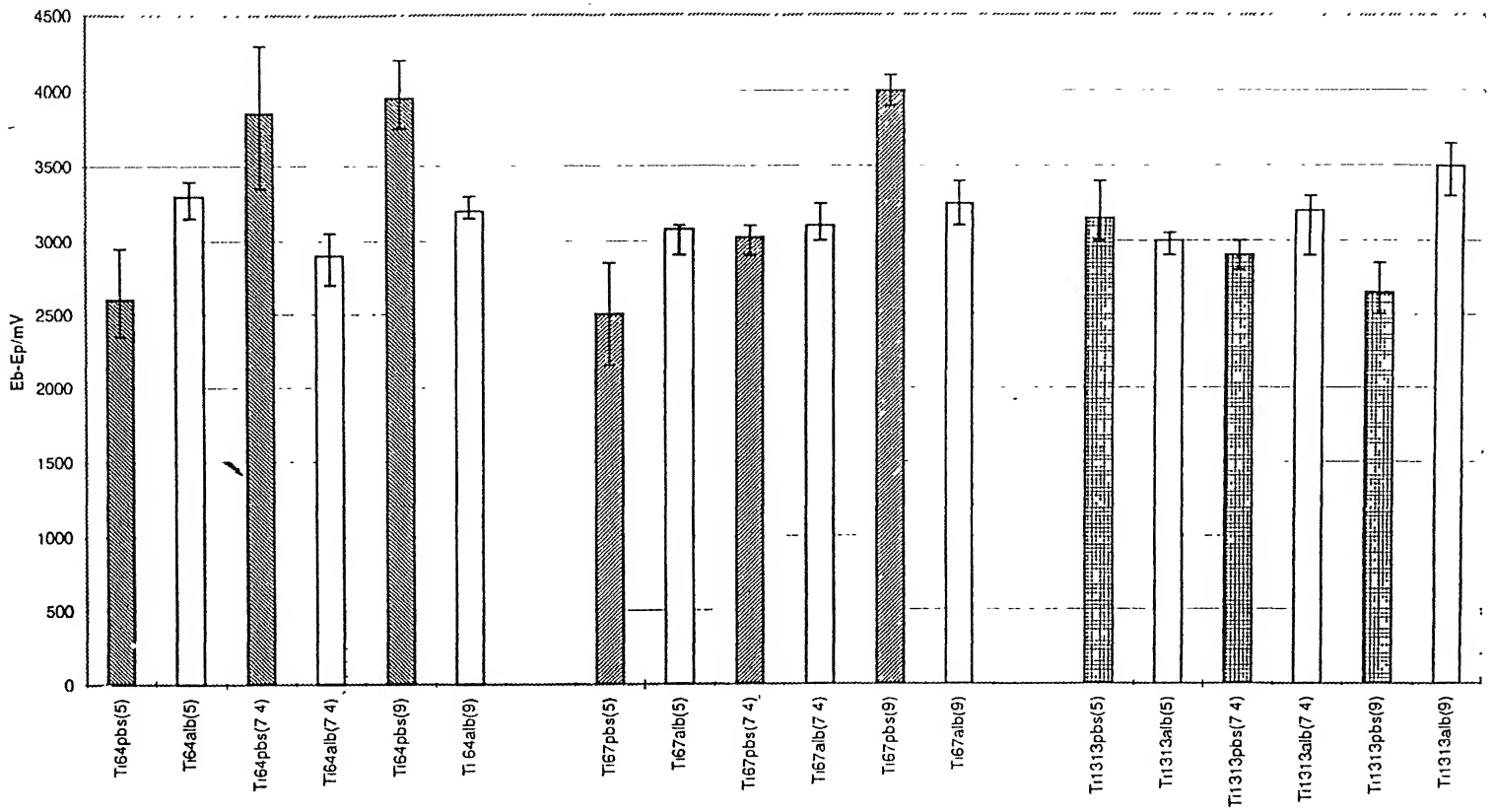

Figure 4: E_b–E_p values for all three Ti alloys in PBS and 1 mg/ml bovine albumin solution at different pH values, presented as the mean and the range of three measurements. Ti64=Ti–6Al–4V, Ti67=Ti–6Al–7Nb, Ti1313=Ti–13Nb–13Zr, PBS=phosphate-buffered saline, Alb=bovine albumin, the value in parenthesis is the pH of the electrolyte [98].

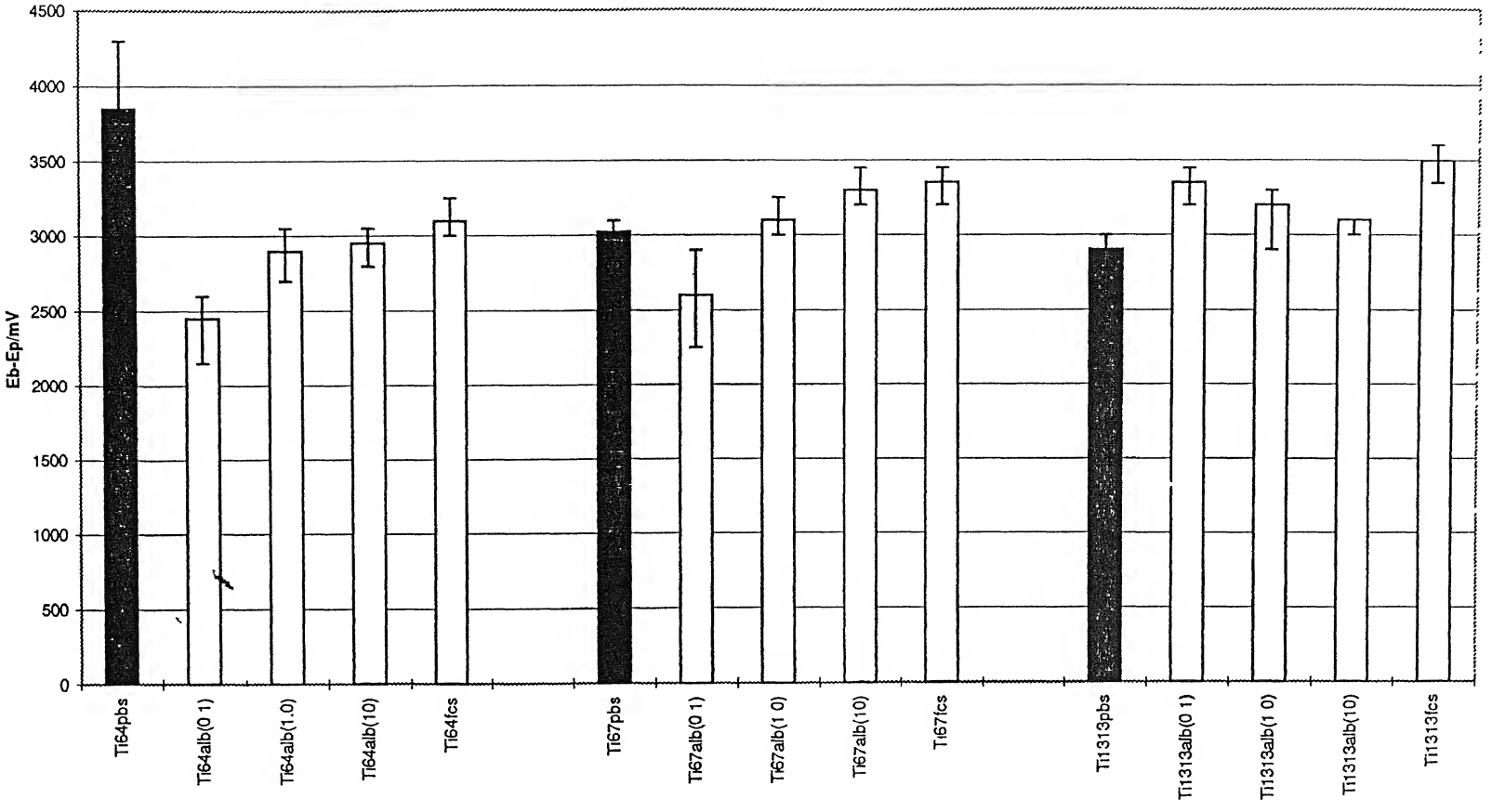

Figure 5: E_b–E_p values for all three Ti alloys in PBS, bovine albumin at different concentrations and 10% foetal calf serum, presented as the mean and the range of three measurements. Ti64=Ti–6Al–4V, Ti67=Ti–6Al–7Nb, Ti1313=Ti–13Nb–13Zr, PBS=phosphate-buffered saline, Alb=bovine albumin, fcs=10% foetal calf serum and the value in parenthesis is the concentration of albumin in mg/ml [98].

the corrosion resistance of Ti–6Al–4V and Ti–6Al–7Nb decreased, whereas that of Ti–13Nb–13Zr was seen to increase but only slightly [98].

When albumin, at a concentration of 1 mg/ml, was added, the effect of pH on the corrosion resistance of Ti–6Al–4V and Ti–6Al–7Nb was reduced whereas for Ti–13Nb–13Zr the addition of albumin caused a decrease in corrosion resistance as the pH increased, although again the changes were small. From Figure 5 the corrosion resistance of the alloys, in environments containing progressively increasing concentrations of albumin, can be evaluated. It was observed that by adding albumin (0.1 mg/ml) to PBS, the corrosion resistance increased for Ti–6Al–4V. For Ti–6Al–7Nb and Ti–13Nb–13Zr the changes in corrosion resistance were smaller showing a slight increase for Ti–6Al–7Nb and a slight decrease for Ti–13Nb–13Zr.

As the concentration of albumin increased the corrosion resistance of Ti–13Nb–13Zr appeared to remain at the same level, whereas, that for the other two alloys tended to decrease. The Ti–6Al–4V alloy was more corrosion resistant in all the albumin solutions than in PBS, whereas the Ti–6Al–7Nb and Ti–13Nb–13Zr alloys were generally less corrosion resistant in protein solutions than in PBS. The addition of foetal calf serum produced a similar effect with each alloy, as had the presence of higher concentrations of albumin.

2.2.3 Repassivation of Titanium alloys

Titanium alloys are used in orthopaedic applications and there is concern about the release and subsequent build up of material in the tissues. It is unlikely that the passive layers on these alloys will be broken down electrochemically in the physiological environment. It is known, however, that the integrity of the passive layer can be influenced by wear [99]. It is important therefore to investigate the repassivation processes of these alloys in a biological environment. In this study electrochemical techniques were used to break down the passive layer so that one could investigate the repassivation and the interaction of proteins with this process. To understand

comprehensively how corrosion takes place in terms of charge transfer at the metal/electrolyte interface, it is necessary to consider an accepted model for the charge distribution in terms of a charge double layer structure (Figure 6). In this case, a double-layer is present due to hydroxylated ions at the metal surface and charge transfer can occur within the layer depending on whether the metal oxide is stable (i.e. acting as a cathode) or whether it is passivating up to and beyond removal of its protective oxide layer (i.e. as an anode).

When the passive layer is broken the titanium alloy is able to release ions into solution until the passive layer is rebuilt. The action of rebuilding this layer results from the chemical interaction of anions in the environment reacting with the surface [100]. It is hypothesized that any anions in the environment may have a bearing on the final composition of the repassivated layer and its ability to form. Cyclic polarization studies were used to assess the ability of the surface to repassivate and hardness measurements to investigate the properties of the repassivated surface [101].

Examination of the surface under a microscope following cyclic polarization indicated an evidence of pit formation. This evidence and the presence of hysteresis during cyclic polarization suggests that the passive layer is being broken down and repassivated under these experimental conditions. The difference between the breakdown potential and the repassivation potential is related to the reactions that are taking place at the surface of the material as repassivation occurs. This study [98] revealed that proteins in the environment might be interacting with the repassivating process and thus influencing the properties of the passive layer. When the pH of the environment changes the proteins will have a different charge owing to their zwitterion character and therefore it is reasonable to suspect that they may interact with the repassivation process in a different way [98].

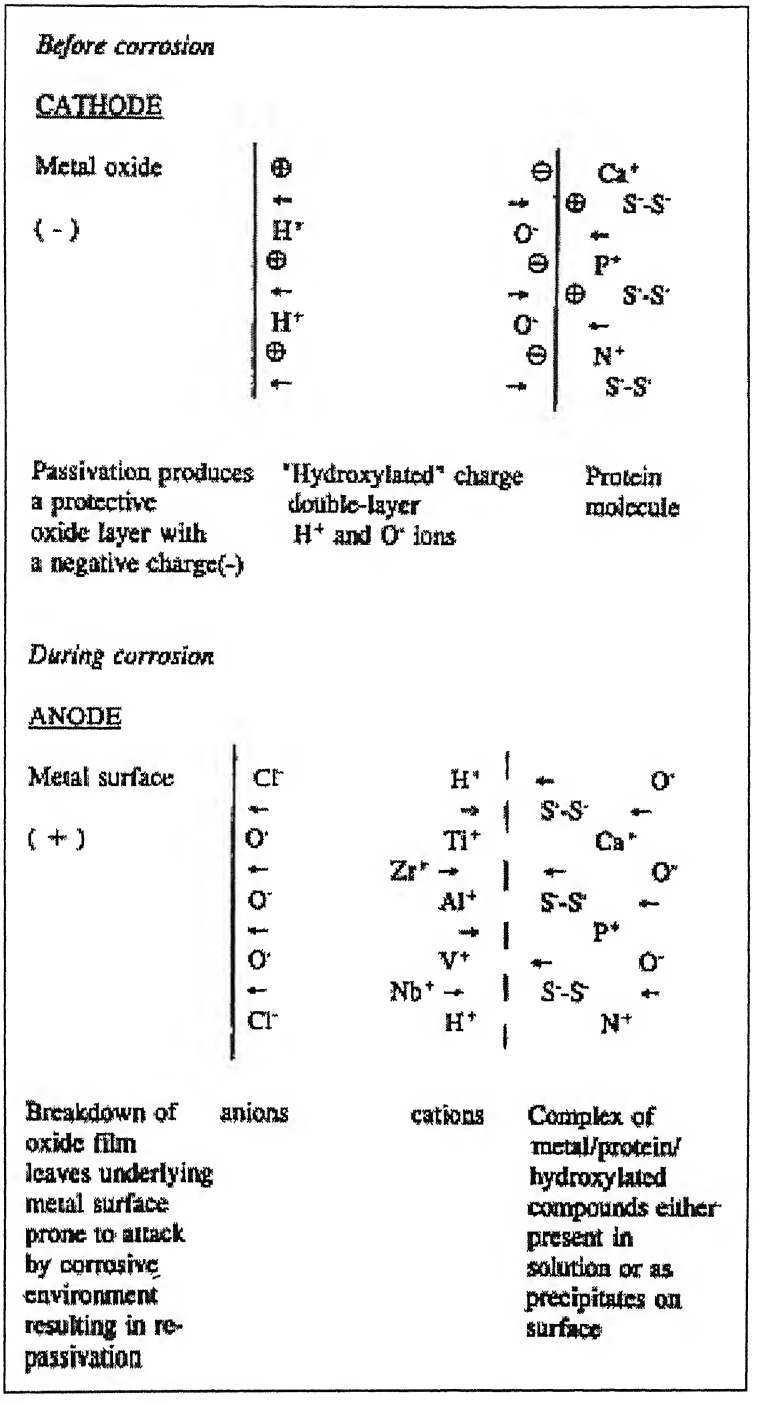

Figure 6: Theoretical model of charged double layer showing the transfer of charge at the metal/oxide/protein interfaces before and during the corrosion process.

In an environment without the presence of proteins it was observed that as the pH increased the corrosion resistance of Ti–6Al–4V and Ti–6Al–7Nb was reduced. In other words, the repassivation process became more difficult and therefore there was the possibility of greater release of metal ions into solution. This occurred with these two alloys owing to the solubility of Al and V ions and their increased solubility in the presence of increased hydroxyl concentration. The investigation showed that, under the same conditions the corrosion resistance of Ti–13Nb–13Zr increased slightly although the changes were very small. This could be explained by the lower solubility of Zr and Nb ions, in comparison with Al and V, thus repassivation occurs in preference to dissolution [102]

From the experimental work performed by M.A. Khan et al. [98], it was clear that when albumin is added to the phosphate buffer saline (PBS) solution at the three pH levels it appears to reduce the effect of pH on the corrosion resistance of Ti–6Al–4V and Ti–6Al–7Nb. Proteins can interact with the corrosion reactions in several ways and thus shift the position of equilibrium. For example, proteins can bind to metal ions and transport them away from the interface thus encouraging further dissolution or proteins may adsorb onto the metal surface thus restricting the diffusion of oxygen to the surface thus make it harder for the surface to repassivate. Both these mechanisms might be expected to decrease the corrosion resistance of the alloy. Data [103] suggests that the proteins are increasing the corrosion resistance of the alloy, in particular, at the higher pH level. At these pH levels albumin has a negative charge since its isoelectric point is 4.9. It may be possible that under these conditions metal/ protein/ hydroxide complex forms and becomes adsorbed to the surface restricting metal dissolution. Following corrosion in PBS at pH 7.4 the hardness of all the surfaces was reduced but this reduction was small for Ti–6Al–4V and greatest for Ti–13Nb–13Zr. As the pH of the PBS was increased or decreased the hardness of the repassivated surface was significantly reduced for all the alloys suggesting that the repassivated surface had a different character to the original Ti oxide surface [98].

2.2.4 Corrosion and wear behavior of Ti-13Nb-13Zr alloy

Ti-13Nb-13Zr is a new titanium alloy, which has a unique combination of properties that may make it an attractive choice for a variety of applications. Originally developed for use in biomedical implants, this alloy combines a low elastic modulus; high strength, excellent hot and cold workability, superior corrosion resistance, and the ability to be surface hardened to improve wear properties [104]. Research on this age-hardenable alloy has shown that the mechanical properties can be controlled over a significant range through hot working, heat treatment and cold working [104]. The elastic modulus of Ti-13Nb-13Zr can be varied between approximately 6 and 12 Msi, and strengths as high as 190 ksi have been achieved. Further, the material does not seem to exhibit some of the typical processing difficulties encountered in some age-hardenable beta-Ti alloys. For example, in wire drawing trials, Ti-13Nb-13Zr yielded exceptionally good surface finish in the "as-drawn" condition with over 85% cold work.

Localized aggressive environments (pH<1.7) may be expected as a result of the increasing modular design of modern orthopedic implants, where tight joints can occur in conjunction with mechanical abrasion of implant surfaces [105]. The resulting critical corrosion related issues include the possibility of local deaeration, separation of anodes and cathode sites, and the metal dissolution/hydrolytic acidification/chloride ion (Cl^-) migration mechanism, promoting a local build up of acidity and high Cl^- concentrations adjacent to the implant. This could result from increased passive dissolution and/or abrasion-repassivation. The issue of local acidification and Cl^- accumulation points toward crevice corrosion. However, crevice corrosion which is defined by local depassivation and active dissolution and which can result in mechanical failures, is not expected for Ti exposed to low pH solutions at temperatures <75 deg. C [106]. Instead, the primary concern resulting from localized acidification is the accelerated passive dissolution and/or, but not necessarily depassivation and active dissolution of the implant resulting from a high flux of foreign metallic ions into the physiological system. The active and passive rates of dissolution of titanium

are known to be functions of pH [107-108]. Consequently, an examination of the potential-pH diagram of titanium at 37^0C is necessary to provide preliminary information regarding the regions of possible accelerated passive and/or active corrosion.

The revised Pourbaix diagram suggests that the thermodynamically stable state of Ti is the titanium anion (Ti^{3+}) at pH<1.49 within the range of open potentials near the expected deaerated open circuit potential (OCP) for Ti e.g. -0.2 V to -0.7 V vs. a saturated calomel reference electrode (SCE). Concerning the abrasion repassivation Beck showed that Ti^{3+} was the dominant dissolved species resulting from the scratch–repassivation of Ti discs [110] and Baes and Mesmer reported that Ti^{3+} is hydrolysable [111].

Moreover, Kolman and Scully [108] have shown that Ti^{3+} occurs over the duration of repassivation as a result low overall current efficiency of TiO_2 formation after mechanical depassivation. Indeed The pH near a crack tip in Ti-8% Al-1% Mo-1% V has been reported to be as low as 1.7 [105]. Also Beck reported a pH<1.3 near a corroding pit exposed to neutral Cl^- solution [112]. In addition, Ti^{3+} hydrolysis can produce pH as low as 0 when 1 M titanium chloride is added to deaerated water [108].

Consequently, an improved implant alloy should exhibit better resistance to anodic dissolution at pH <0, as well as improved passivation and repassivation behaviors to limit Ti^{3+} production compared to currently available Ti-based implant alloys. It is known that titanium exhibits a high resistance to pitting corrosion in Cl^- containing solutions as aggressive as 5 M HCl, where Ti exhibited pitting at 13.2 V_{SCE} [113]. This E_{pit} is far more positive than the expected OCP values of Ti-based alloys in aerated Ringer's solution and deaerated 5 M HCl. In Ringer's solution, the tested commercial Ti-based implant alloys all exhibited spontaneous passivity and similar i_P values except DH (diffusion hardened) Ti-13 Nb-13Zr alloy, which exhibited low i_P.

In contrast, most of the tested commercial implant alloys, including Ti-13Nb-13Zr (Solution treated, Solution treated and aged) exhibited active to passive transitions indicative of incomplete passivity in deaerated 5 M HCl. Only ST (solution treated) Ti-15Mo-3Nb-3Al and DH Ti-13Nb-13Zr exhibited

spontaneous passivity in deaerated 5 M HCl. While not spontaneously passive in 5 M HCl, Ti-13Nb-13Zr (ST and STA) exhibited increased resistance to active anodic dissolution, improved passivity, and enhanced resistance to localized corrosion in comparison to CP Ti [114].

E_{pit} values for Ti-13Nb-13Zr (ST and STA) in 5 M HCl were measured and compared to previously reported E_{pit} values of Ti and Ti-6Al-4V in comparable solutions (Table 7). In 5 M HCl at 37^0 C, ST and STA Ti-13Nb-13Zr resisted pitting and did not experience localized corrosion events at potentials as high as 22.8 V_{SCE} (upper limit of the potentiostat) [114].

Table 7:

Experimental and literature-based E_{pit} values of commercial implant alloys in Cl^- solutions.

Material	Heat Treatment	E_{pit} (V_{SCE})	Solution Experimental Condition	Reference
CP Ti	Annealed	+ 13.2 V	5 M HCl (22^0C)	113
CP Ti	Annealed	+ 10 V	5 M HCl (37^0C)	115
Ti-6Al-4V	Hot rolled and Hot forged	+ 5.9 V	5 M HCl (37^0C)	107
Ti-13Nb-13Zr	Solution Treated	> +22.8 V	5 M HCl (37^0C)	114
Ti-13Nb-13Zr	Solution Treated and aged	> +22.8 V	5 M HCl (37^0C)	114

2.3 Electrochemical Corrosion Testing

2.3.1 Electrochemical Corrosion

Corrosion can be defined as the degradation of a metal by an electrochemical reaction with its environment [116]. Corrosion is an electrochemical process. Electrochemical processes require anodes and cathodes in electrical contact and ionic conduction path through an electrolyte. The electrochemical process includes electron flow between the anodic and cathodic areas; the rate of this flow corresponds to the rates of oxidation and reduction reactions that occur at the surfaces. Monitoring this electron flow provides the capability of assessing the kinetics of the corrosion process, not simply the thermodynamic tendencies for the process to occur spontaneously but also the accumulated metal loss registered after the test. Measurements of this type are known as electrochemical measurements of corrosion [117-118].

Electrochemical techniques are finding increased use in corrosion research and in engineering applications. Such methods are practical because the corrosion behavior of material-electrolyte combinations is a direct function of the mechanisms as well as the kinetics of the electrochemical reactions responsible. The availability of better electrochemical techniques and the demonstrated accuracy of such methods for investigating corrosion phenomena have been the subject of several recent technical symposia [119-120].

All metals are found in their low energy state ores, in the form of their oxides, sulfides, carbonates or more complex compounds. Large amount of energy is supplied in order to extract a pure metal from its ore. This pure metal is in a high-energy state and hence they try to come back to the low energy state by recombining with the environment. This process is called corrosion. Figure 7 shows the thermodynamic energy profile for metals and their compounds. The thermodynamic aspects of corrosion will be briefly discussed. All the interactions between elements and compounds are governed by the free energy changes (ΔG). Any reaction is said to be

spontaneous when ΔG for the reaction is negative. At room temperature most of the chemical compounds of metals have lower free energy than the pure metals and hence most of the metals have an inherent tendency to corrode.

In all kinds of aqueous corrosion, there are two reactions occurring at the metal/liquid interface; an electron producing reaction (anodic or oxidation reaction) and an electron consuming reaction (cathodic or reduction reaction). The corrosion reaction for the creation of a wet electrochemical cell requires four basic requirements, the cathode on which the reduction reaction occurs, an anode on which oxidation occurs, an electrolyte to act as the conducting medium for ions and a electrical connection for electron to flow between the anode and cathode.

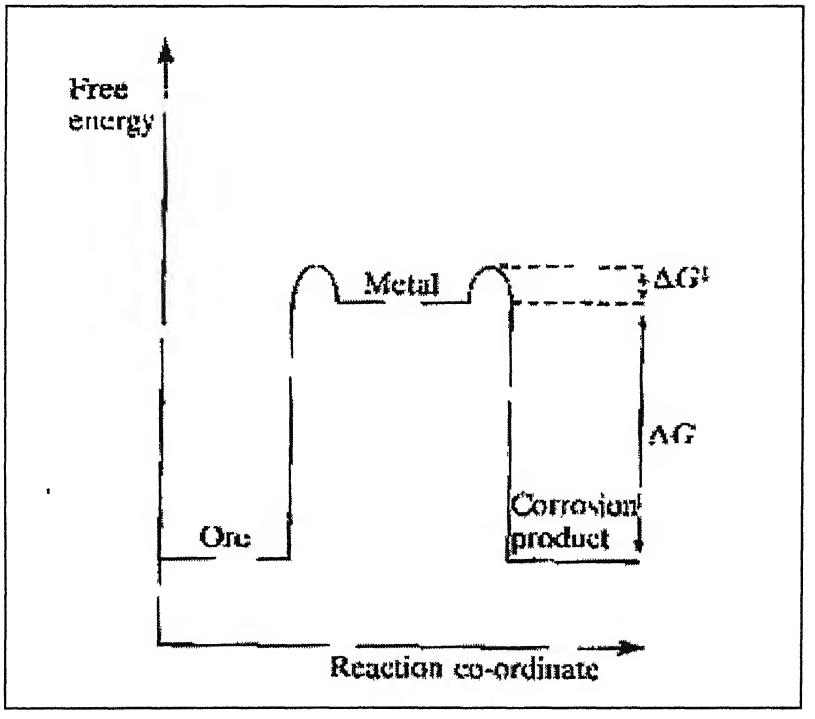

Figure 7: The thermodynamic energy profile for metals and their Compounds.

The anodic reaction is invariably corrosion of the metal as shown in equation 1. Several cathodic reactions can occur during corrosion [116]. The simplest of them is reduction of hydrogen ions (equation 2). Another is reduction of an oxidized ion in solution (redox reaction) as in equation 3.

Another reaction is reduction of dissolved oxygen as in equation 4. In the absence of any of these reactions water reduction will occur as in equation 5.

$M \longrightarrow M^{n+} + ne^-$ (Anodic Reaction) (1)

$2H^+ + 2e^- \longrightarrow H_2$ (Hydrogen Reduction Reaction) (2)

$Fe^{3+} + e^- \longrightarrow Fe^{2+}$ (Redox Reaction) (3)

$O_2 + 4H^+ + 4e^- \longrightarrow 2H_2O$ (Oxygen Reduction Reaction) (4)

$2H_2O + 2e^- \longrightarrow H_2 + 2OH^-$ (Water Reduction Reaction) (5)

A basic wet corrosion cell is shown in the Figure 8. The potential difference between the anode and the cathode could be measured by using a voltmeter in the circuit.

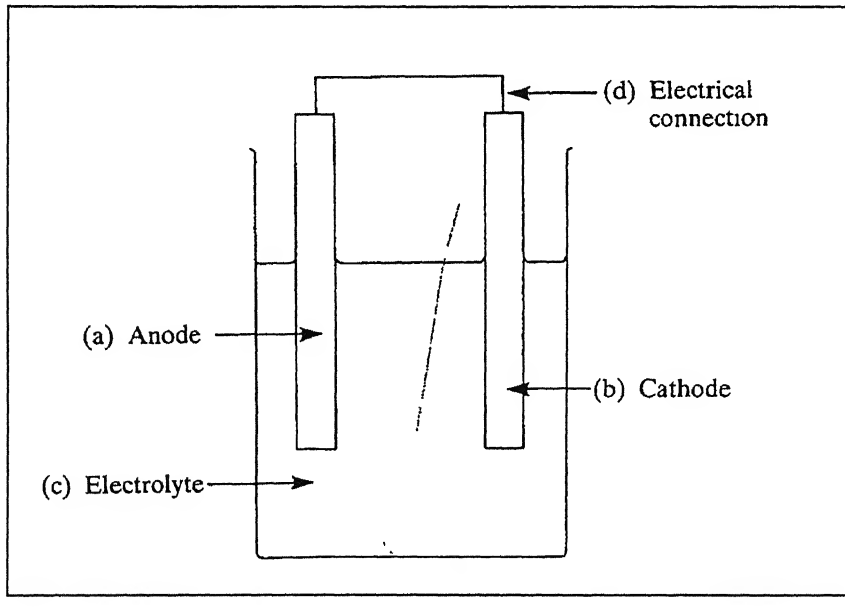

Figure 8: A basic wet corrosion cell [2].

But this gives only the potential difference between the electrodes and in order to measure the absolute potential we need a third electrode. This third electrode is called as the standard electrode against which all the measurements can be made. The standard hydrogen electrode, saturated

calomel electrode (SCE) etc. are usually used as the standard electrodes. Table 8 gives some commonly used standard electrodes and their potentials.

Table 8: Standard reference electrode potentials [2].

Electrode	Electrolyte	Potential (V)
Calomel (SCE)	Saturated KCl	+0.2420
Calomel (NCE)	1.0 M KCl	+0.2810
Calomel	0.1 M KCl	+0.3335
Silver/Silver Chloride (SSC)	1.0 M KCl	+0.2224
SSC	Sea Water	+0.25
Copper/Copper Sulphate (CSE)	Sea Water	+0.30
Zinc	Sea Water	-0.79

2.3.2 Polarization

When a metal is not in equilibrium with the solution of ions, the electrode potential differs from the free corrosion potential by an amount known as the polarization [116]. It can also be said as overpotential or overvoltage. Polarization is a very important corrosion parameter as it is useful in calculating the rates of the corrosion process. The deviation of the equilibrium potential is a combination of an anodic polarization of metal and a cathodic polarization of the environment. If the electrons are made available to the metal, the potentials at the surface becomes more negative, suggesting that excess electrons with their negative charges accumulate at the metal/solution interface. This negative potential charge with respect to the reversible condition is called as cathodic polarization. Similarly, when electrons are removed from the metal, there will be a deficiency of electrons on the metal surface interface, which produces a positive potential change, called anodic polarization [121]. In an aqueous electrolyte solution the surface will reach a steady potential called free corrosion potential, E_{corr}, which depends on the ability and rate at which electrons can be exchanged by the anodic and cathodic reactions.

When an adherent surface film forms on anodic polarization under oxidizing conditions, this is termed as passivation [116]. Passivity of metals has been a subject of significant research. The nature of the passive films that form on a wide variety of materials has been explored utilizing special electrochemical characterization techniques like impedance spectroscopy, ellipsometry, etc. [116].

The mechanism of passive film formation can be understood by modern electrochemical theory, with the aid of polarization diagrams. The polarization diagram is a plot between the potential (i.e. the thermodynamic axis) and current density (i.e. the kinetic axis). The changes in the current density as a function of polarization (i.e. deviation of potentials away from equilibrium) is represented in these polarization diagrams and several processes related to corrosion (and electrochemistry) can be easily understood utilizing these diagrams. The anodic polarization diagram for a metal exhibiting passivity (i.e. condition of corrosion resistance due to formation of an adherent non-dissolving passive film on anodic polarization under oxidizing conditions) is schematically depicted in Figure 9 [122]. It must be remembered that experiments have to be performed by controlling the potential and measuring the current (i.e. either potentiostatically or potentiodynamically) rather than vice versa, in order to understand passivation phenomenon [116]. At the equilibrium reversible potential of the metal (E_{rev}), the exchange current density (i_o) depicts the rate of the forward reaction (i.e. corrosion) being equal to the rate of the reverse reaction (i.e. reduction).

On anodically polarizing the material, thermodynamic conditions for the formation of a stable surface film are established at point A. On further anodically polarizing the material, the passive film nucleates on the surface from point B onwards and this indicates the potential for initiation of passivity (E_{ip}). On further increasing the potential, the film starts covering the surface laterally and at optimum coverage, the critical current density (i_{crit}) is achieved (point C), corresponding to which the primary passivation potential

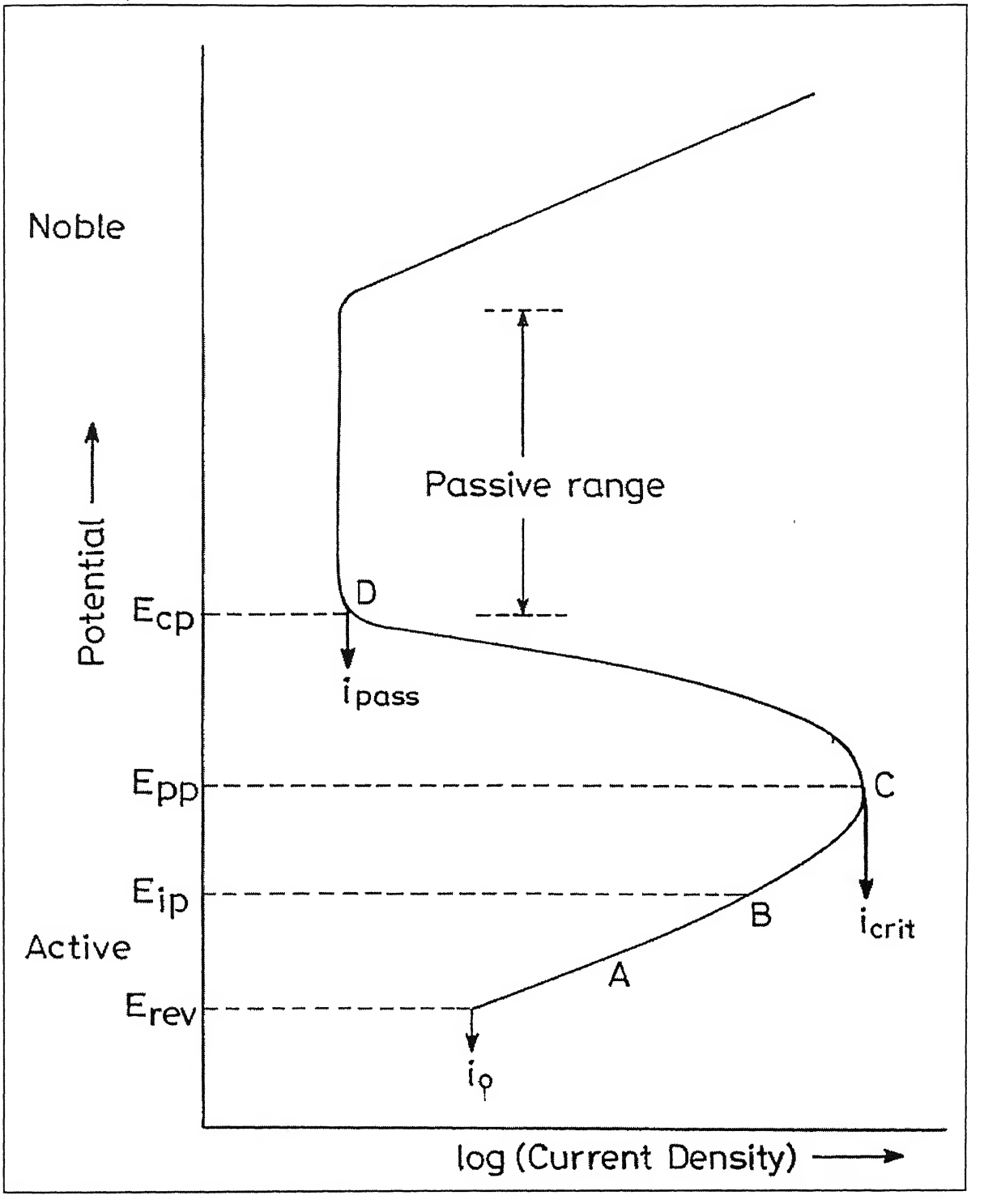

Figure 9: Schematic anodic polarization diagram for an active-passive metal illustrating important passivity parameters.

(E_{pp}) is defined. On further anodic polarization beyond E_{pp}, the surface passive film completely covers the surface and the current density decreases with increasing anodic polarization until the point D, when the passive film completely covers the surface. The potential corresponding to point D is referred to as the potential for complete passivation (E_{cp}). On polarizing past this potential, the current density remains constant with increasing potential in the passive range (Figure 9). On further anodically polarizing the material, several reactions can lead to the destruction of passivity (i.e. indicated by increasing current density with increasing potential), which is understood by the breakdown potential, E_b. Some of the processes leading to increasing current density with polarization beyond the breakdown potential are oxygen evolution, transpassive dissolution due to conversion of the passive film forming ion to a higher oxidation state, pitting caused by destabilization of the passive film due to the presence of halide ions or changes in the nature of the passive film (for example anodizing wherein there is a change in porosity of the passive film).

In the passive region, the current density remains constant with increasing anodic polarization, which is due to thickening of the passive film [122]. It is important to note the fine dimensions of the passive films. The current density remains constant over a significant range of potential in the passive range, and this is called the passive current density (i_{pass}). The passive current density is dictated by the constant rate of dissolution of the metal ions into the electrolyte from the passive film surface. The increasing anodic positive potentials in the passive range are accommodated by thickening of the film.

After the above discussion on the anodic polarization characteristic, the development of free corrosion potentials needs to be addressed. Modern electrochemical theory states that equilibrium corrosion condition obtains when the net cathodic rate is equal to the net anodic rate. Practically, this implies that the free corrosion potential will be established at the potential where the cathodic polarization curve (i.e. of the cathodic reaction) intersects the anodic polarization curve. The rate of the anodic reaction is therefore

directly related to the rate of chemical reduction reaction(s) at cathodic areas. The cathodic reaction in de-aerated solutions is hydrogen evolution, given by

$$2H^+ + 2e \rightarrow H_2 \quad \text{(acidic)} \quad (1)$$

$$2H_2O + 2e \rightarrow H_2 + 2OH^- \quad \text{(neutral or alkaline)} \quad (2)$$

The hydrogen evolution reaction proceeds rapidly in acids, but slowly in alkaline or neutral media. Dissolved oxygen in the electrolyte takes part in the cathodic reaction in accordance with one of the following reactions.

$$4H^+ + O_2 + 4e \rightarrow 2H_2O \quad \text{(acidic)} \quad (3)$$

$$O_2 + 2H^+ + 4e \rightarrow 2OH^- \quad \text{(neutral/alkaline)} \quad (4)$$

$$2H_2O + O_2 + 4e \rightarrow 4OH^- \quad \text{(alkaline)} \quad (5)$$

Dissolved oxygen reacts with hydrogen/water adsorbed at random on the metal surface, independent of the presence or absence of impurities. Therefore, the oxidation reaction proceeds as rapidly as oxygen reaches the metal surface.

The oxygen reduction reaction will be considered to illustrate the development of free corrosion potentials (FCP) or mixed potential under atmospheric corrosion conditions. The cathodic polarization curve corresponding to oxygen reduction reaction can intersect the anodic polarization curve at different locations and based on this; different conditions of passivity (stable or unstable) or active behavior can be realized. Three possible situations are depicted in Figure 10. In Figure 10a, the cathodic polarization curve intersects the anodic curve in the active region and the FCP is established at the potential corresponding to the intersection of both these curves. The metal corrodes in the active state. In practical cases, this situation generally depicts corrosion of fresh surface of metal, free of any surface film. In case the anodic polarization curve intersects the cathodic polarization curve *only* in the passive region, then the FCP would be established in the passive region. This is the condition of stable passivity (Figure 10b). When the cathodic polarization curve intersects the anodic

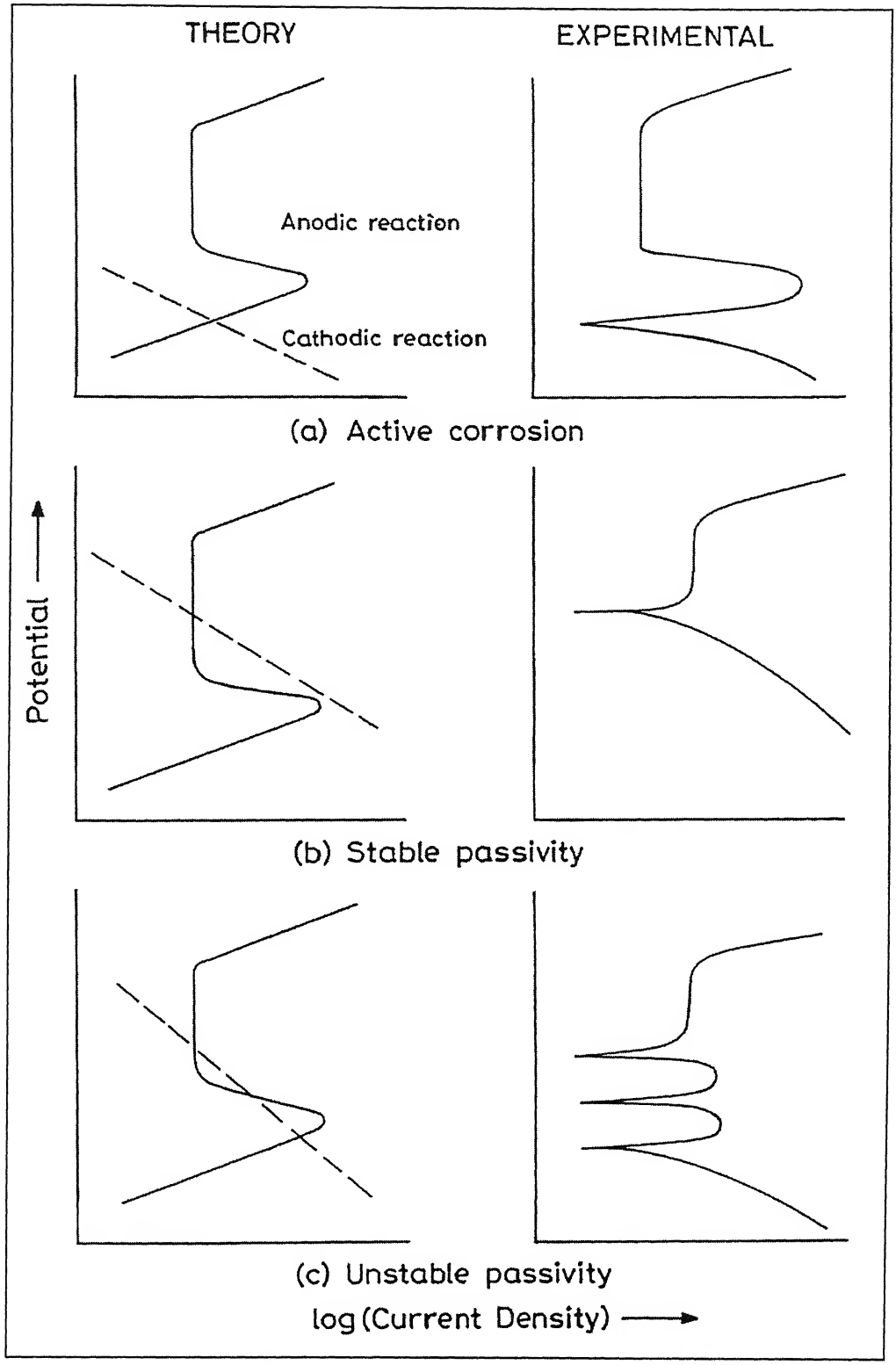

Figure 10: Schematic illustrations outlining the theoretical aspects governing the development of experimental polarization diagrams: (a) active behavior, (b) stable and (c) unstable passive behavior.

polarization curve as shown in Figure 10c, there are three potentials where the anodic and cathodic current densities are equal. The FCP that the material will achieve depends on its prior surface condition. In case a fresh surface is exposed without any film present, then the FCP would establish in the active region, whereas if there is a pre-existing passive film, the FCP would establish in the passive region. The schematic depicted in Figure 10c is indicative of unstable passivity and the experimental polarization diagram for this situation would show the existence of a cathodic loop [116]. The above discussion establishes that surface electrochemical potential depends upon the nature of the surfaces as well as the cathodic reaction kinetics.

2.3.3 Corrosion Rates

There are two methods available for measurement of corrosion rate using polarization methods, namely Tafel extrapolation and polarization resistance. The polarization methods to measure corrosion rates have their inherent advantages [123]. The main advantage of these methods is that the time taken for conducting experiments is relatively short, whereas the conventional weight loss methods require several days. The polarization methods are highly sensitive, and accelerating factors such as elevated temperature, to increase rates is generally not necessary. Moreover these methods are non-destructive and several repetition experiments can be carried out using the same sample.

The mixed potential theory forms a basis for explaining the polarization techniques. The mixed potential theory consists of two simple hypothesis:

1. Any electrochemical reaction can be divided into two or more partial oxidation and reduction reactions.

2. There cannot be net accumulation of electrical charge during a chemical reaction i.e., corrosion reaction the sum of the anodic oxidation currents should be equal to the sum of the cathodic

reduction currents. In other words the total rate of oxidation should be equal to total rate of reduction [124].

Consider the reactions for zinc getting corroded in an acid solution. Then the anodic and cathodic reactions are given by,

$$Zn \longrightarrow Zn^{2+} + 2e^{-} \quad \text{(Anodic reaction)} \qquad (7)$$

$$2H^{+} + 2e^{-} \longrightarrow H_2 \quad \text{(Cathodic reaction)} \qquad (8)$$

These reactions are called as the half-cell reactions and the potential corresponding to them are called cell potential. The potentials cannot coexist separately on an electrically conducting surface. The potentials will polarize to an intermediate value called as the corrosion potential or mixed potential (E_{corr}). When there is no external current flowing into the system, then the equilibrium potential attained is called free corrosion potential (E_{corr}) [121]. As the reactions polarize on the same surface the change in potentials is given by,

$$\eta_a = \beta_a \log (i_a/i_o) \qquad (9)$$

$$\eta_c = \beta_c \log (i_c/i_o) \qquad (10)$$

where η_a and η_c are anodic and cathodic polarization, β_a and β_c are the Tafel constants, i_a and i_c are the anodic and cathodic currents, respectively. At E_{corr} the rate of anodic and cathodic reactions are equal and is equal to the current density, i_{corr}. The half-cell reactions for dissolution of Zn in acid are shown in the Figure 11. This figure is also called as Evans diagram and represents active corrosion of the metal.

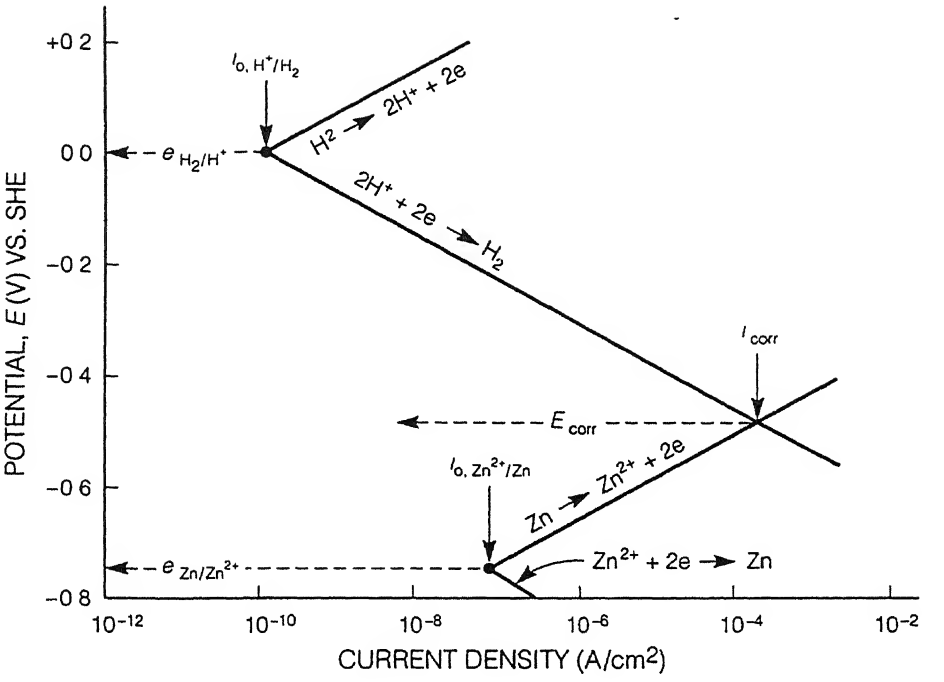

Figure 11: Polarization diagram for dissolution of Zn in acid (active corrosion case).

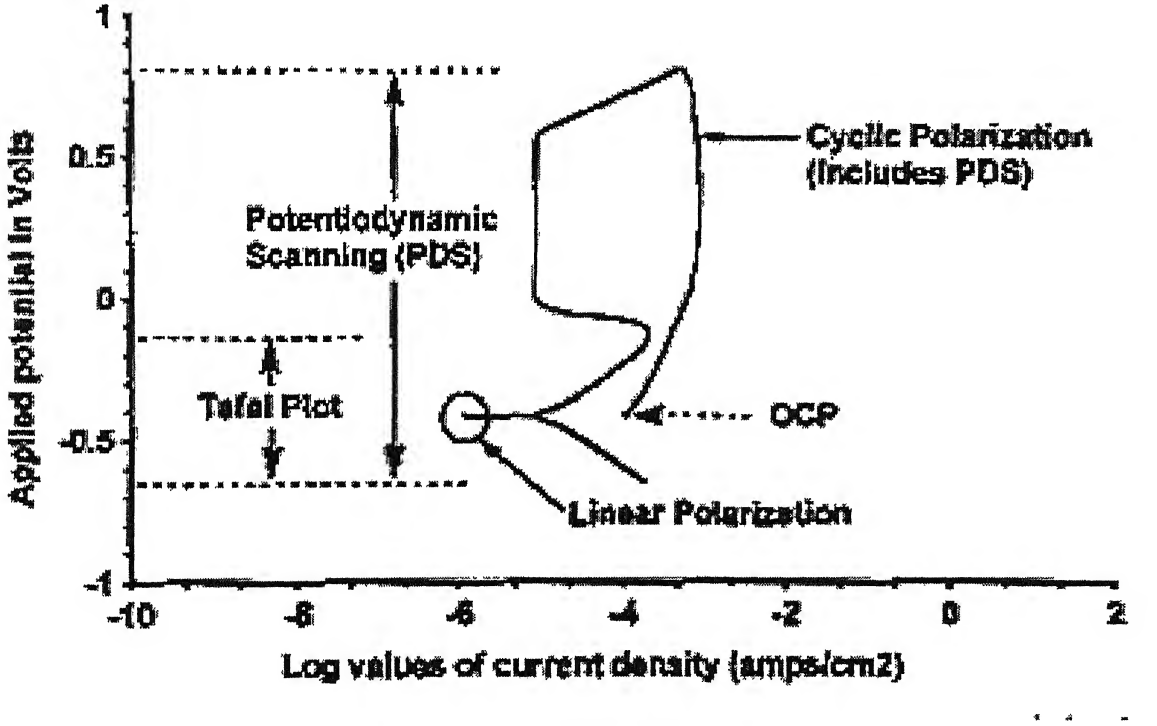

Figure 12: Various types of polarization methods.

The various polarization techniques that are commonly used are linear polarization, Tafel extrapolation, potentiostatic polarization and cyclic polarization. These four polarization techniques are summarized in the Figure 12.

Linear Polarization

The linear polarization uses the smallest potential spectrum of all the polarization techniques. Linear polarization is measured at approximately ±20 mV from the open current potential. Consequently it allows repeated measurements on the same electrode, enabling it to be used for long term corrosion monitoring and for determining the steady state corrosion rate [125]. A typical linear polarization curve is shown in the Figure 13. The slope of the polarization curve gives the polarization resistance, R_p. From the value of R_p the i_{corr} value is calculated using the formula,

$$i_{corr} = [1/(2.303R_p)]\ [(\beta_a\beta_c)/\ (\beta_a + \beta_c)] \qquad (11)$$

where $R_p = (\Delta E/\Delta i)$, the slope of the curve.

The corrosion rate is directly proportional to the corrosion current and can be converted into corrosion rate using the formula,

$$\text{Corrosion rate in mil/year (MPY)} = i_{corr}\ (\Lambda)\ (1/\rho)\ (\varepsilon) \qquad (12)$$

where, $\Lambda=1.2866X10^5$ [equivalents.sec.mils]/[columbs.cm.years]
ρ is the metal density in g/cm^3 and ε is the equivalent weight. There are various assumptions made in the equation (12) which are listed below,

1. The reactions of the systems are reversible.
2. The corrosion reaction is controlled by the activation energy.
3. There is no change on the electrode surface during polarization.
4. Polarization is due to corrosion.

The energy barriers for the forward and reverse reactions are symmetrical.

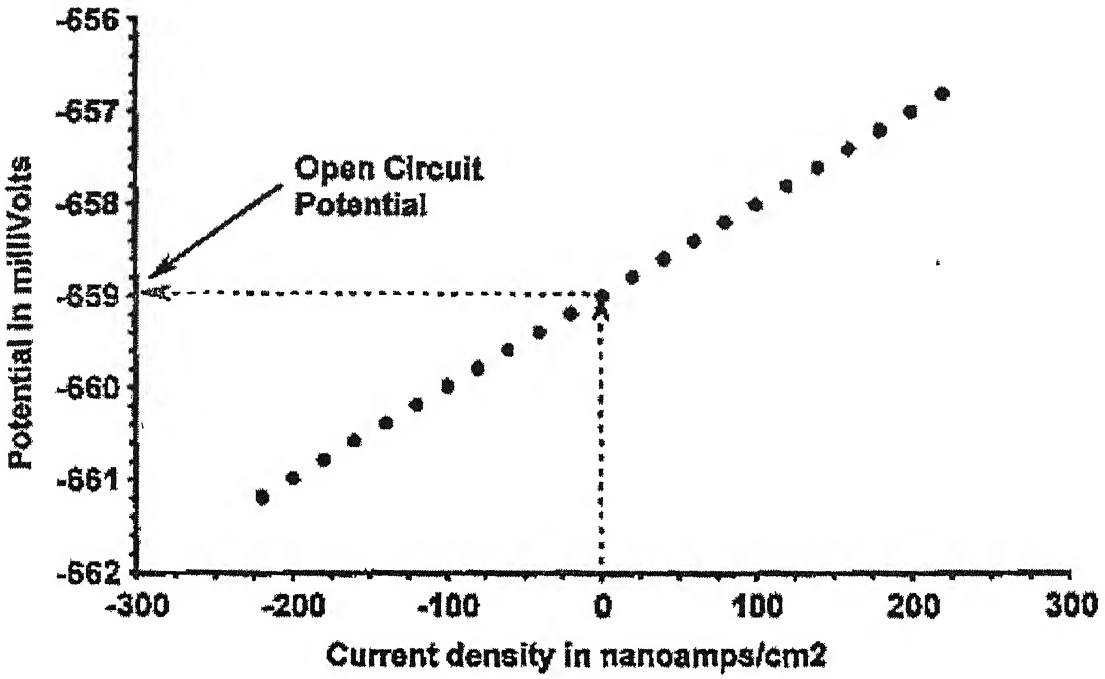

Figure 13: Schematic diagram of a linear polarization plot.

The linear polarization suffers from a lot of limitations. It is difficult to obtain linear data in high resistance solutions or when the metals having extremely low corrosion rates and if localized corrosion such as pitting or crevice corrosion is present. This method cannot determine the type of kinetics that controls the corrosion rate.

The main advantage of linear polarization method is that it is a non-destructive test and can be repeatedly used on the same test electrode, to continuously monitor corrosion fro long times. The other DC methods damage test electrode surface to the extent that measurements can either only be repeated a limited number of times on a test electrode because polarization causes test electrode surface roughening (Tafel plots); or only one measurement can be made on a test electrode because polarization induces pitting (cyclic polarization and potentiodynamic scanning). However, the other methods provide information that linear polarization does not provide about localized corrosion and corrosion mechanisms.

Linear polarization can be used to determine when a test electrode is at its steady state rate so that another DC measurement (e.g., cyclic polarization) can be made at steady state [126].

Tafel Extrapolation

The Tafel extrapolation method was introduced to illustrate the application of mixed potential theory. The Tafel extrapolation method uses a wider potential spectrum than linear polarization and hence provides more information. The linear polarization plot provides information about the corrosion rate, whereas the Tafel plot provides information about the corrosion rate as well as the kinetic data. The Tafel plot is carried out normally in a potential range of ±250mV from FCP. An idealized Tafel plot is shown in the Figure 14. The figure shows distinct anodic and cathodic polarization regions and the inflection point of the two curves gives the FCP. The linear region in the graph is extrapolated and the slopes of the linear regions are calculated. These are called as Tafel slopes. The linearity over which the Tafel slopes are calculated should have one decade of magnitude. A vertical line is drawn from the infliction point to the X-axis to give the corrosion current (Figure 15). From the value of corrosion current the rate of corrosion can be calculated using equation 12. In certain cases, where dilute solutions are used, concentration polarization and ohmic resistance effects are likely at higher current densities. In such cases, Tafel extrapolation is carried out only in the cathodic region. The cathodic polarization slope is extrapolated and is allowed to intersect the corrosion potential E_{corr}. From this inflection point the corrosion current is calculated [116].

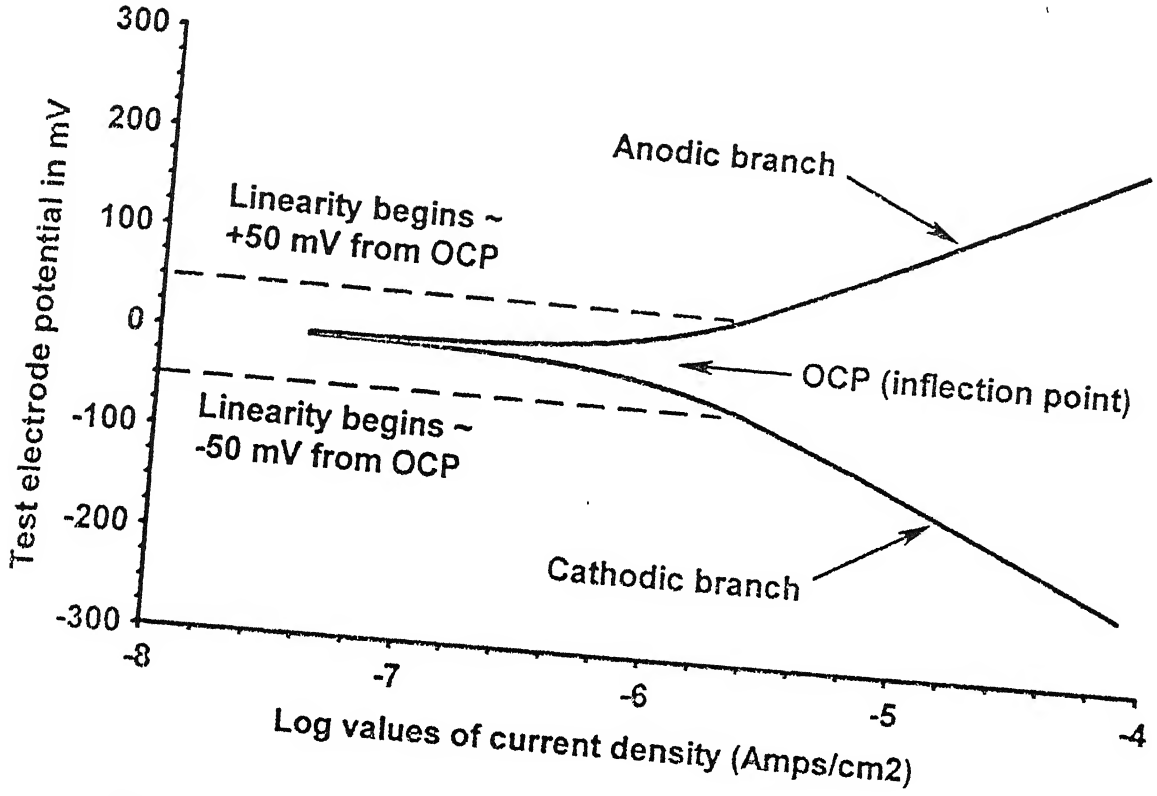

Figure 14: Tafel plot for activation controlled corrosion rates.

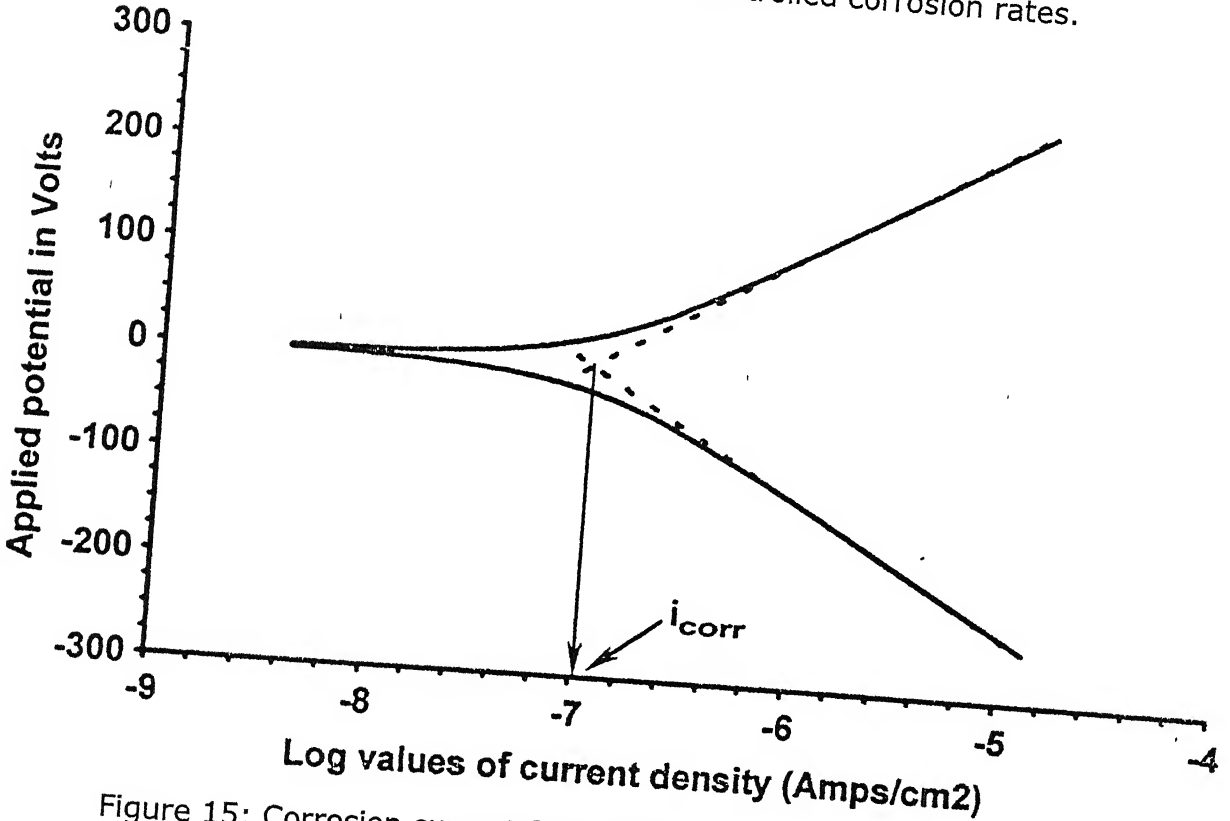

Figure 15: Corrosion current from activation controlled Tafel plots.

The main limitation of Tafel extrapolation when compared with the linear polarization is that the test electrode can be polarized only for a limited number of times. This is due to the surface roughening that takes place with each polarization. Moreover the Tafel plot cannot predict about the passive behavior of the system studied. It cannot be used for studying the localized corrosion behavior of the system [127].

Tafel slopes have units of Volts per current-density-decade, where a decade is one order of magnitude current density, such as from 0.10 amp/cm^2 to 1.0 amp/cm^2 in Figure 16.

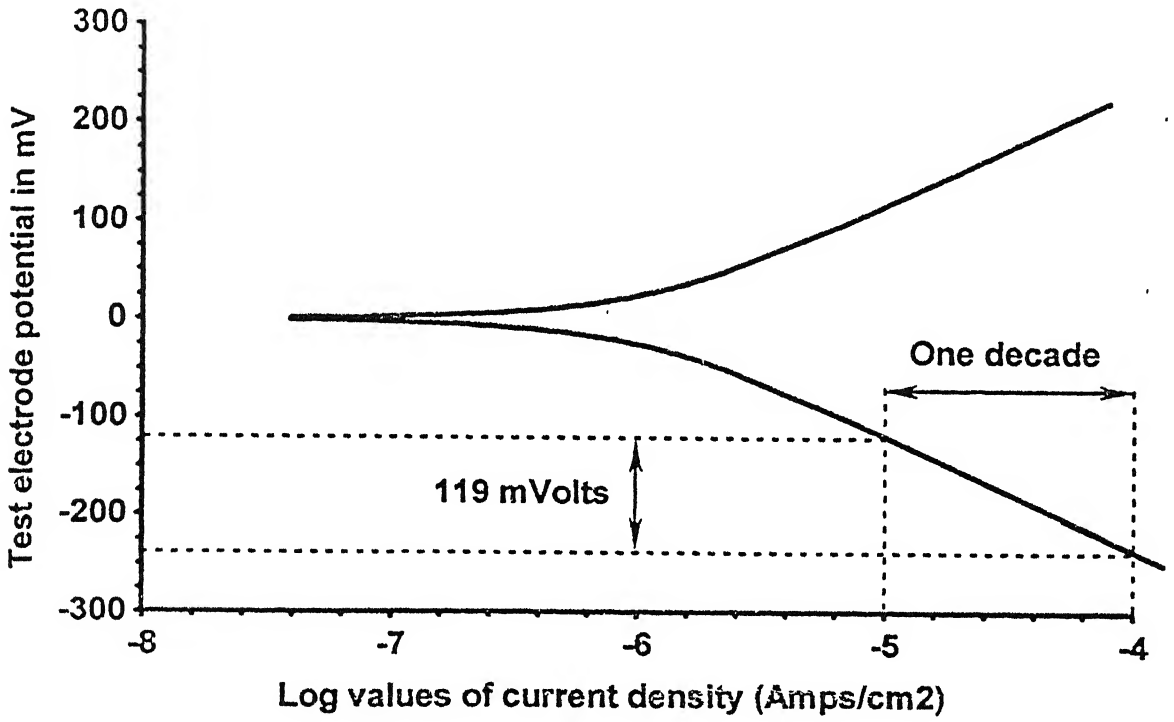

Figure 16: Determining Tafel slopes from Tafel plots.

Potentiodynamic Polarization

The corrosion rates can also be determined from the potentiodynamic polarization curves using the Tafel extrapolation method [128]. The potentiodynamic polarization is carried out in a wider range of potential spectrum of −250 mV to +1600 mV from FCP and gives much more details about the sample's response to the environment. The potentiodynamic

polarization provides data about the metal behavior i.e., whether the metal is active or passive or active passive in the given environment. The plot elucidates the properties of the passive film and the effect of inhibitors on the corrosion behavior of the metal. Depending upon the nature of potentiodynamic polarization curve, alloys can be divided into active alloys and active-passive alloys. For an active metal the corrosion rate increases linearly with increase in the anodic polarization potential. This is due to the non-protective oxide layer, which forms on the metal surface. For an active passive metal the corrosion rate increases with polarization potential up to a critical current density after which it falls down rapidly due to the formation of a protective passive film (Figure 17) [125].

The potentiodynamic polarization curve can be used for a quick evaluation of the material for application in a certain environment. The schematic diagram in Figure 18 shows the selection criterion of an alloy depending upon the nature of the environment. The figure shows four types of alloys and cathodic reactions corresponding to three environments. For a reducing atmosphere, as in 1, either the non-passivating alloy or the partially passivating alloy B is superior because they have better corrosion resistance in the active conditions. The alloys C and D produce strong passivity and hence alloying elements like chromium should be added. This makes the alloys more expensive and thus unjustifiable for the service condition [116]. For a moderately oxidizing atmosphere, number 2, the alloy C would be recommended because the reduction curve exceeds the critical current density and it is the only alloy showing stable passivity. In alloy B, the reduction curve exceeds critical current density, but the passive region is not broad enough to ensure good passive resistance. Alloy D is in a state of borderline passivity, with both active and passive states possible. For strong oxidizing condition in 3, alloy D is recommended as the reduction curve exceeds critical current density and the corrosion rate is low. In alloy C, the passivity breaks in this condition and it is in the transpassive region. Alloys A and B are not resistant to high oxidizing conditions.

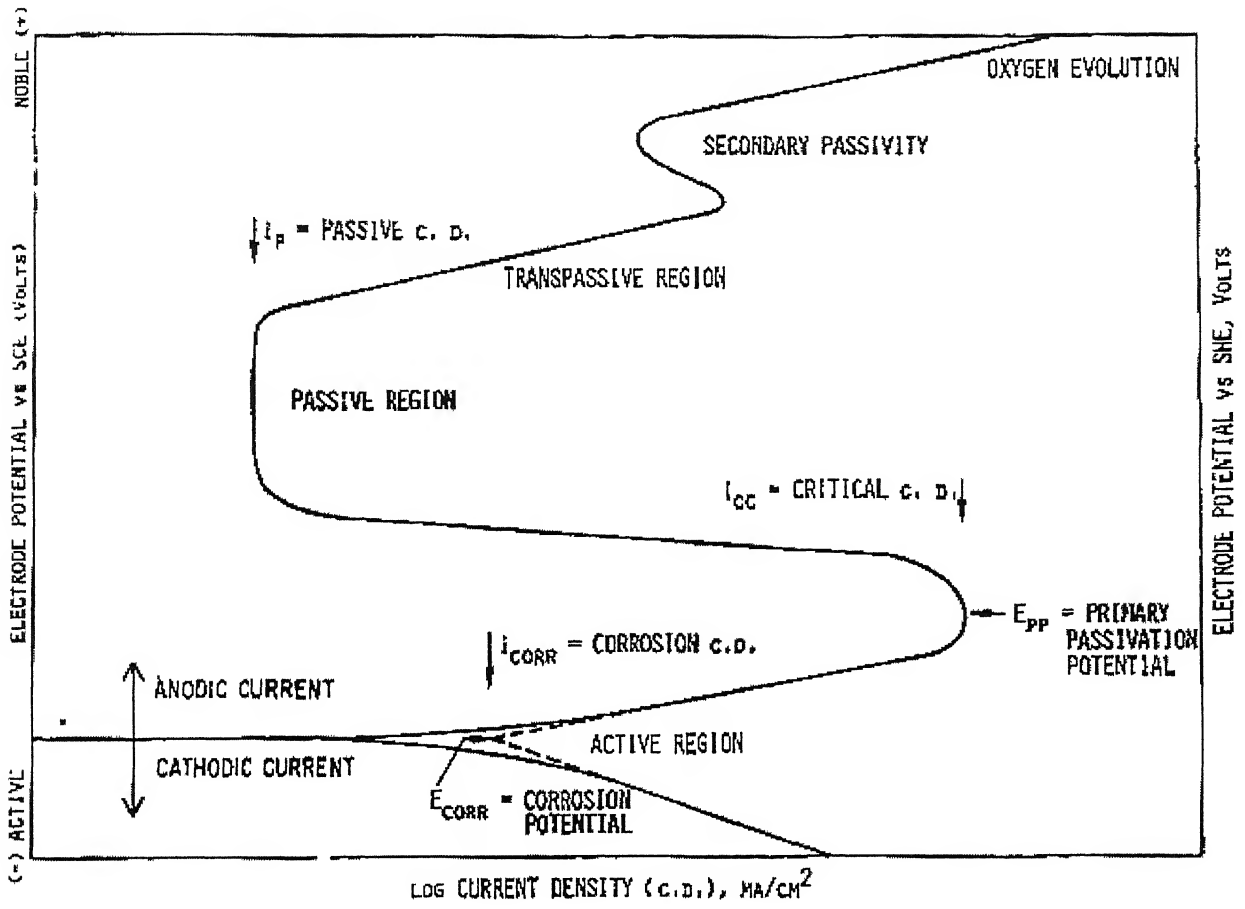

Figure 17: Potentiodynamic polarization plot for active-passive metal.

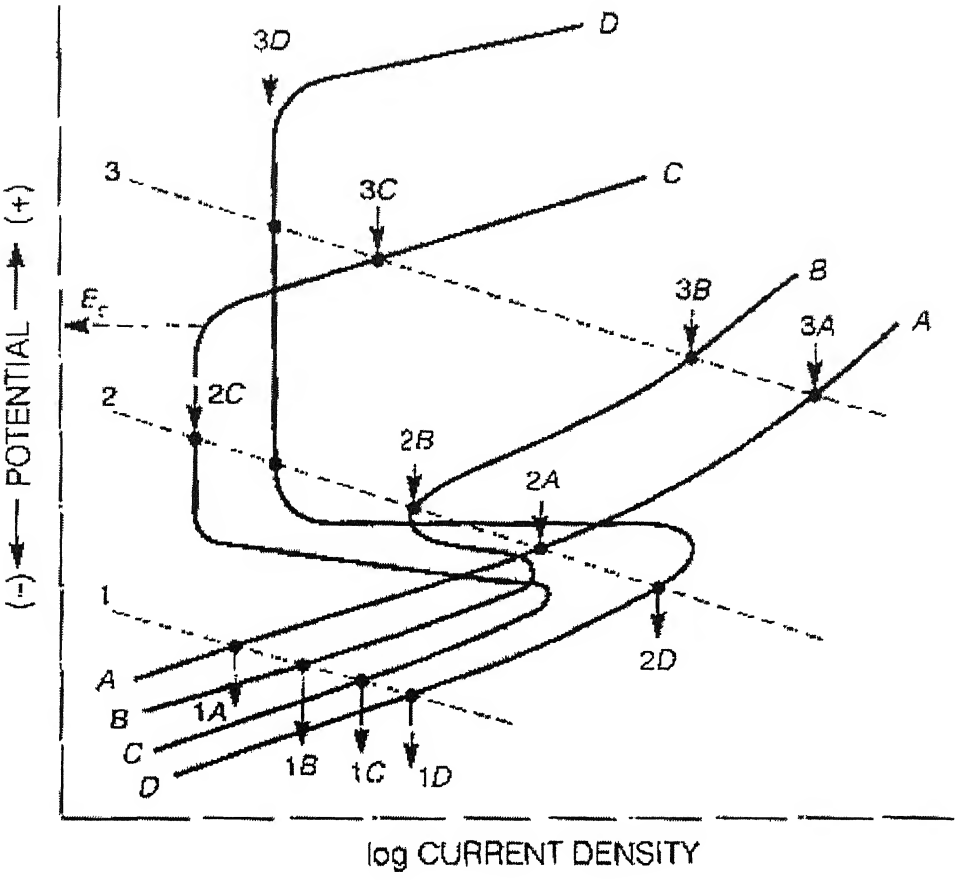

Figure 18: Schematic polarization diagrams illustrating the selection of alloy depending upon the nature of the environment.

The main limitation of potentiodynamic polarization that the sample surface gets disturbed after the experiment is completed. Hence the test can be conducted only once at a time. Moreover the exact corrosion rate cannot be predicted accurately by this method.

2.4 Tribological behavior of Titanium alloys

Although many investigations are reported in literature about the corrosion resistance of Ti-based alloys, the detailed tribological study of these important biometallic alloys in simulated body fluid solution is limited. In particular, no study according to the present literature survey has been undertaken to investigate the friction and wear behavior of titanium-based

alloys in simulated body fluid environment to assess its potential as an implant material. The reported tribological results with Ti-based alloys are summarized as follows.

Bundinski [136] investigated the fretting wear resistance of commercially pure titanium and age hardenable Ti-6Al-4V alloys using a reciprocatory pin on plate wear tester. In the fretting test a number of counterbody materials, e.g. WC-Co, Stellite, 17-4 stainless steel, 316 stainless steel including CP titanium are used. Self mated titanium shows the highest wear damage, whereas Ti-6Al-4V experiences less wear damage against stellite. The investigation revealed that both CP titanium and Ti-6Al-4V alloys have lower abrasive wear resistance than 300 series stainless steel. In the investigated materials, material transfer and plastic deformation were identified as predominant wear mechanism under unlubricated sliding conditions.

Mercer and Hutchings [139] reported the friction and wear behavior of CP titanium and Ti-6Al-4V against alumina in different testing environment (air, argon, N_2, O_2). A pin on disc wear tester was used and testing parameters include a normal load of 1.96N and a sliding speed of 0.63 m/sec and test duration of 1 hour. A steady state coefficient of friction of about 0.6 is measured during the wear testing of Ti-6Al-4V under all the gases. This friction value is also the characteristic of the sliding of the self-mated titanium. The analysis of reported wear data revealed that wear loss of Ti-6Al-4V is highest in O_2 atmosphere and lowest in inert atmosphere (argon). The major wear mechanism in different atmosphere is identified as abrasion. The extensive formation of a non-protective TiO_2 layer in pure oxygen atmosphere is reported to be the major cause for high wear rate.

Chapter 3

EXPERIMENTAL PROCEDURE

3.1 Materials

The materials used in the present investigation were (all compositions are in weight %):

- **Commercial Pure Titanium**
- **Ti-15Al**
- **Ti-5Al-2.5Fe**
- **Ti-6Al-4V**
- **Ti-6Al-4Fe**
- **Ti-6Al-4Nb**
- **Ti-13.4Al-29Nb**
- **Ti-13Nb-13Zr**
- **316L Stainless Steel**

The titanium alloys (CP Titanium, Ti-15Al, Ti-5Al-2.5Fe, Ti-6Al-4V, Ti-6Al-4Fe, Ti-6Al-4Nb, Ti-13.4Al-29Nb, and Ti-13Nb-13Zr) used in present study were obtained from Defense Metallurgical Research Laboratory (DMRL), Hyderabad, India. The 316L stainless steel was obtained from Salem Steel Plant and its composition (weight %) was Cr-17.64%, Ni-11.13%, Mo-2.58%, Mn-1.68%, Si-0.23%, P-0.025%, C-0.020%, S-0.002% and rest iron. The compositions of the alloys (as received) mentioned above are in weight % and they are nominal compositions provided by the supplier. All the titanium alloys except Ti-6Al-4V, 316L and CP Titanium were received in pancake form. Ti-6Al-4V, CP titanium and 316L were obtained in rolled sheet form. Dimensions of CP titanium sheet were 20 cm × 20 cm and thickness 1cm. 316L sheet was of dimension 20 cm × 20 cm and 0.5 cm thickness. The dimension of Ti-6Al-4V was 10cm × 10cm and 1cm thickness.

3.2 Sample Preparation

Specimens for electrochemical studies were cut from the samples using a diamond cutter (Buehler-ISOMET). The areas to be exposed for studies were in the form a square shape of 1 cm x 1 cm and thickness 0.5 cm. The schematic of the Figure 19 shows how the samples were obtained for the electrochemical study. The samples from the pancake were cut from the portion towards the center and top surface was mounted for the experimental study as shown in the Figure 19. In case of rolled sheet, the long transverse direction was mounted and samples were taken from the edge of the sheet. A covered wire lead was attached to the back of the specimen by soldering with the help of a small amount of conducting paste. Following this, each specimen was cold mounted into a thermosetting liquid and powder in the form of a 3 cm. diameter rod and height of about 3 cm. The time duration taken by the mixture of thermosetting liquid and powder to dry and harden was two hours. Cold mounted specimen was then polished up to 4/0 finish on emery paper and then polished using 0.5μ alumina powder. The specimens were than washed with distilled water followed by ultrasonic cleaning with acetone.

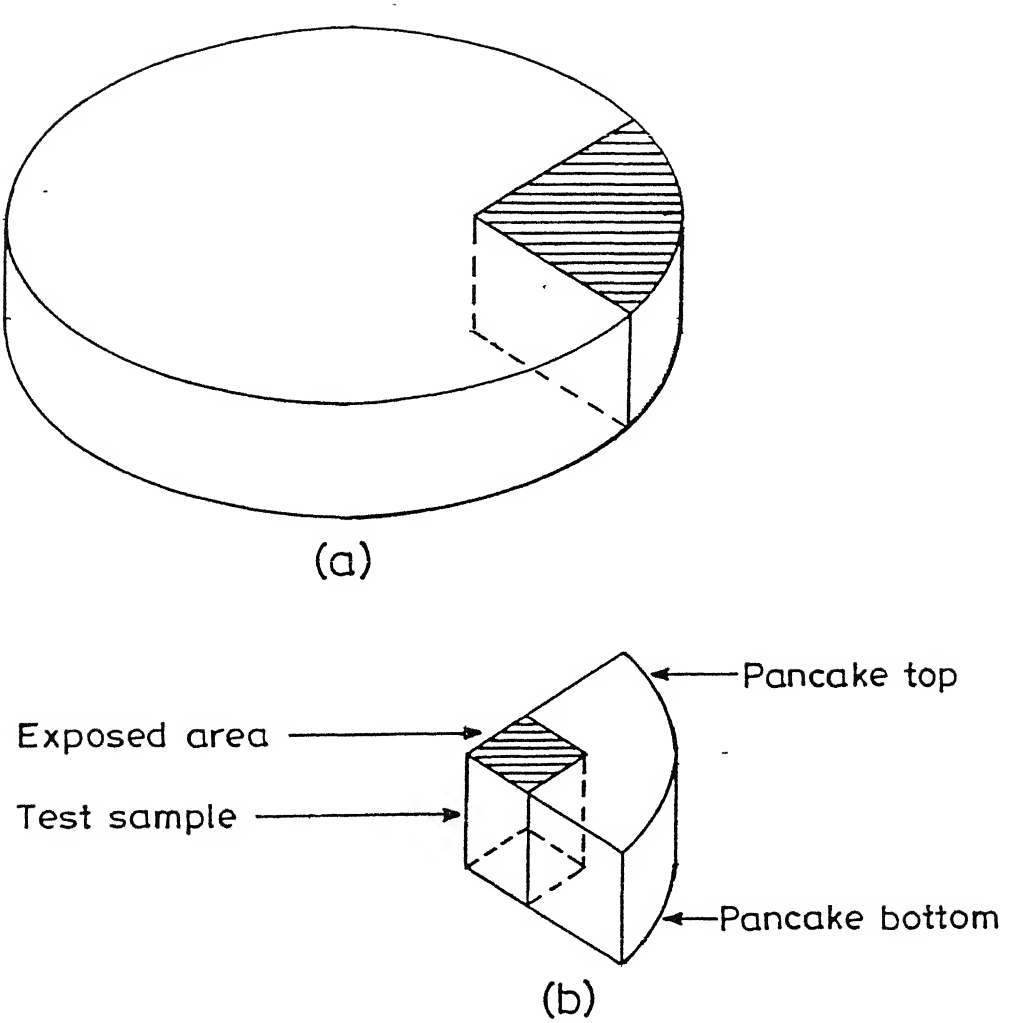

Figure 19: Basic diagram showing (a) Pancake, and (b) cut samples from the Pancake for Electrochemical and Tribological study.

3.3 Electrochemical Studies

The electrochemical studies on the specimens were carried out in a potentiostat, Model 263A supplied by EG&G Instruments Inc., Princeton Applied Research, USA. It possessed a very high range of sensitivity from 100 μA to 1A. The electrolyte used for testing was Hank's solution, prepared in the laboratory from laboratory grade chemicals. The basic diagram of a potentiostat connected with the working cell is shown in Figure 20. The potentiostat is basically composed up of an ammeter, an electrometer and a power supply. There were four probes from the potentiostat plugin, which are connected to the working electrode, reference electrode and counter electrode. The fourth probe was grounded. The working cells for the potentiostat are of two types, the flat cell or the round cell. The flat cell can be used for testing flat samples and can only be used when the surface of the sample is flat. The round cell can be used for any sample and usually the samples are mounted before using in the round cell. The round bottom cell was used in the current investigation.

The schematic representation of the round bottom cell is shown in Figure 21. Graphite was used as the counter electrode. The potential of the working electrode was measured against saturated calomel electrode (SCE), inserted into the salt bridge, whose other end was placed close to the working electrode. The potential of the reference SCE was +242 mV with respect to standard hydrogen electrode (SHE). The samples that were used in this cell were usually mounted to expose only a specific surface area (1 cm^2) of the sample to the corrosive medium. The polarization experiments in this investigation were conducted using mounted samples in the round cell and this cell was placed over a heating mantle having a temperature control attachment so as to maintain a constant temperature of 37°C (human body temperature) during the experimental procedure.

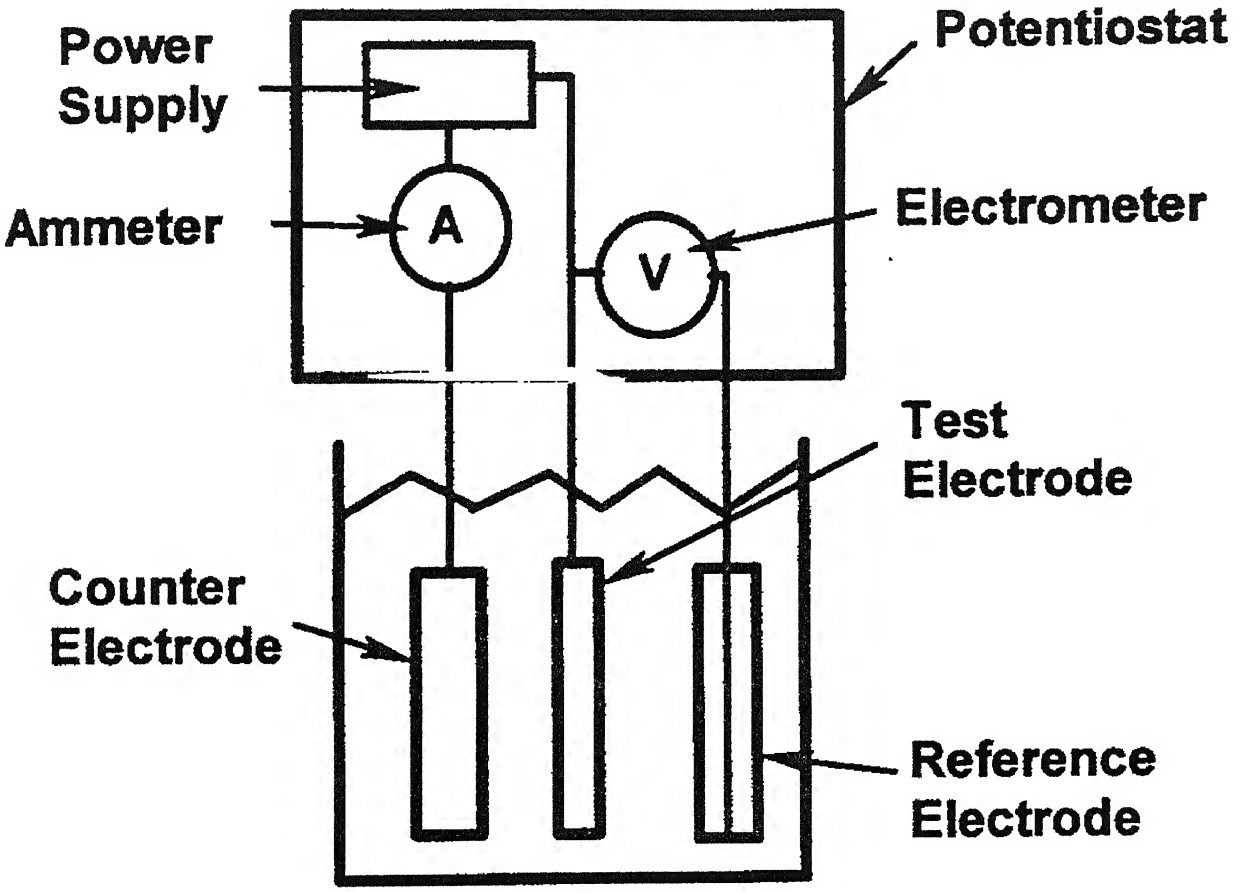

Figure 20: The basic diagram of a potentiostat connected with the working cell.

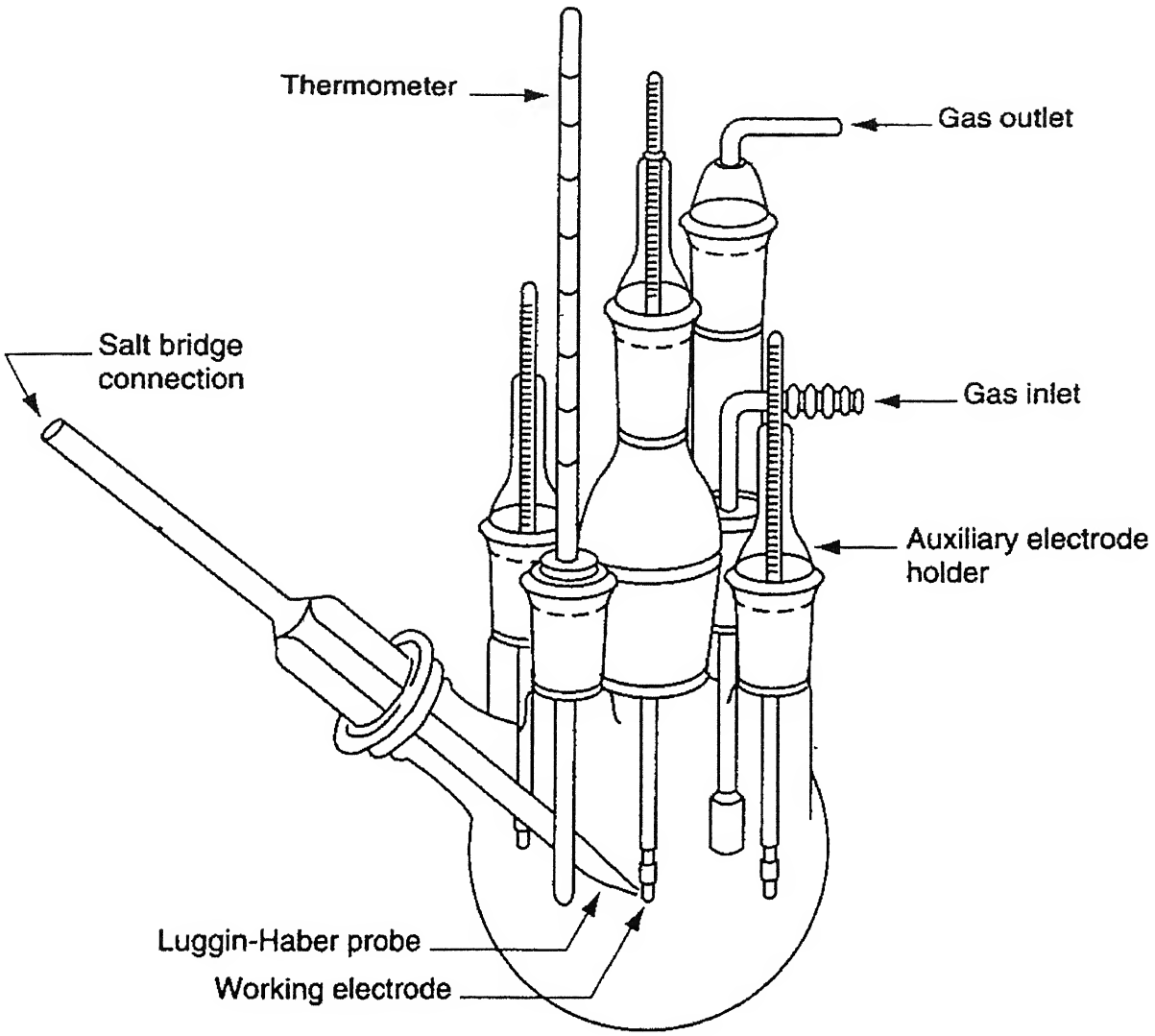

Figure 21: Schematic representation of round bottom Cell.

Electrochemical behavior of the materials were tested by using electrochemical techniques in Hank's solution of pH 7.4, known to simulate body fluid environment, at 37°C (98.4°F), which is equivalent to human body temperature. The accuracy of temperature maintained in present investigation was +2°C. Temperature control for the E_{corr} stabilization and Tafel experiments was relatively easy as compared to potentiodynamic polarization experiments because the experiment run time taken was shorter. These experiments were started at 39°C and after completion of the experiment the temperature observed was between 37°C to 38°C. For potentiodynamic polarization, the temperature was increased up to 39°C and power for the heating mantle was switched off, and after the temperature touched 37°C during the course of the experiment, the experiment was kept at hold for about 2 minutes and power for heating mantle was again switched on so as to increase the temperature by 1°C. Temperature of the cell was monitored using a thermometer. The power for the heating mantle was switched off before starting all electrochemical experiments so as to avoid interference and noise in the data because of the electric field of the mantle.

3.3.1 Solution Preparation

The composition of Hank's solution chosen for the electrochemical and tribological study is provided in Table 5. The medium used for preparation of the body fluid solution (Hank's solution) was double distilled water. In order to achieve full dissolution of the chemicals in the medium, addition of NaCl, KCl, $CaCl_2$, $NaH_2PO_4.2H_2O$ and $NaHCO_3$ was taken after the other chemicals ($MgSO_4.7H_2O$, Glucose, KH_2PO_4 and $MgCl_2.6H_2O$) were completely dissolved. Continuous stirring with the help of magnetic stirrer (Remi 2 LH) aided dissolution. A slight temperature of about 30°C was also applied, in case of any residual chemicals were observed at the bottom of the flask. The pH of the solution was precisely maintained at 7.4 and strictly checked every time after the solution preparation using a pH meter (Ecoscan, Eutech

Instruments, Singapore). Freshly prepared Hank's solution was used for each experiment.

3.3.2 Tafel Extrapolation

The Tafel extrapolation experiments were carried on from ± 250 mV from free corrosion potential (FCP), that is E_{corr}. The FCP was stabilized before conducting each Tafel experiment. The scan rate used for Tafel experiments was 0.166 mV/s, as per ASTM standard [129]. The linear portion of the cathodic polarization line was extrapolated to meet the horizontal line drawn from zero current potential value, and from the point of intersection of the two lines the anodic slope was extrapolated. The corrosion rate was also obtained by this method. This methodology was adopted as the alloy exhibited stable passive behavior, and therefore well-defined Tafel slopes were not observed in anodic Tafel plot. The anodic slopes obtained for the alloys were very high due to the stable passive nature. The slopes β_a, β_c, and i_{corr} were calculated using the Tafel curves obtained. Duplicate tests were performed and in some cases, triplicate experiments were performed, especially if the duplicate result was markedly different from the original result.

3.3.3 Potentiodynamic Polarization

The potentiodynamic polarization experiments were carried out in the potential range of −700 mV to +1600 mV for all the samples after stabilizing E_{corr}. E_{corr} was stabilized prior to all experiments. The potentiodynamic polarization experiments were also carried out at a scan rate of 0.166 mV/s. The passivation parameters like breakdown potential (E_b), passivation current (i_{pass}) and passivation range (E_b-ZCP) was estimated from the potentiodynamic polarization curves. Duplicate tests were performed.

3.4 Microstructural Characterization

The specimen surfaces used in the polarization study, was microstructurally characterized after electrochemical testing. The surface of the mounted specimens was polished with 2/0, 3/0 and 4/0 emery papers and then mechanically wheel polished in fine cloth using 0.5μ alumina powder. They were then degreased using acetone before etching. The etching was done by immersing the samples in 10% HF and 5% HNO_3 (rest distilled water) etching reagent for 5 to 10 seconds at room temperature. The etching time and amount of etchant needed was different for all the samples. Etching of the samples could not be done in a single step. A slight variation in etchings time of about 2-3 seconds caused over etching of samples and samples had to be prepared again for etching. In the special cases for Ti-6Al-4V, Ti-13.4Al-29Nb and Ti-15Al, the etchant had to be diluted with the addition of few drops of doubled distilled water, and this solution provided better etching of these samples.

The microstructures were recorded using an optical microscope (Axiolab A, Zeiss, Germany), attached with a digital camera (CE, Japan). They were later analyzed in an image-analysis program (Image-Pro Plus, version 4.1, Media Cybernetics, USA). In order to calculate the volume fraction of the beta phase in titanium alloys, a 23X18 grid was used and the sample was observed at different magnifications of 100X, 200X and 500X. The number of points falling in the feature of interest was calculated manually and divided by the total number of points. The result provided the volume fraction.

3.5 Tribological Tests

The tribological behavior of the biometallic alloys was evaluated using a commercial ball on flat fretting wear tester (DUCOM, Bangalore, India). The details of the equipment are shown in Figure 22a. 'Fretting' is defined as low amplitude reciprocatory tangential sliding. It can be noted that majority of the wear tests of biomaterial combinations are subjected to standard reciprocating motion, similar to real contact conditions prevalent in human body. An inductive displacement transducer monitored the displacement of the flat sample. The friction force was recorded with a piezoelectric transducer attached to the holder that supports the counterbody. The friction coefficient was obtained from the on-line measured tangential force.

The polished CP Titanium, Ti-6Al-4V, Ti-5Al-2.5Fe, Ti-13Nb-13Zr alloys were used as flat (stationary) materials. Ti-6Al-4V was chosen for tribological analysis as it is commercially used as a stem material in total hip joint replacement (THR) assembly. CP titanium was selected as a reference material. Detailed analysis of corrosion results, as presented in Chapter 4, reveals that Ti-5Al-2.5Fe and Ti-13Nb-13Zr has optimum combination of corrosion rate and passivity range, and therefore, these materials were also considered for tribological characterization. The friction and wear behavior of the Ti-based alloys are also compared with that of as-cast Co-28Cr-6Mo alloy (commercial Portasul-2* grade), an important biomaterial used in THR assembly. Here, it can be recalled that the commercial THR assembly consists of a femoral stem made of Ti-based alloy and a femoral head made of Co-28Cr-6Mo alloy.

An 8 mm diameter bearing grade (commercial SAE 52100 grade) steel ball was used as the moving counterbody. The flat samples were provided a 4/0 finish followed by cloth polishing using 0.5μ alumina powder. Prior to the fretting tests, both the flat and ball were ultrasonically cleaned in acetone. The test plate with the sample was placed in the chamber as shown in Figure 22a. The chamber was completely filled with simulated body fluid

solution (Hank's solution). In order to simulate severe wear conditions, all the tests were performed at a high load of 10N. Other parameters include test duration of 10,000 cycles with relative displacement stroke between the flat and ball set to 80 μm and the frequency 10 Hz (see Fig. 22b). This combination of testing parameters resulted in a gross slip fretting contact with a linear sliding speed of 0.0032 m/s. The composition of simulated body fluid i.e. Hank's solution having a measured pH of 7.4, is given in Table 5. The temperature and relative humidity during the wear tests were 37°C and 40% respectively. These parameters were maintained by placing the fretting wear tester in an environmental chamber provided with temperature and humidity control. The accuracy of the temperature and humidity maintained in this investigation was ±1°C and ±5% respectively.

Detailed microstructural characterization of the worn and ultrasonically cleaned flat surfaces was performed (after wear tests) with a Leitz optical microscope and SEM (JEOL JSM-840A). The wear scar diameters (both in the sliding and in transverse directions) were measured in the optical microscope and wear volumes were computed according to the equation proposed by Klaffke [130]. The use of this equation given below, is reported to be justified for the present fretting conditions. It is supposed to provide errors less than 5% when the wear scar diameter is larger than twice the Hertzian contact diameter.

$$W_V = d_1^3 / 8R \left[\prod d_1/8 + 4\delta/3 \right] \qquad (13)$$

were d_1= wear scar diameter normal to the fretting direction

R= radius of the ball

δ= ½ of the stroke

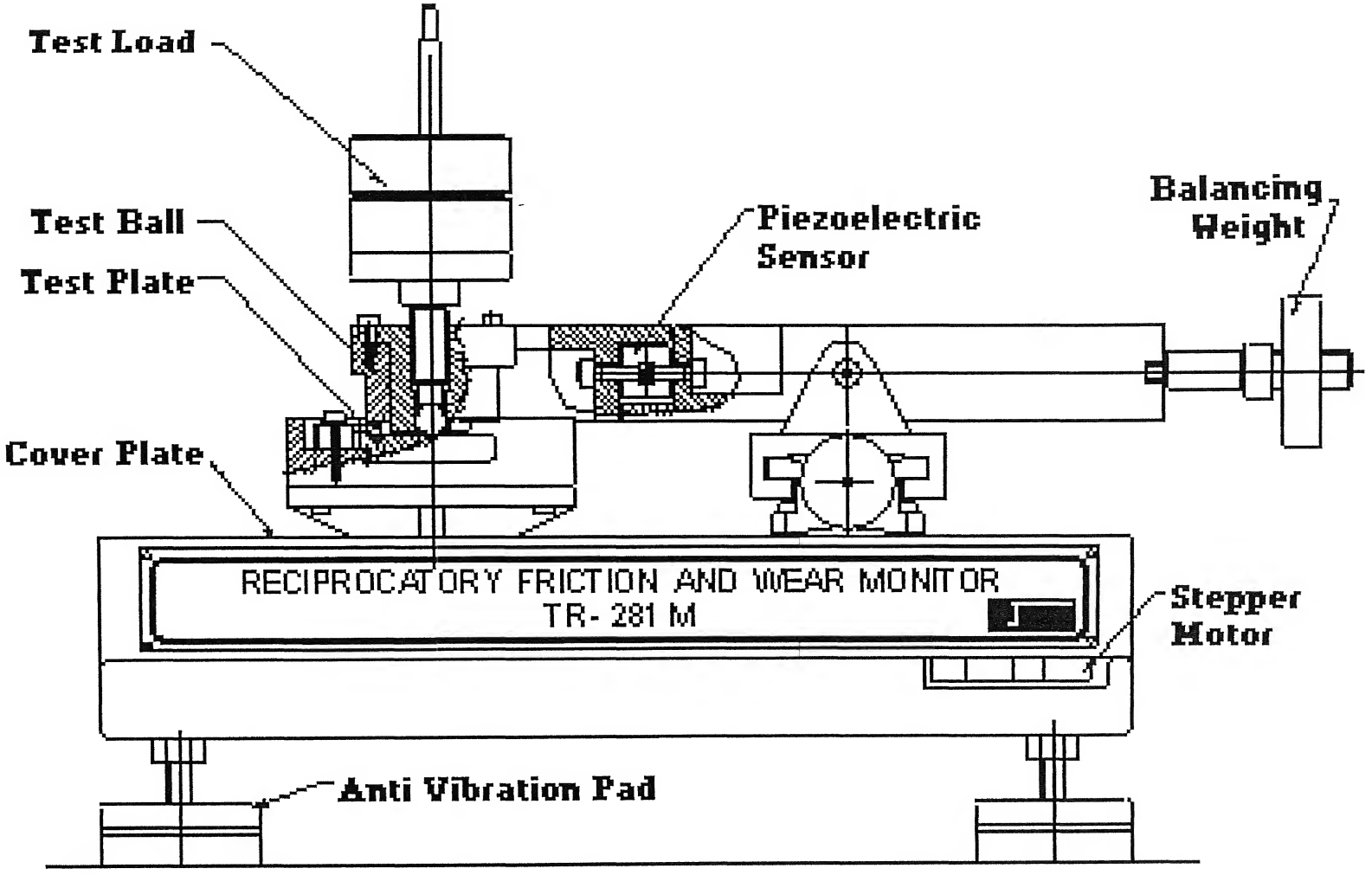

Figure 22 (a): Schematic of the fretting wear tester, manufactured by DUCOM, India.

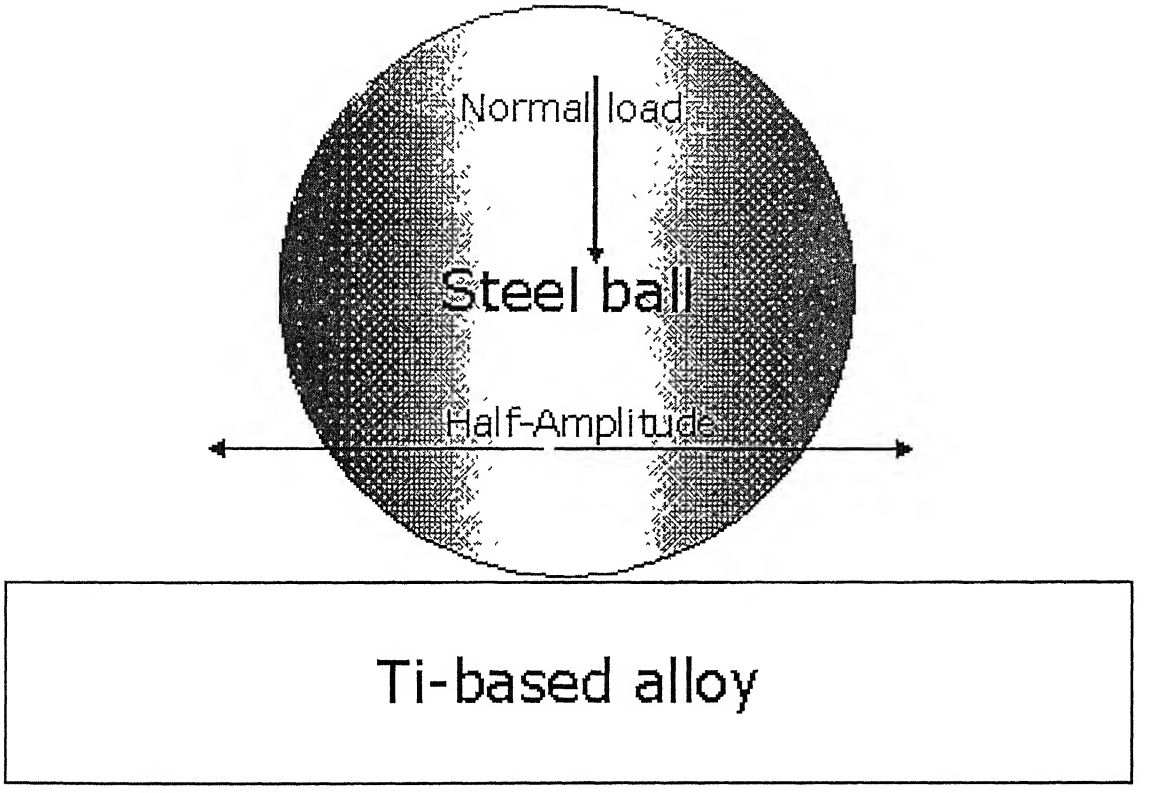

Figure 22 (b): Schematic representation of the fretting of Ti-based alloy against steel.

Chapter 4

RESULTS AND DISCUSSIONS

The results obtained in the present study are first outlined and this is followed by a discussion of the results.

4.1 Potentiodynamic Polarization

Duplicate test results of stabilization of free corrosion potential (E_{corr} vs. time) for all the samples along with their corresponding Tafel and potentiodynamic polarization experiments are provided in Appendix A. All the materials showed almost the same nature of E_{corr} stabilization, typically depicted in Figure 23. The potential moved towards noble potential on immersion and stabilized in a relatively short period of time. However the E_{corr} stabilization for Ti-13Nb-13Zr was different in some experiments compared to other alloys (Figure 24). In this case the free corrosion potential shifted towards the active direction before stabilization. The reason for the observed variation is not known, but it could be related to the nature of surface film that forms on the surface of Ti-13Nb-13Zr. The microstructure of the alloy could also have an effect and this will be discussed in detail later. The experiment for this particular alloy was repeated four times and all these are reported in Appendix A and B.

Potentiodynamic polarization curves for the different Ti-based alloys used in present study are shown in Figure 25 and 26. The nature of polarization curves indicates that the samples passivated immediately on immersion in the solution. The polarization behavior can be termed as stable passivity. This behavior was noted for all the samples. Duplicate test results have been provided in Appendix A. Based on these duplicate tests, the appropriate polarization curves have been used in the discussion in Figure 25 and 26. The passivation parameters like breakdown potential (E_b), passive

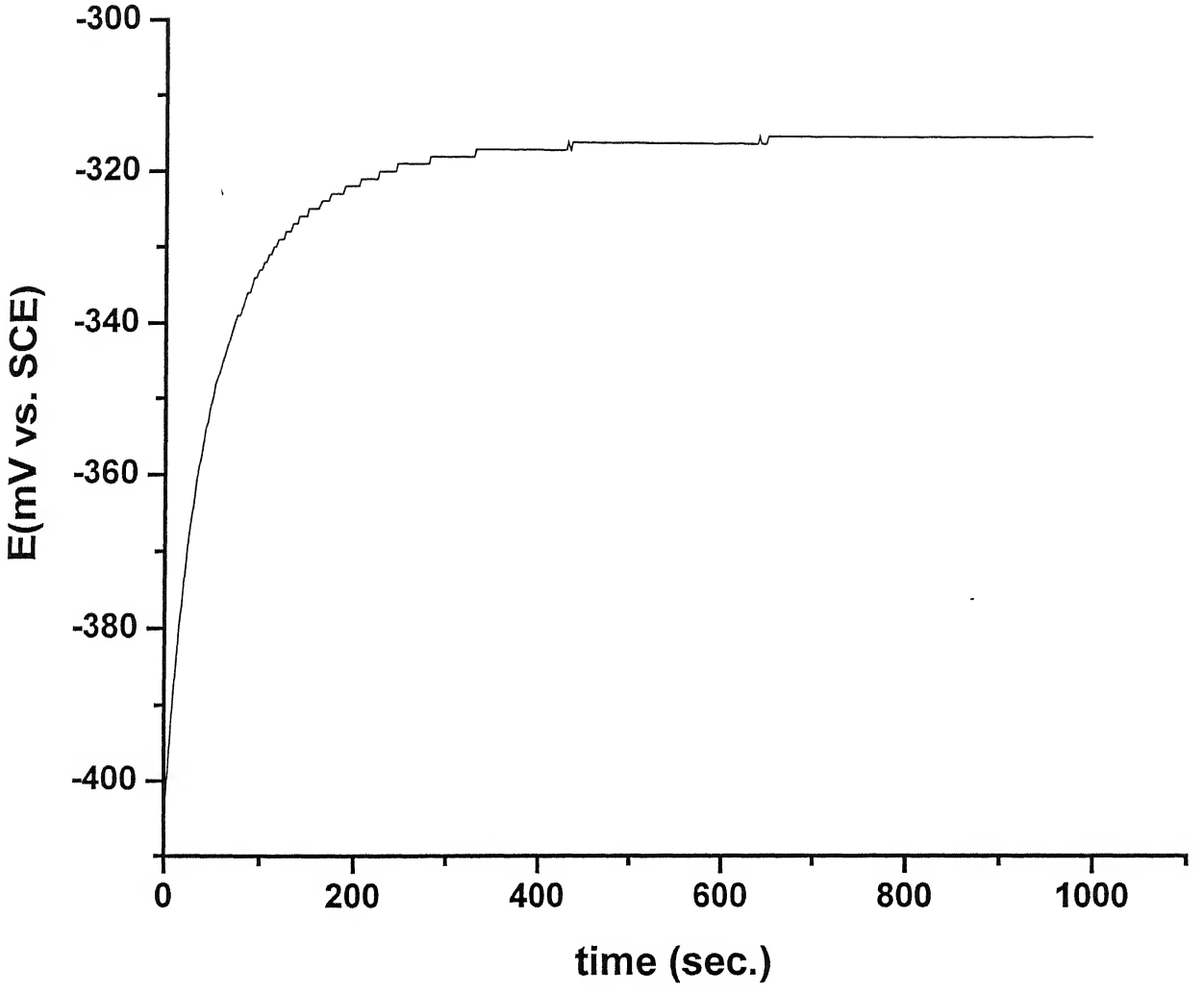

Figure 23: Open circuit potential as function of time for Ti-6Al-4Fe in Hank's solution at 37°C temperature and 7.4 pH.

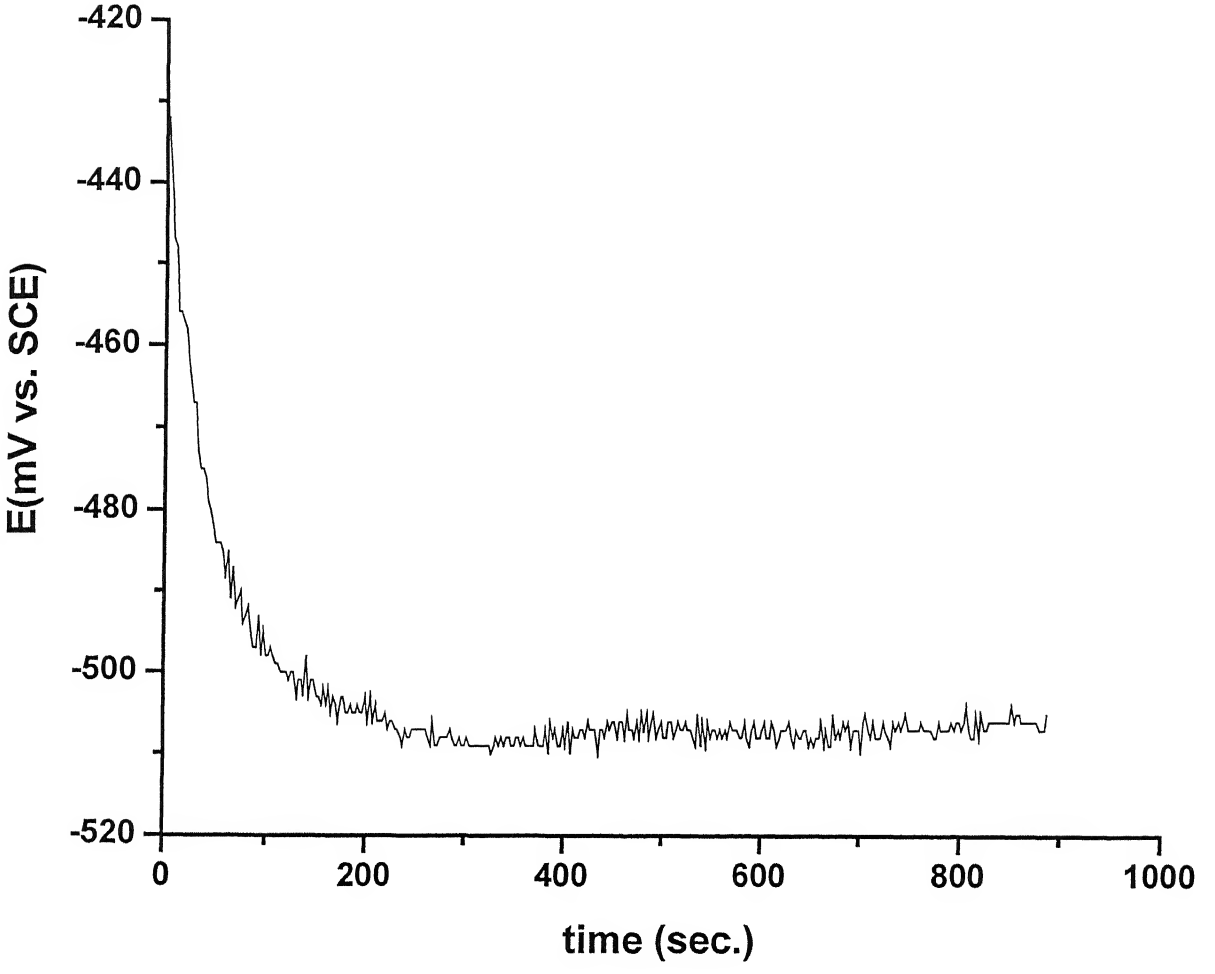

Figure 24: Open circuit potential as function of time for Ti-13Nb-13Zr in Hank's solution at 37°C temperature and 7.4 pH.

current density (i_{pass}) and the passivation range (E_b-ZCP) were estimated from the polarization curves and they are tabulated in Table 9. The passivation parameters from duplicated polarization experiments have been tabulated in Appendix B. The polarization experiment was repeated three times for Ti-13Nb-13Zr (Figure 31 and 32 of Appendix A). In two of these experiments, the free corrosion potential stabilized in the noble direction. The conservative data (i.e. larger i_{pass}) has been reported in Table 9 and Figure 26. This incidentally, corresponds to the condition when the FCP stabilized in the active direction. The zero current potential (ZCP) obtained from the potentiodynamic polarization curves, of all Ti-alloys was in the range of −400 to −650 mV except for Ti-6Al-4Nb which was more noble (−170mV). This can be compared to the ZCP of −281mV for 316L steel.

4.1.1 Passive Current Densities

Passive current densities were obtained from the middle of the straight-line portion of passive region. The passive current densities of the alloys investigated were of the same order of magnitude (1.2 to 6.8 $\mu A/cm^2$). Commercial pure titanium exhibited the highest passive current density of 6.8 $\mu A/cm^2$. Addition of alloying elements like aluminum, niobium, iron, zirconium and vanadium lowered i_{pass}. There was no drastic effect of alloying of 2.5%Fe, 4%V, 4%Fe and 4%Nb on the passive current density. The i_{pass} for Ti-5Al-2.5Fe, Ti-6Al-4V, Ti-6Al-4Fe and Ti-6Al-4Nb was 1.2, 1.5,1.3 and 1.4 $\mu A/cm^2$, respectively. Aluminum addition alone resulted in some decrease in i_{pass}. While the i_{pass} decreased with Al addition, the combined addition of Al with another element (Nb, V and Fe) decreased i_{pass} further (Table 9).

4.1.2 Breakdown Potential

The highest breakdown potential (E_b) of 1290 mV was exhibited by Ti-6Al-4V; E_b values for Ti-5Al-2.5Fe and CP titanium were almost comparable (Table 9). Addition of aluminum in large amount (of 15%) significantly lowered the breakdown potential of Ti. However the addition of

niobium seems to enhance the breakdown potential, increasing E_b value from 750mV (for Ti-15Al) to 979mV (for Ti-13.4Al-29Nb) (Table 9).

On alloying Ti with Al, and additional elements like Nb, Fe and V, the breakdown potential was not significantly affected. Increase in Fe content seems to have lowered the breakdown potential (E_b for Ti-6Al-4Fe is 1170mV). Ti-13Nb-13Zr exhibited a breakdown potential of 1200 mV, which is marginally less than that of Ti-6Al-4V and CP titanium. The lowest breakdown potential was exhibited by 316L steel. This was much lower compared to other Ti alloys. Earlier investigations of 316L stainless steel and Ti-6Al-4V in deaerated simulated body fluid Hank's solution at 37°C have reported an E_b value of 280 mV (vs. SCE) for 316L stainless steel and 1900 mV for Ti-6Al-4V [95]. The comparative results of the present study are reasonable.

4.1.3 Passive Range

The passive range in the case of materials exhibiting stable passive behavior is provided by the difference between breakdown and zero current potentials. The highest passive range was exhibited by CP titanium, and then Ti-5Al-2.5Fe and followed by Ti-13Nb-13Zr (1700mV). Addition of aluminum apparently decreased the passive range considerably, as can be noted from data for Ti-15Al. Niobium addition enhanced the passive range (Table 9) as can be noted from data for Ti-15Al and Ti-13.4Al-29Nb. The passive range for Ti-6Al-4V, Ti-6Al-4Fe and Ti-6Al-4Nb were comparable although the range was lower for Ti-6Al-4Nb. It must be noted that ZCP was at a relatively noble potential for Ti-6Al-4Nb compared to others and could be the reason for the apparent decrease in passive range. The passive range was low in the case of 316L (about 319 mV) as compared to other Ti-alloys, which were in the range of 1300-1890 mV.

The thin oxide film that forms on titanium surface is impervious and quite protective against chloride ion attack. The excellent corrosion resistance of titanium alloys results from the formation of this very stable, continuous, highly adherent, and protective oxide film. Titanium metal is

highly reactive and possesses extremely high affinity for oxygen. Therefore, beneficial surface oxide films form spontaneously and instantly when fresh metal surface is exposed to air or moisture [131]. 316L stainless steel is particularly predisposed to pitting corrosion due to inclusions of a dissimilar material trapped in the metal during a manufacturing process. These impurities may initiate pitting corrosion in relation to a grain boundary and thus can lead to component failure [28]. The addition of a minimum of 2% of molybdenum content in type 316 stainless steel has been shown to reduce the tendency for pitting-type corrosion in chloride environments. In the present study, the stainless steel sample was free of second phase impurities and moreover the alloy was 316L, i.e. containing Mo additions. Therefore, the ease of pitting must be related to the presence of chloride ions in the solution. Hoar and Mears [30] postulated that chloride ions accelerate the corrosion of stainless steel by penetrating the oxide film. The chloride-contaminated film then loses its passivating quality and a local attack on the metal follows, creating a pit.

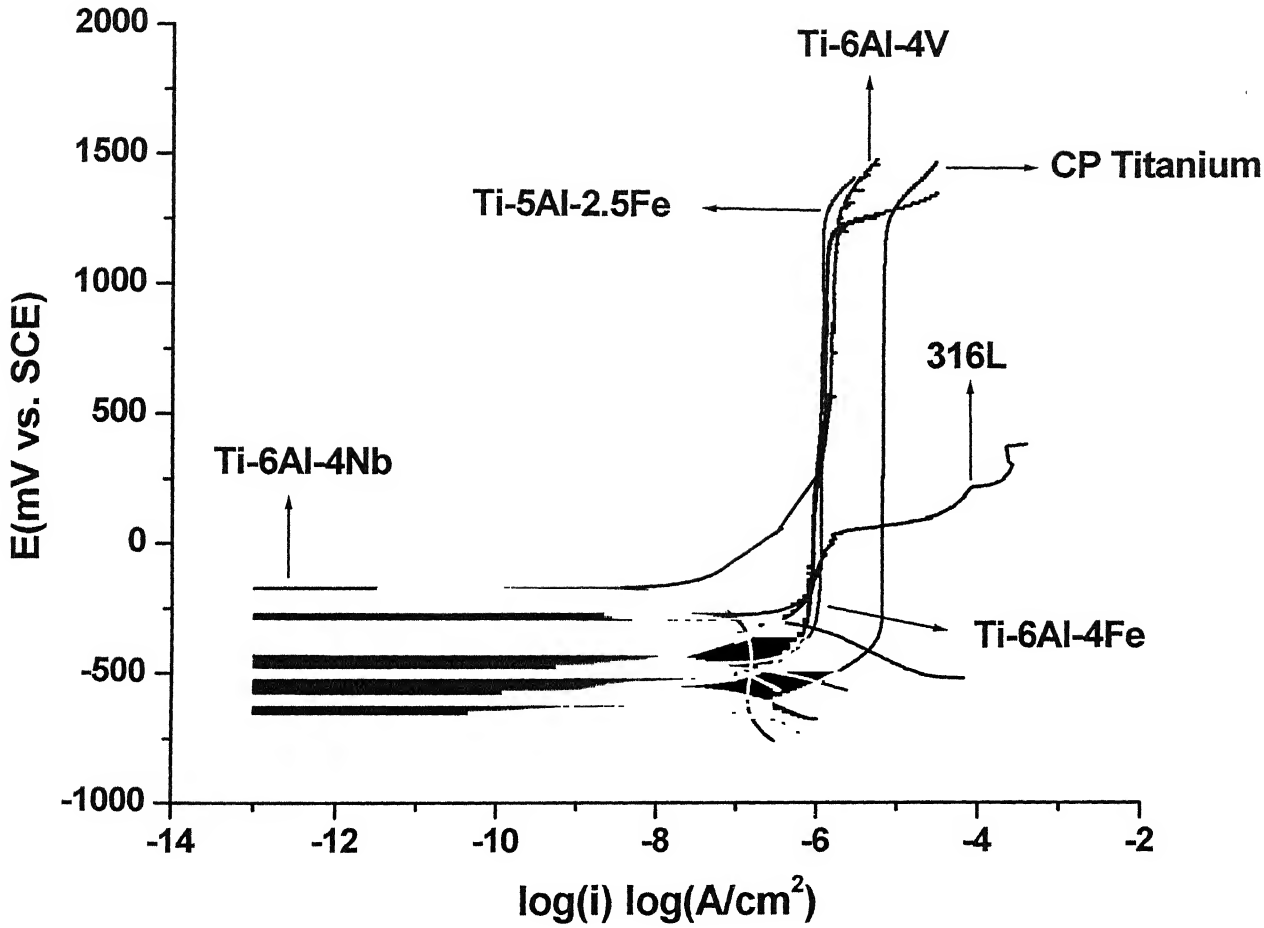

Figure 25: Potentiodynamic polarization curves for one set of samples in Hank's solution at pH 7.4 and 37°C temperature.

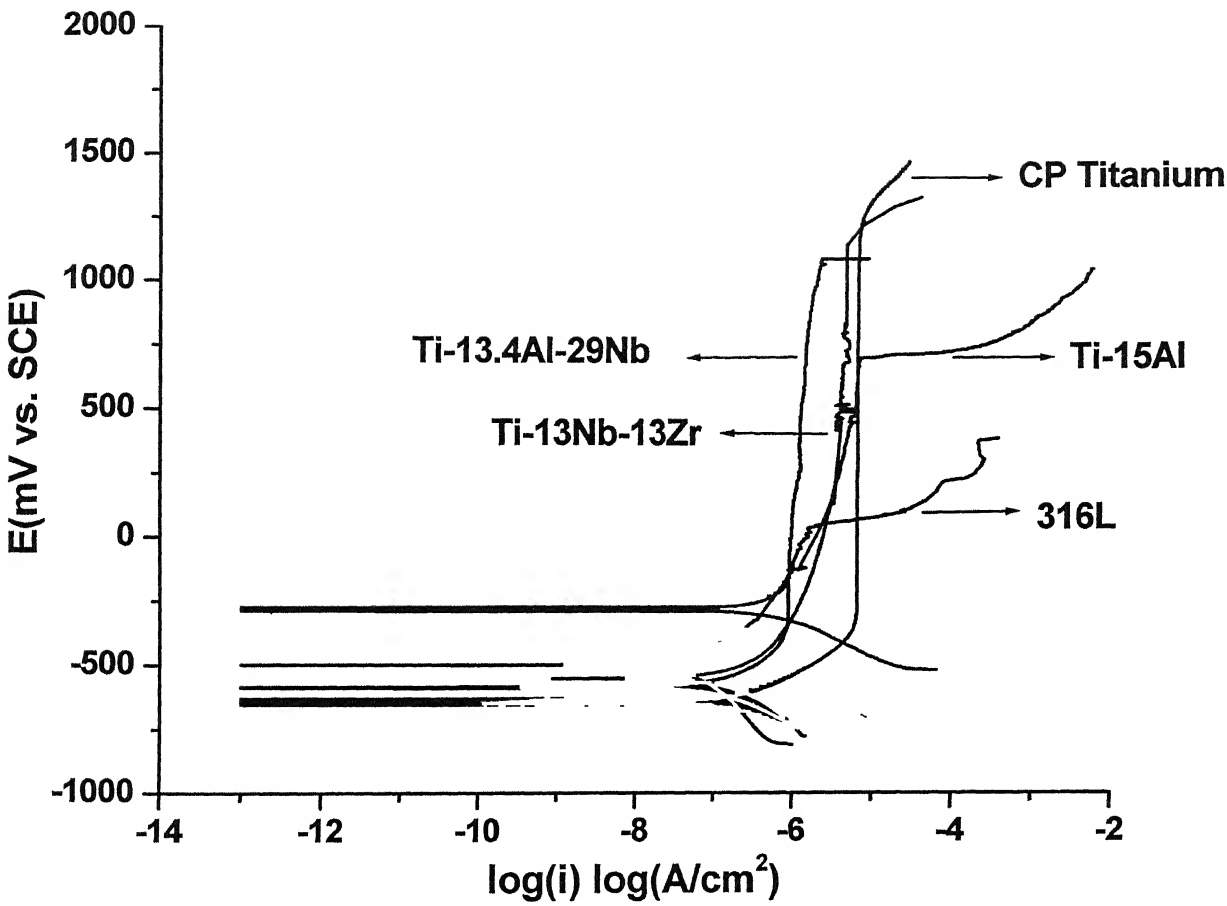

Figure 26: Potentiodynamic polarization curves for another set of samples in Hank's solution at pH 7.4 and 37°C temperature.

Table 9: Passivation parameters of the samples in Hank's solution at pH 7.4 and 37°C. temperature. All the potentials are with respect to SCE.

Material	**Z_{cp} (mV vs. SCE)**	**E_b (mV vs. SCE)**	**i_{pass} ($\mu A/cm^2$)**	**E_b - ZCP (mV vs. SCE)**
C.P. Titanium	-648	1250	6.8	1898
Ti-15Al	-548	750	2.5	1298
Ti-5Al- 2.5Fe	-562	1240	1.2	1802
Ti-6Al-4V	-400	1290	1.5	1690
Ti-6Al-4Fe	-470	1170	1.3	1640
Ti-6Al-4Nb	-170	1182	1.4	1352
Ti-13.4Al-29Nb	-585	979	1.3	1564
Ti-13Nb-13Zr	-500	1200	4.3	1700
316L Steel	-281	37	1.0	319

4.2 Tafel Extrapolation

The Tafel extrapolation results for all the Ti-based alloys have been presented in Figure 27 and 28. All the experiments were duplicated so as to ensure reproducibility of test results. The original as well as duplicate experimental curves are shown in Appendix A and data from these curves are tabulated in Appendix B. Tafel slopes β_c (cathodic tafel slope) and β_a (anodic tafel slope) possess units of mV per current density decade, where a decade is one order of magnitude current density such as from 0.10 amp/cm^2 to 1.0 amp/cm^2.

Corrosion current density for activation controlled Tafel plot is obtained from the intersection of the anodic and cathodic linear extrapolations at zero current potential. This is shown in Figure 2 of Appendix A for commercial pure titanium. The methodology of obtaining cathodic and anodic Tafel slopes and for calculating corrosion current density is shown in this figure.

The cathodic portion of the Tafel slopes exhibited lenearities in the curve, whereas such well-defined linear portion could not be ascertained in the anodic portion due to stable passivity behavior exhibited by the samples in the solution. The cathodic Tafel slopes ranged between 120 and 250 mV/decade while the anodic Tafel slopes were of the same order. This corrosion current density in Amps/cm^2 can be converted to corrosion rate in mpy (mils per year) using Equation 12. Corrosion rates for all the materials were calculated using the same procedure. Table 10 provides the results of the Tafel extrapolation for the materials used in the study.

Alloying of aluminum alone to CP titanium has not improved the corrosion resistance to a great extent. From the corrosion current (i_{corr}) value and corrosion rates calculated for Ti-5Al-2.5Fe, Ti-6Al-4V, Ti-6Al-4Fe and Ti-6Al-4Nb it can be seen that their corrosion rates are comparable with that of CP titanium. Ti-6Al-4Fe gives the i_{corr} (Figure 27) and corrosion rate of 0.199 μA/cm^2 and 0.041 mpy. No effect on corrosion rate is observed with increased percentage of iron. On comparing the data for Ti-13.4Al-29Nb and Ti-6Al-4Nb, increased percentage of niobium addition has not drastically

affected i_{corr}.

Ti-13Nb-13Zr alloy exhibited the least corrosion current density (i_{corr}) and corrosion rate as compared to other materials investigated. This fact is also corroborated by potentiodynamic polarization studies (Figure 26) as the i_{corr} value calculated from potentiodynamic polarization curves for this material was also the lowest (0.063 $\mu A/cm^2$). This is comparable to the corrosion rate determined by Tafel extrapolation studies. The lower corrosion rate of Ti-13Nb-13Zr in simulated human body conditions may probably result due to lower metal ion release during the spontaneous passivation of the alloy. The corrosion products of the minor alloying elements, niobium and zirconium have to be also considered in addition to titanium [114]. It has been reported that modification of passive TiO_2 layer by niobium oxide (Nb_2O_3) or zirconium oxide (ZrO_2) reduces Cl^- ingress into the oxide layer thereby improving the structural integrity of the oxide film such that pit initiation events were reduced [114]. Titanium (Ti), Niobium (Nb), and Zirconium (Zr), which are used in Ti-13Nb-13Zr, were reported by Steinemann as causing minimal negative tissue response when introduced into the surrounding tissue as ions during the alloy dissolutions [35]. Apart from possessing higher corrosion resistance Ti-13Nb-13Zr alloy, has sufficient alpha phase to provide the necessary mechanical properties. The presence of strong passivating elements like Zr and Nb in sufficient amounts and their uniform distribution can also be the probable reason for superior mechanical properties exhibited by this alloy.

316L steel exhibited the maximum corrosion rate of 0.16 mpy and minimum breakdown potential. Corrosion current for 316L steel is 0.421 $\mu A/cm^2$ as compared to that of Ti-alloys, which are in the range of 0.01 to 0.2 $\mu A/cm^2$. This higher corrosion rate of 316L steel may be due to the presence of chloride ion in the solution. It is highly susceptible to pitting corrosion. The ability of 316L stainless steel to repassivate in biological environments is also considerably less as compared to other biomaterials [95]. The most significant difference between 316L stainless steel and titanium alloys is absence of a true potentially independent passive region in

316L stainless steel. The anodic polarization curve had a positive slope indicating that the passive/oxide film is not truly protecting the material from corrosion even in its passive region. The passive region is also small and transition to transpassive region occurs at a fairly active potential (Figure 26). It is reported that this material does not exhibit a protection potential, and if it does the hysteresis is large enough to indicate that the material is not capable of repairing/ repassivating/ quickly if any damage occurs to the passive oxide layer [53]. The corrosion rates of this alloy increase significantly when subjected to crevice and/or fretting conditions [132] within the range of clinically relevant potential-pH combinations and hence this material is at the best biotolerant. The results of the present study indicate the lower corrosion resistance of this alloy compared to titanium alloys.

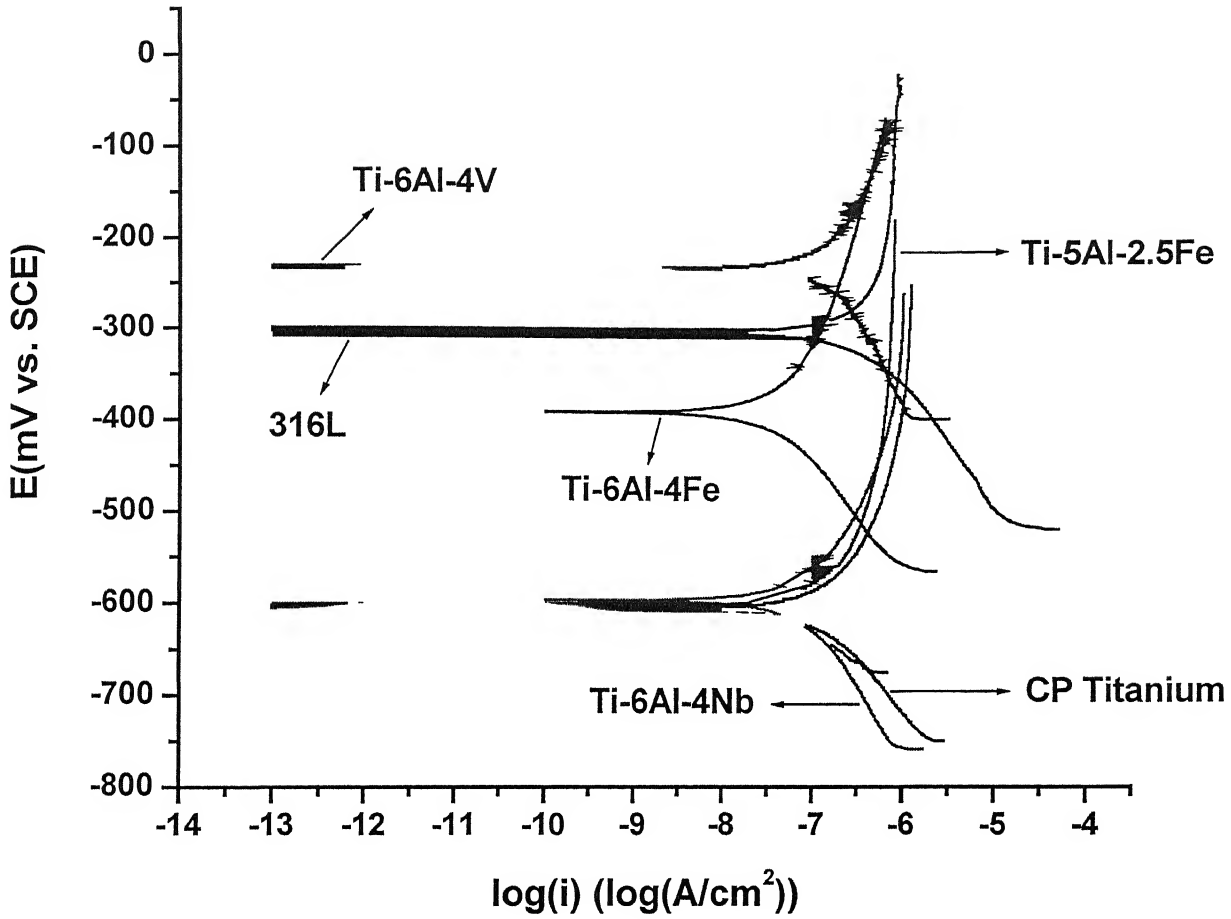

Figure 27: Tafel extrapolation curves for a set of samples in Hank's solution at pH 7.4 and 37°C temperature.

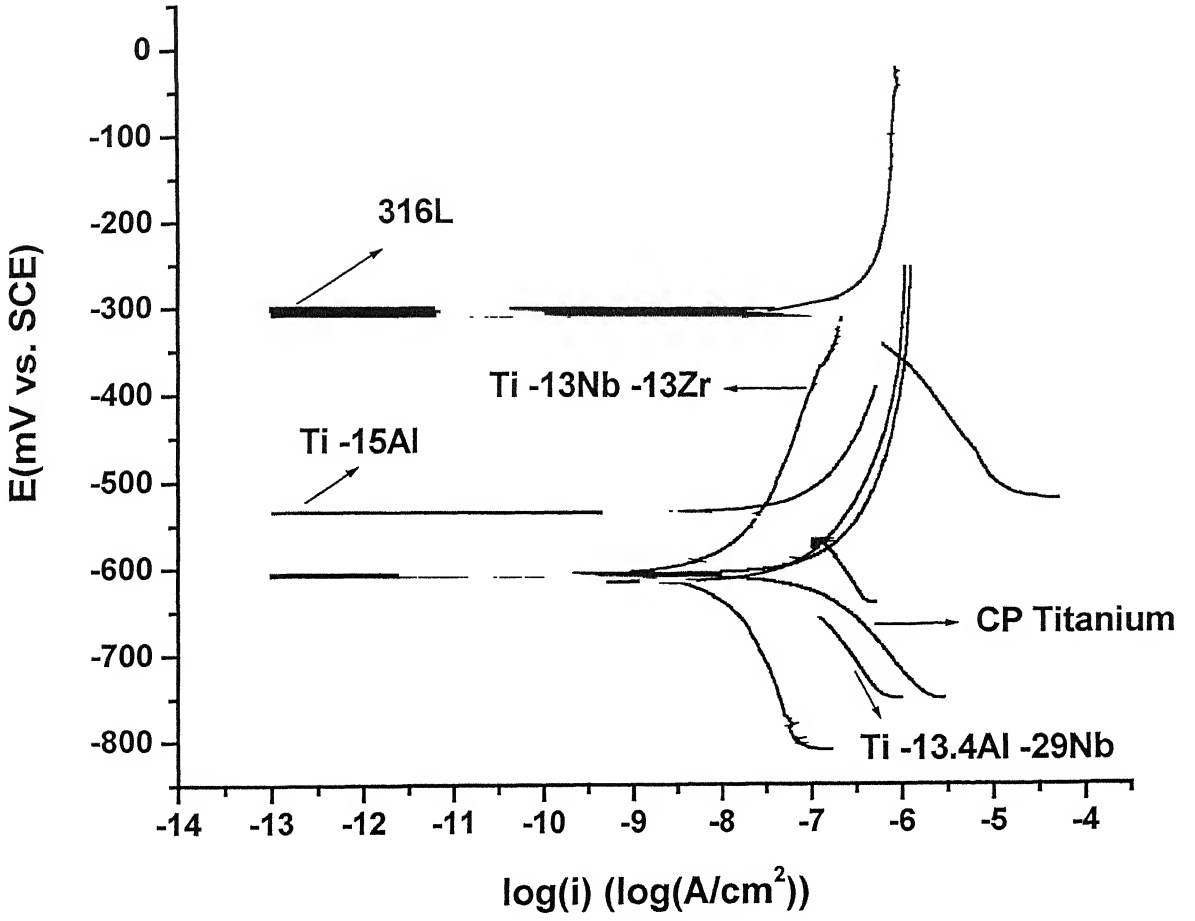

Figure 28: Tafel extrapolation curves for another set of samples in Hank's solution at pH 7.4 and 37°C temperature.

Table 10: Corrosion rates determined by Tafel extrapolation method for different biomaterials.

Material	ZCP (mV vs. SCE)	β_c (mV/dec)	β_a (mV/dec)	i_{corr} ($\mu A/cm^2$)	Corrosion rate mils per year (mm/year)
C.P. Titanium	-563	-137	145	0.080	0.036 (0.0009)
Ti-15Al	-534	-154	160	0.080	0.028 (0.0007)
Ti-5Al- 2.5Fe	-604	-121	170	0.121	0.042 (0.0010)
Ti-6Al-4V	-271	-181	106	0.160	0.0550 (0.0013)
Ti-6Al-4Fe	-478	-120	120	0.199	0.041 (0.0010)
Ti-6Al-4Nb	-596	-158	185	0.100	0.0300 (0.0007)
Ti-13.4Al-29Nb	-616	-138	134	0.067	0.024 (0.0006)
Ti-13Nb-13Zr	-607	-249	202	0.0125	0.0045 (0.0001)
316L Steel	-303	-145	382	0.421	0.16 (0.0040)

4.3 Microstructural Characterization

Titanium can exist in two allotropic modifications; that is, it exists in more than one crystallographic form. At room temperature, titanium has a hexagonal close-packed (hcp) crystal structure, which is referred to as "alpha" phase. This structure transforms to a body-centered cubic (bcc) crystal structure, called beta phase, at 888°C (1621°F). It is common to separate Ti alloys into four categories, referring to the phases normally present. The alloy categories generally are called alpha and near alpha which contains little or no beta stabilizers, alpha-beta and beta which contains substantial volumes fraction of beta phase, typically 0.05 to 0.40 or which can be quenched in thin sections to completely retain the metastable beta phase. Sometimes a category of near beta alloys is also considered [133].

These categories denotes the general type of microstructure after processing. The microstructures of titanium are complex. They are often the direct result of composition, processing and post processing heat treatments. The most important beta stabilizing elements are the so-called beta isomorphous elements such as V, Nb, Mo, Fe and Ta, while the alpha stabilizing elements are Al, O and N. Other common alloying additions are Sn and Zr, which are neutral because they have minimal effect on beta transus [133].

Microstructural characterization of the materials in this study was undertaken after the electrochemical testing. This ensured that the reported microstructure was for the surface used in the electrochemical tests. The cast pancake was expected to reveal differences in structure and therefore, the surfaces that were tested were taken up for microstructural analysis. In the microstructures, beta phase appeared as dark and alpha as white phase. In addition, the microstructural variation to be noted is a result of the composition. Beta volume fraction was calculated for these materials and a correlation between volume fractions of beta phase, corrosion current density

and corrosion rate and grain size was attempted. The results of microstructural analysis are tabulated in Table 11. The analysis of the microstructures is discussed in the following sections in different categories (i.e. alpha, near alpha, beta and near beta).

4.3.1 Alpha and Near Alpha Phase Titanium Alloys

Pure titanium is single-phase alpha at room temperature. As with any single-phase alloy, the microstructure of CP titanium depends on whether or not it has been cold worked and the specific type of annealing employed. In addition, upon cooling from the beta region which begins at 882°C, the structure depends on the cooling process followed because the process directly affects the progression of the beta-to-alpha transition and the final alpha grain size shape. The equiaxed recrystallized grains of alpha in microstructure of CP titanium is evident in Figure 29 (a) and (b). Alpha grain boundaries as seen in the microstructure of CP titanium are quite regular which suggests that the material was cold rolled and annealed in the alpha region. No traces of interstitial elements were observed, which may be the reason for enhanced corrosion resistance of this grade in reducing chloride environments. The interstitial elements oxygen and nitrogen greatly strengthen pure titanium; grades of higher purity (low interstitial content) are lower in strength and hardness, and have a lower transformation temperature, than those higher in interstitial content [133]. Customarily CP titanium is selected for its excellent corrosion resistance, especially in application where high strength is not required. Yield strength of commercially pure grades vary from about 170 MPa to 480 MPa simply as a result of variation in interstitial and impurity levels, with strength increasing as the oxygen/nitrogen (and iron) content increases [134].

Alpha formers such as aluminum can increase the strength of titanium alloys by solid solution strengthing; there is an increase in strength of approximately 55 MPa for each 1% aluminum [134]. However, aluminum enrichment of alpha phase was found to be detrimental to the passivity of

titanium, as seen earlier. The microstructures of Ti-15Al are shown in Figure 29 (c) and (d).

In the alloy containing 15% aluminum, the grain boundaries were not observed. White precipitated alpha phase can be seen. Fraction of beta phase for Ti-15Al was also higher as compared to CP titanium. Microstructures show a coarse lenticular plate like structure, which are alpha platelets formed by slow cooling from beta region (1040°C to 1090°C). The passive range of the alloy was much lower compared to CP titanium. The range decreased from 1898 mV to 1298mV. The protective passive film may also have been affected by other factors like composition and grain boundaries. The properties of alpha and near alpha alloys are not altered greatly by heat treatment. They are employed in solution annealed and stabilized conditions [134]. Near alpha alloys are much more susceptible to the formation of Ti_3Al, which promotes stress-corrosion cracking (SCC). It has been reported that nature of oxide film on this alloy basically remains unaltered in the presence of minor alloying constituents. Consequently, small additions (<2 to 3%) of most commercially used alloying elements or trace alloy impurities generally have a little effect on basic corrosion resistance in normally passive environments [131].

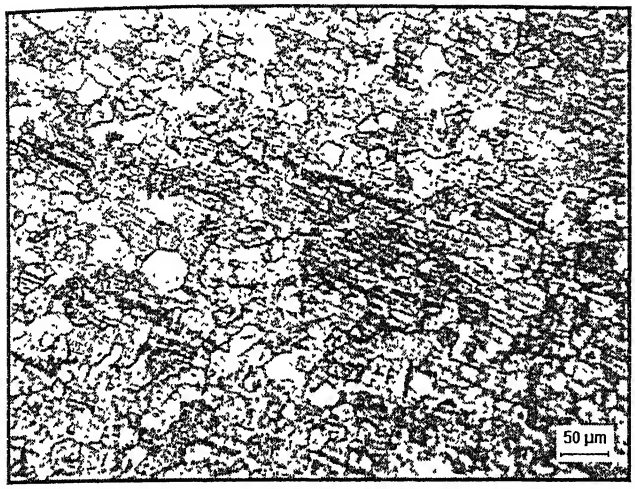

(a)

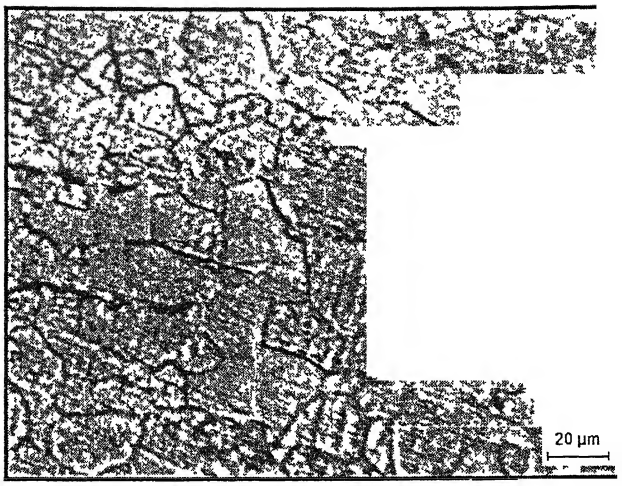

(b)

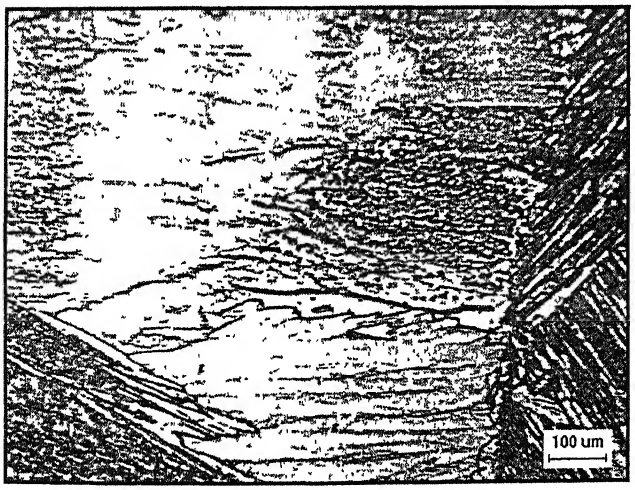

(c)

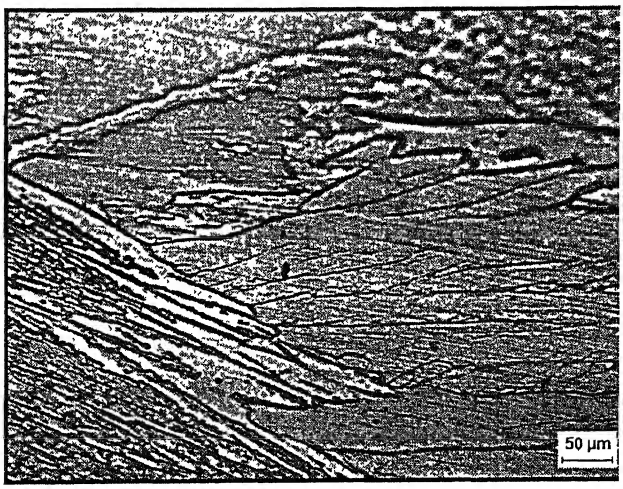

(d)

Figure 29: Optical micrographs of CP titanium at (a) 200X (b) 500X and Ti-15Al at (c) 100X (d) 200X. The microstructures were obtained on the area used for electrochemical testing in simulated body fluid solution at 37°C and 7.4 pH.

4.3.2 Alpha-Beta Titanium Alloys

The alloys Ti-6Al-4V, Ti-6Al-4Nb, Ti-6Al-4Fe and Ti-5Al-2.5Fe possess a two-phase alpha-beta structure owing to addition of vanadium, niobium and iron which are beta stabilizers. Aluminum is an alpha stabilizer. Alpha is the dominant phase in all these alloy combinations as evident from the microstructures (Figure 30 and 31). Ti-5Al-2.5Fe is in near alpha-beta class; the alpha phase dominates the properties of this alloy to greater extent as compared to Ti-6Al-4V, Ti-6Al-4Fe and Ti-6Al-4Nb. Ti-5Al-2.5Fe contains much less % of beta than other alpha-beta alloys investigated which have about 38-39% beta phase.

Owing to two-phase equiaxed microstructure, Ti-6Al-4V is more susceptible to corrosion as the compositional difference across the grain boundaries increases which leads to the galvanic cell formation. This equiaxed structure may have resulted by extensive mechanical working (>75% reduction) of the material in alpha-beta phase field, where the breakup of lamellar alpha into equiaxed alpha depends on the exact deformation procedure. This equiaxed structure can also be obtained by recrystallization annealing followed by slow cooling [135]. The resulting structure is fairly fine grained with a grain size of 22.4 μm (Figure 30a and b). This alloy is not as corrosion resistant as alpha, near alpha alloys and beta alloys. The high corrosion rate of 0.055 mpy for Ti-6Al-4V (Table 11) may be due to the fine-grained equiaxed structure.

Addition of niobium increases the grain size considerably to 826μm as evident from Figure 30 (c). White plates are alpha and dark plates are beta. This is a typical Widmanstatten type of structure. Grain boundary alpha can also be seen in the microstructure in a transformed beta matrix. The plate like alpha precipitates that nucleate and grow below the beta transus producing a Widmanstatten structure [137]. The plates often precipitate in colonies of the same crystallographic orientation (Figure 30 c), presumably because of autocatalytic nucleation. Volume fraction of beta phase remains

almost same (Table 11). This is a high strength alloy developed for femoral component in hip prosthesis. Corrosion rate for this alloy is lower as compared to other alpha beta alloys.

Figure 31 shows the micrographs for Ti-6Al-4Fe and Ti-5Al-2.5Fe. Grain size for the two alloys were comparable but volume fraction of beta phase was higher in case of Ti-6Al-4Fe. This alloy shows a lamellar structure with a coarse grain size of 635 μm. It is a fairly fine lamellar, colony structure produced by air-cooling with transformed beta phase appearing dark. Alpha phase appears to be fine needle like (acicular alpha). Ti-5Al-2.5 Fe is also possessed a coarse grained structure (735μm). This alloy is designed for permanent implants in human body. Cast implant devices, such as sockets of hip prosthesis, are readily produced. A special application of this alloy is porous implant devices. Pore size (>50μm) makes it possible to secure implants via tissue growth into the pores. Examples for such devices are heart pacemaker electrodes and dental implants [131]. The fine lamellar widmanstatten alpha beta structure for this alloy (Figure 31c), which is formed by solutionizing over beta transus followed by air cooling has been reported to give greatest fracture toughness [137]. Blocky and fine plate like acicular alpha and transformed beta (dark) and alpha at prior beta grain boundaries are also seen in the micrograph of Ti-5Al-2.5Fe.

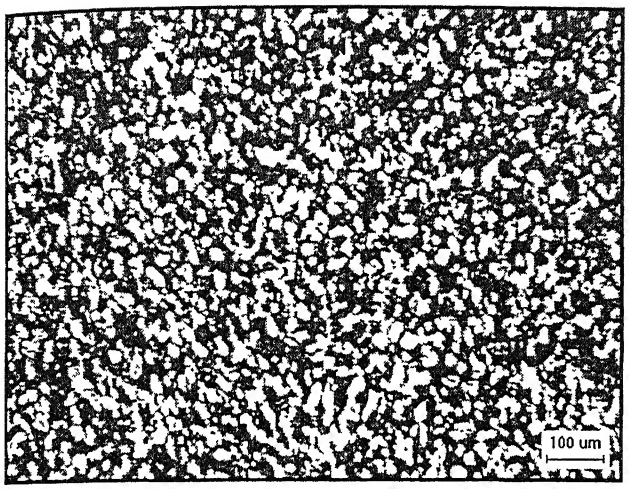

(a)

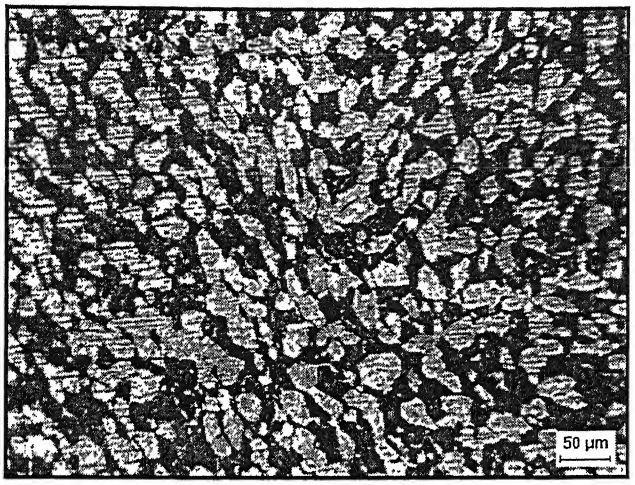

(b)

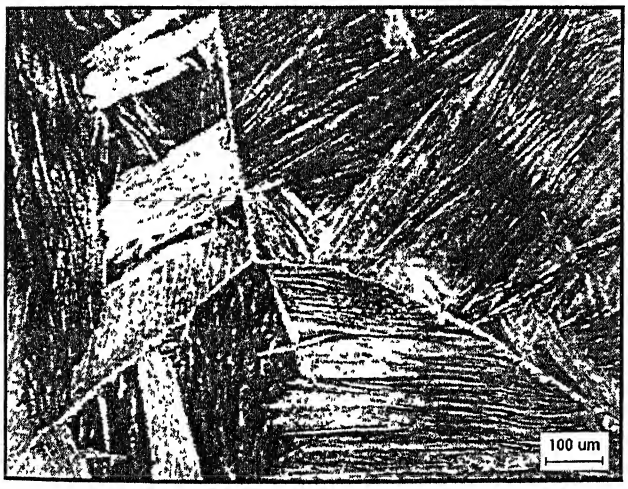

(c)

(d)

Figure 30: Optical micrographs of Ti-6Al-4V at (a) 100X (b) 200X and Ti-6Al-4Nb at (c) 100X (d) 500X. The microstructures were obtained on the area used for electrochemical testing in simulated body fluid solution at 37°C and 7.4 pH.

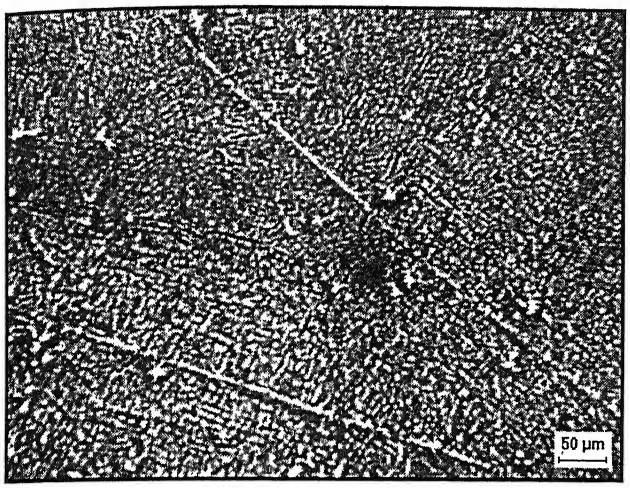

(a)

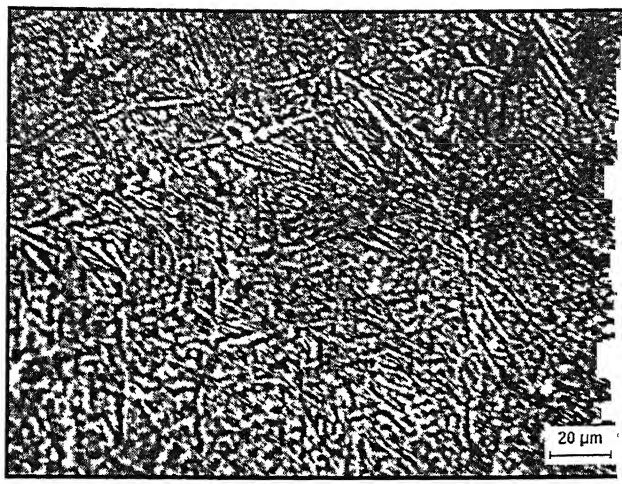

(b)

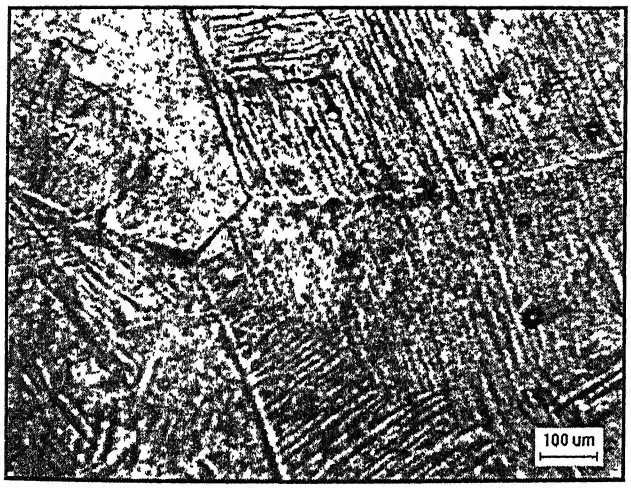

(c)

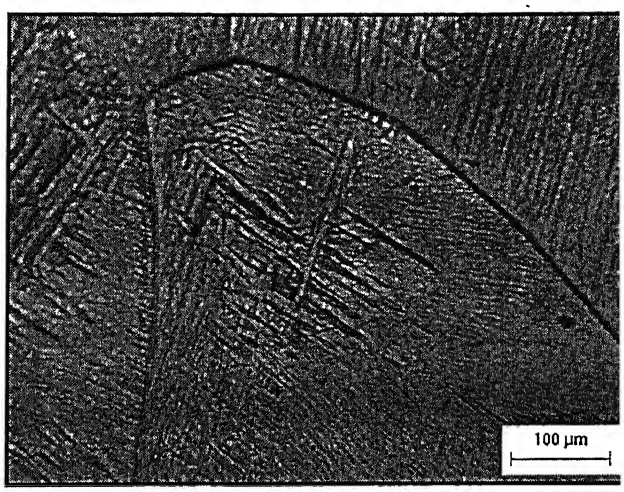

(d)

Figure 31: Optical micrographs of Ti-6Al-4Fe at (a) 200X (b) 500X and Ti-5Al-2.5Fe at (c) 100X (d) 200X. The microstructures were obtained on the area used for electrochemical testing in simulated body fluid solution at 37°C and 7.4 pH.

4.3.3 Beta and Near Beta Titanium Alloys

Ti-13.4Al-29Nb alloy contains aluminum in addition to niobium (which is a beta stabilizer), in order to strengthen the alpha phase also aluminum addition minimum 3% is needed to suppresses omega transformation effectively at lower temperature and longer times [137]. Fine needle like precipitated alpha in beta phase is evident from the microstructure of Ti-13.4Al-29Nb. Uniform distribution of this alpha phase can be seen. Also there is no evidence of occurrence of extensive grain boundary alpha, there is a precipitate free zone.

Ti-13Nb-13Zr contains sufficient beta phase stabilizer in the form of niobium to retain the beta phase at room temperature and zirconium is a neutral element added which strengthens and stabilizes the beta phase and prevents the formation of alpha phase on cooling through the transformation temperature range. It also enhances the corrosion resistance above the level achieved by molybdenum and suppresses omega transformation to prevent embrittlement [137]. This beta titanium alloy is developed specifically for use in biomedical applications. Titanium, niobium and zirconium are highly resistant to corrosion reported by Steineman as causing minimal negative tissue response [91]. This alloy shows improved wear resistances because of presence of zirconium, which is a neutral phase, thus reducing the potential for generation of particulate, wear debris [136].

The microstructure of Ti-13Nb-13Zr (presented in Figure 32 c and d) exhibited extremely fine elongated primary alpha in beta matrix. Its structure, as is evident from the micrograph is fibrous in nature, which compares well with the structure of bone, hence leading to a better fixing of the implant material between the tissues [104]. It has been reported that Ti-13Nb-13Zr has been found to provide the preferred combination of high strength, increased ductility and flexibility desired for orthopedic implants. This ductility of the material may be due to the elongated primary alpha (white) seen in the microstructure (Figure 32 c and d). Fracture toughness of

this material is reported to be 73% greater than Ti-6Al-4V. In implant design, material elasticity is an important requisite for producing implants which will adequately transfer stress to surrounding bone to minimize bone atrophy due to stress shielding. Ti-13Nb-13Zr exhibits flexibility with low elastic modulus of 80GPa [106]. This can be attributed to the annealed beta microstructure of the material.

Ti-13Nb-13Zr exhibited the least corrosion rate among all the investigated materials. This may be because of the maximum % of beta phase in the alloy. In order to understand if beta phase amount could dictate the corrosion behavior of the alloys investigated, it was observed that Ti-13.4Al-29Nb alloy (which possessed niobium as beta phase stabilizer), provided a corrosion rate of 0.024 mpy which was still lower than all alpha and alpha-beta alloys but higher than Ti-13Nb-13Zr (which has a corrosion rate of 0.0045 mpy). Prominent grain boundaries can be observed in the microstructure of Ti-13.4Al-29Nb (Figure 32 a and b). Grain size measured for T-13.4Al-29Nb was 453μm but no grain boundaries were observed in case of Ti-13Nb-13Zr.

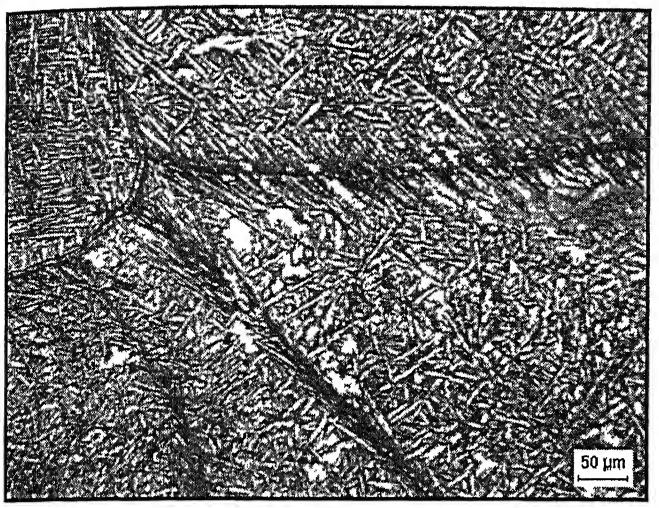

(a)

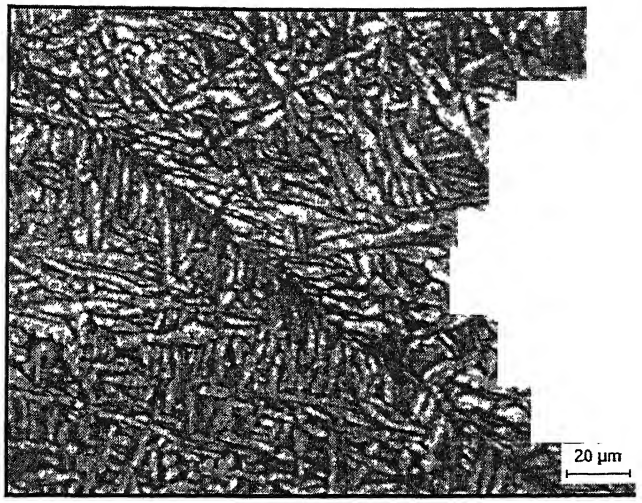

(b)

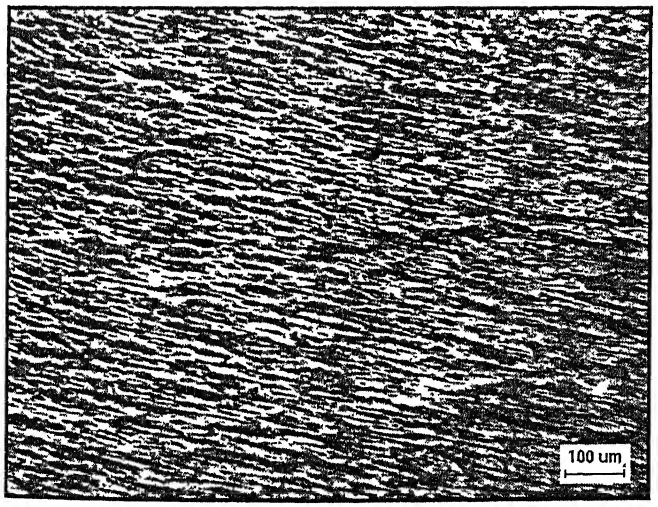

(c)

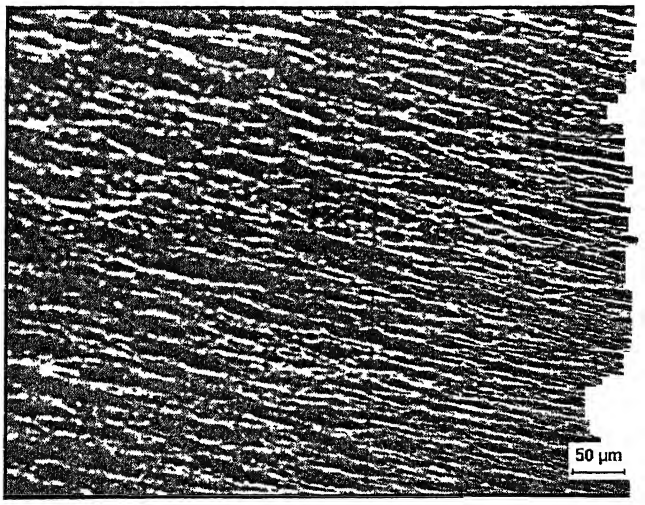

(d)

Figure 32: Optical micrographs of Ti-13.4Al-29Nb at (a) 200X (b) 500X and Ti-13Nb-13Zr at (c) 100X (d) 200X. The microstructures were obtained on the area used for electrochemical testing in simulated body fluid solution at 37°C and 7.4 pH.

Table 11: Beta volume fraction in the Titanium alloys utilized in this study.

Material	Type	Grain Size (μm)	Error ±	i_{corr} ($\mu A/cm^2$)	Corrosion rate mils per year (mm/year)	Volume fraction of beta phase	Error ±
C.P. Titanium	Alpha	25.5	2.5	0.080	0.0360 (0.0009)	0.07	0.02
Ti-15Al	Near Alpha	-	-	0.080	0.0280 (0.0007)	0.19	0.02
Ti-5Al-2.5Fe	Alpha+Beta	735	100	0.121	0.0420 (0.0010)	0.27	0.01
Ti-6Al-4V	Alpha+Beta	22.4	0.9	0.160	0.0550 (0.0013)	0.38	0.02
Ti-6Al-4Fe	Alpha+Beta	635	100	0.199	0.0702 (0.0010)	0.38	0.02
Ti-6Al-4Nb	Alpha+Beta	826	103	0.100	0.0300 (0.0007)	0.39	0.01
Ti-13.4Al-29Nb	Near Beta	453	62.5	0.067	0.0240 (0.0006)	0.41	0.01
Ti-13Nb-13Zr	Beta	-	-	0.0125	0.0045 (0.0001)	0.49	0.02

4.4 Tribological behavior

4.4.1 Friction results

The frictional behavior of commercially pure Titanium, Ti-13Nb-13Zr, Ti-6Al-4V, Co-28Cr-6Mo and Ti-5Al-2.5Fe biomaterials is analyzed. Figure 33 shows coefficient of friction (COF) versus number of cycles for these materials against steel in simulated human body environment. CP titanium, Ti-13Nb-13Zr and Ti-6Al-4V exhibit similar frictional behavior under the present experimental conditions. During the running-in-period (first 500 cycles), COF increases from a low value to a very high value (0.5 to 0.55 for CP titanium, Ti-13Nb-13Zr, and Ti-6Al-4V, 0.43 to 0.42 for Co-28Cr-6Mo and up to 0.325 for Ti-5Al-2.5Fe). Thereafter, COF decreases to a rather stable and steady state value within the next 500 cycles.

Figure 34 plots COF as a function of different material combinations tested. The error bars indicate the standard deviation in the obtained steady state COF values for at least two fretting tests. Little variation (0.01-0.02) in COF values is recorded for all the materials. Comparing the steady state coefficient of friction values (COF), CP titanium shows a higher coefficient of friction of 0.5; whereas COF value for Ti-13Nb-13Zr and Ti-6Al-4V was comparable at 0.48 and 0.46 respectively. It can be noted here that Co-28Cr-6Mo gives a steady state COF of around 0.4. Significantly lower COF is noticed for Ti-5Al-2.5Fe (COF-0.30) as compared to other alloys investigated.

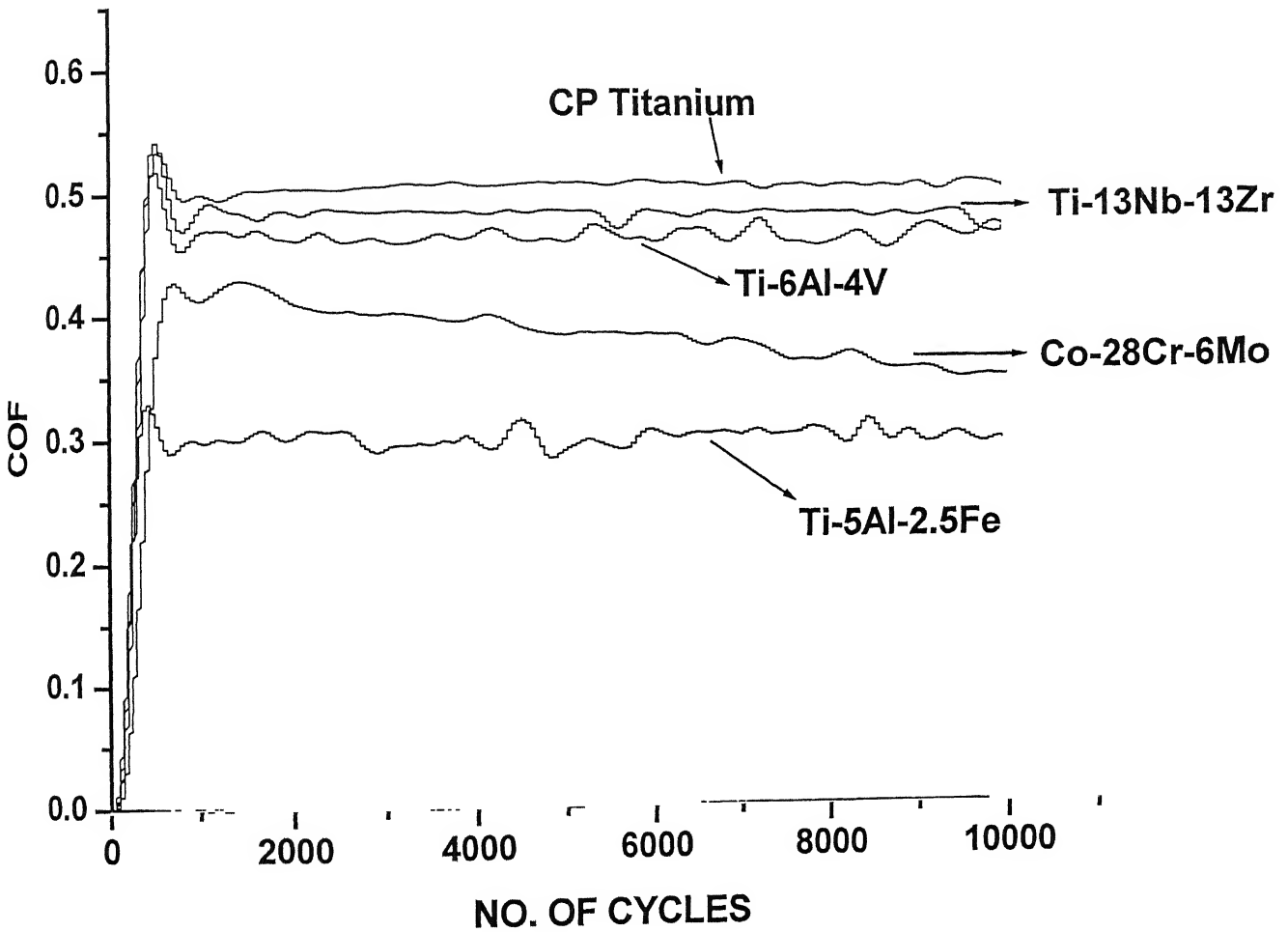

Figure 33: Comparative plot for coefficient of friction (COF) versus number of cycles for potential orthopedic implant materials against steel at 10N load, 10Hz frequency, 80μm displacement stroke.

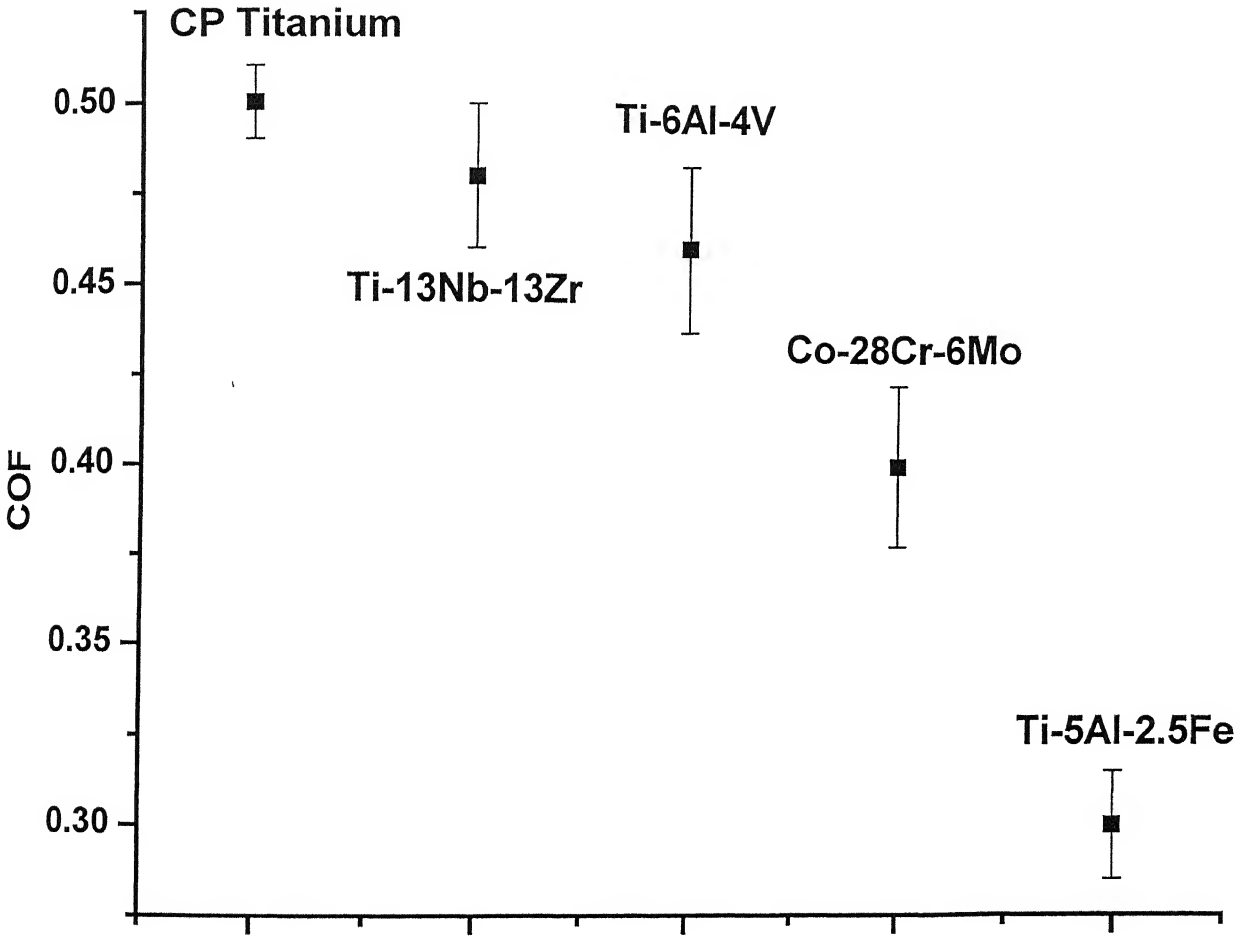

Figure 34: Variation of steady state coefficient of friction for different materials measured during fretting against 8mm diameter steel ball, at 10N load for 10,000 cycles with a frequency of 10Hz frequency for 80μm displacement stroke.

4.4.2 Morphology of worn surfaces

Figure 35 shows the optical micrographs of the ultrasonically cleaned worn surfaces of flats, after fretting against steel ball at 10 N load for 10,000 cycles. It displays the wear scar of the different Ti-based alloys. The wear scar appears circular to elliptical and commonly adherent layer of steel is noted. The accumulation of wear debris around the pit is clearly visible. The wear pit appears to be rather smooth. Steel wear debris is accumulated uniformly at the edges of wear pit in case of Ti-6Al-4V. The worn surfaces in case of CP titanium reveals the evidence of more extensive abrasive scratches.

Figure 36 displays the overview of the worn surface topography on the Co-28Cr-6Mo alloy after fretted against steel. The observation of the rough worn surface is indicative of the high wear rate of the Co-alloy. The adherence of the transfer layer in the central region of the worn surface is also noted.

Figure 37 illustrates the detailed morphological analysis of the fretting scar on commercially pure titanium. Occurrence of extensive grain boundary cracking is clearly visible. The cracks are formed preferentially along the grain boundaries and the material at the worn surface is observed to be plastically deformed.

Figure 38 displays the topographical features of the worn surface on Ti-13Nb-13Zr after it is fretted against steel in simulated body fluid solution. Wear scar is characterized by the presence of deep abrasive scratches (Figure 38c), the transfer layer (Figure 38a and 38b) and extensive cracking (Figure 38d). Detailed analysis of the wear scar further reveals that the cracking occurs both perpendicular as well as along the abrasive scratches. Closer observation also suggests that high plastic deformation probably leads to the cracking of the material during the wear process.

Figure 39 shows the detailed morphological features of the worn surface of Ti-6Al-4V after it is fretted against steel in simulated body fluid solution. The worn surface is characterized by the presence of transfer layer, abrasive scratches and cracking. Detailed investigation of the wear pit reveals the formation of a non-uniform transfer layer along with the grain boundary cracking. The evidence of cracking is more clear in Figure 39c. The formation of irregular shaped wear debris particles is seen in Figure 39d.

The wear characteristic of Ti-5Al-2.5Fe after fretting against steel ball is illustrated in Figure 40. Closer observation of the wear pits reveals smooth appearance of the owned surface along with signs of plastic deformation. Closely spaced deformation bands are also observed. Considerable amount of wear debris is observed to be accumulated around the wear scar. Smooth appearance (Figure 40a) of the wear scar is the indication of the lower coefficient of friction. The detailed view of wear debris is shown in Figure 40d. In another fretting test the formation of tribo chemical oxide layers is well revealed. The oxide layer is found to be discontinuous and heavily cracked. Detailed morphology of oxide layer as shown in Figure 40b and 40c indicate non-protective nature.

SEM micrograph of Co-28Cr-6Mo surface fretted against steel ball is shown in Figure 41. At higher load of 10 N and after 10,000 fretting cycles, the worn surfaces on Co-28Cr-6Mo exhibit signs of severe wear, as illustrated in Figure 41a. The topographical observation shows very rough nature of worn surface characterized by abrasive scratches with extensive plastic deformation and grain pull out. The presence of cracking is also observed in Figure 41b. The cracks are considered to cause delamination induced grain pull out. Also, the observation of such rough worn surfaces correlates well with the measured high COF of 0.4.

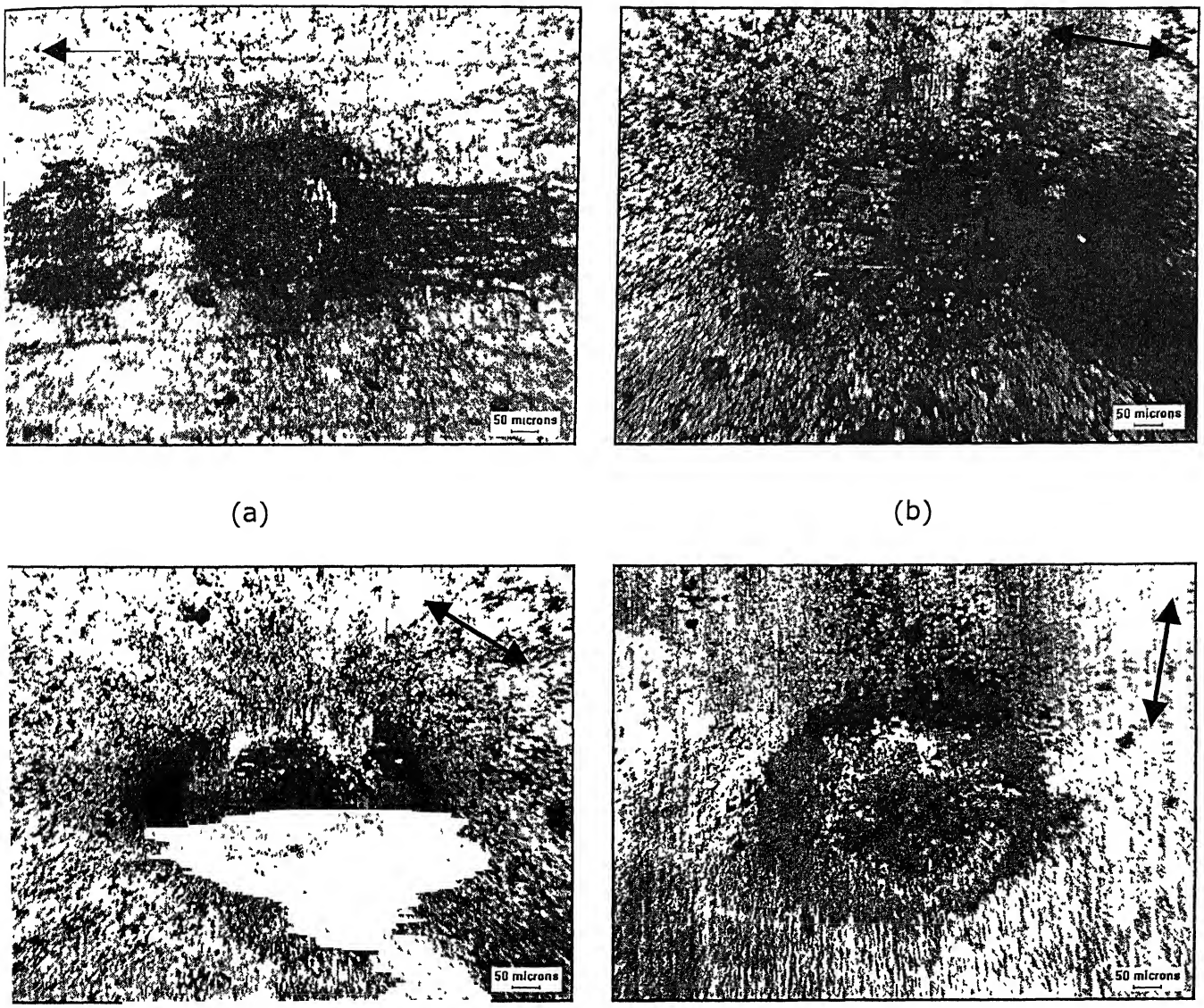

Figure 35: Optical Micrograph of the worn surfaces of (a) CP Titanium (b) Ti-13Nb-13Zr (c) Ti-6Al-4V (d) Ti-5Al-2.5Fe after they were fretted against steel ball at 10N load for 10,000 cycles with a frequency of 10Hz at 80μm displacement stroke. Double pointed arrows indicate the fretting direction.

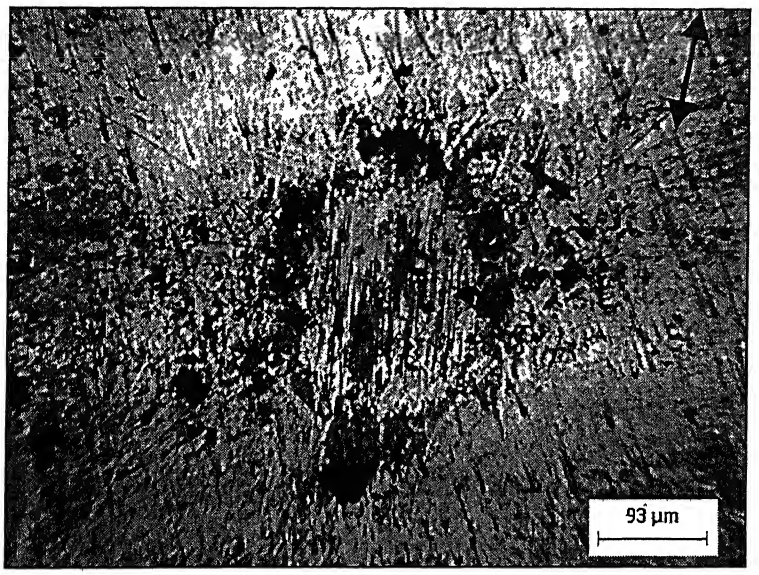

Figure 36: Optical Micrograph of the worn surfaces of Co-28Cr-6Mo flat after they were fretted against steel ball at 10N load for 10,000 cycles with a frequency of 10Hz at 80µm displacement stroke. Double pointed arrows indicate the fretting direction.

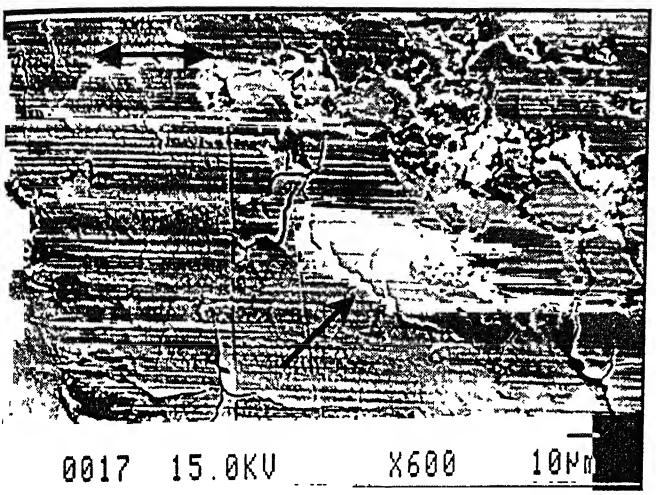

(a)

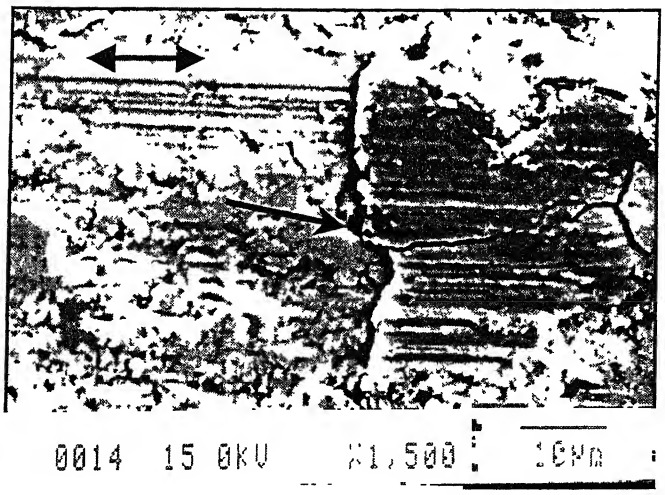

(b)

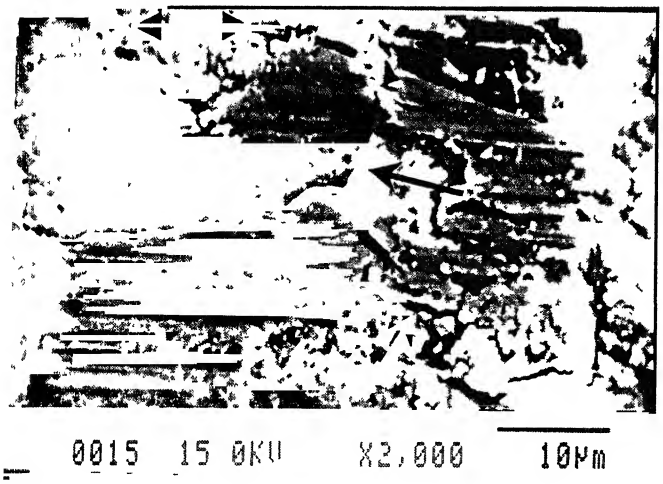

(c)

Figure 37: SEM micrograph of CP Titanium surface fretted against steel ball at 10N load, 10Hz frequency, 10000 cycles and 80µm displacement stroke. Double pointed arrows indicate the fretting direction and single pointed indicate the presence of cracks.

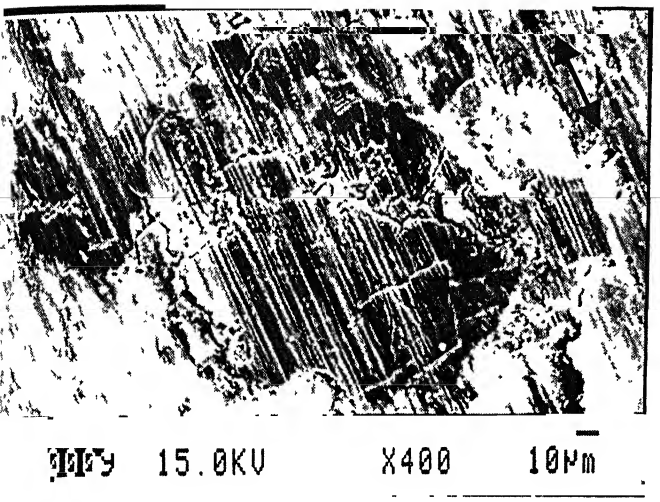

(a)

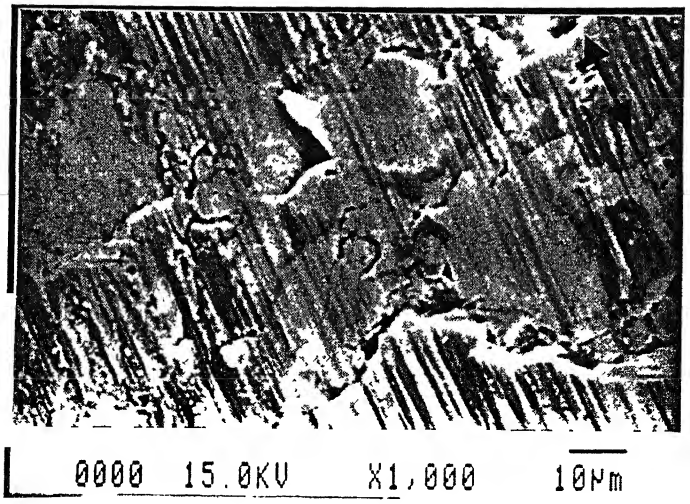

(b)

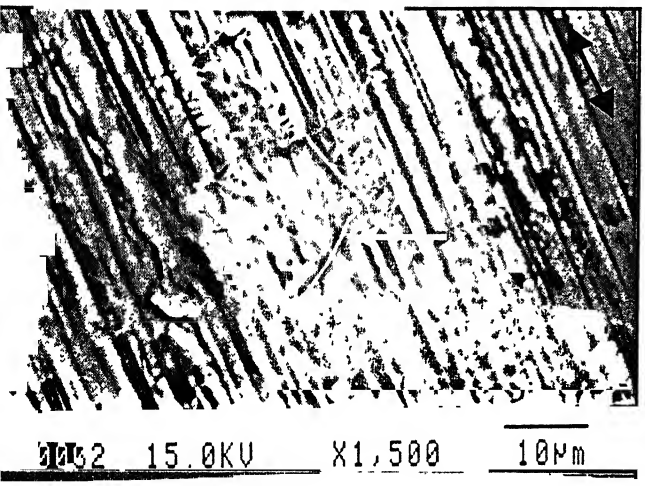

(c)

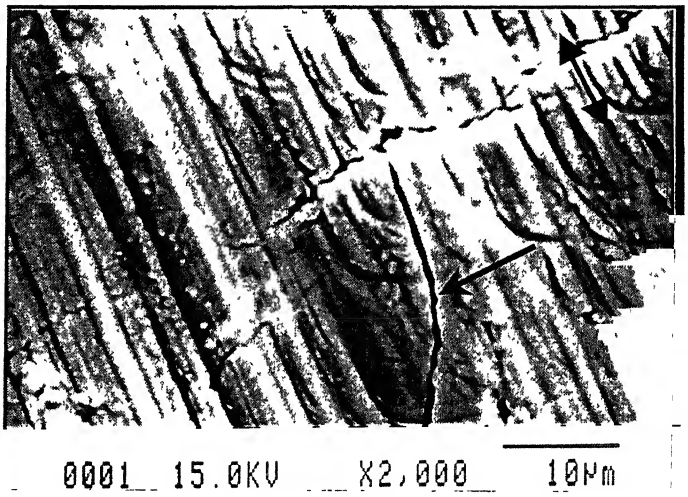

(d)

Figure 38: SEM micrograph of Ti-13Nb-13Zr surface fretted against steel ball at 10N load, 10Hz frequency, 10000 cycles and 80µm displacement stroke. Double pointed arrows indicate the fretting direction and single pointed indicate the presence of cracks.

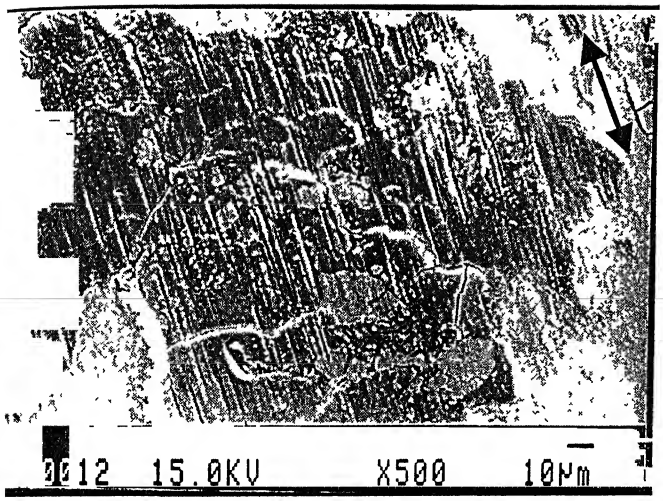

(a)

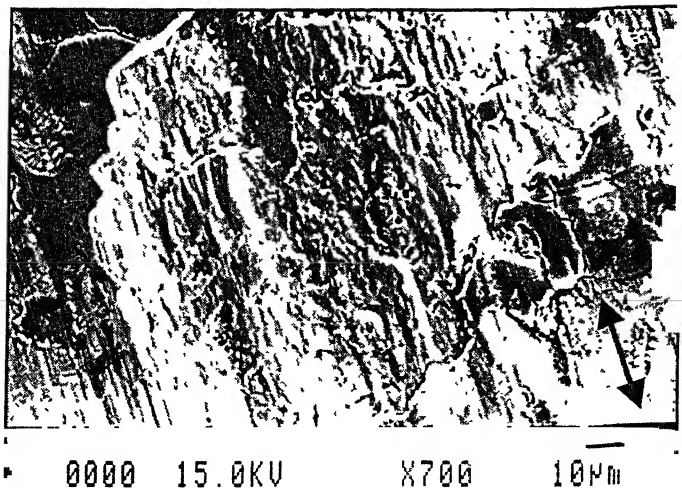

(b)

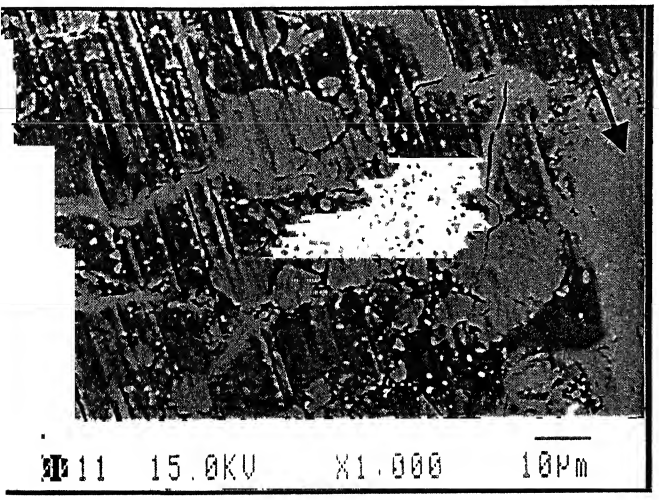

(c)

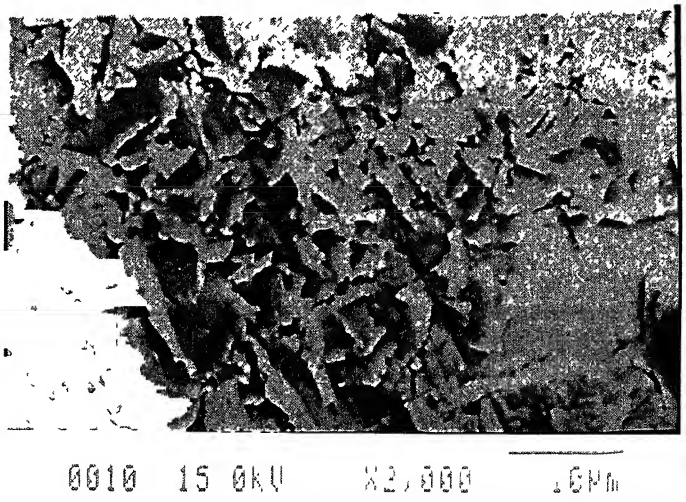

(d)

Figure 39: SEM micrograph of Ti-6Al-4V surface fretted against steel ball at 10N load, 10Hz frequency, 10000 cycles and 80μm displacement stroke. Double pointed arrows indicate the fretting direction and single pointed indicate the presence of cracks.

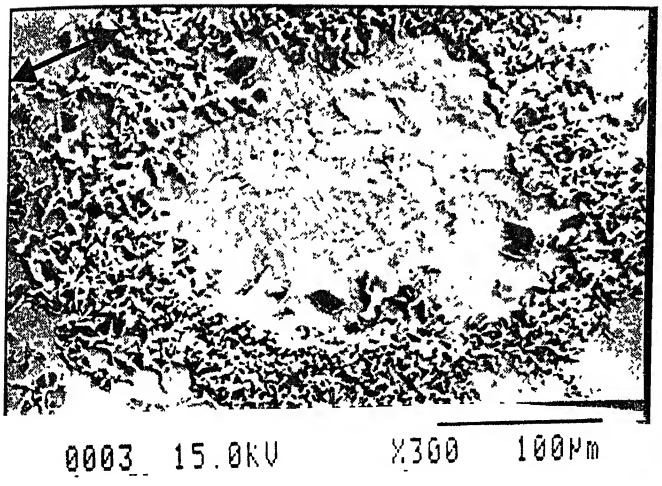

(a)

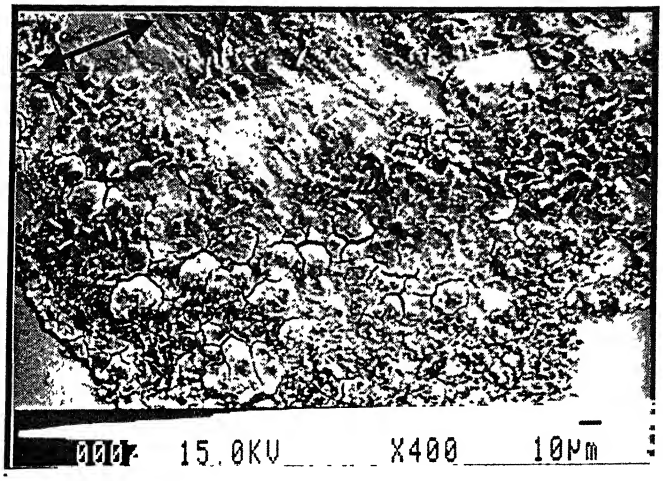

(b)

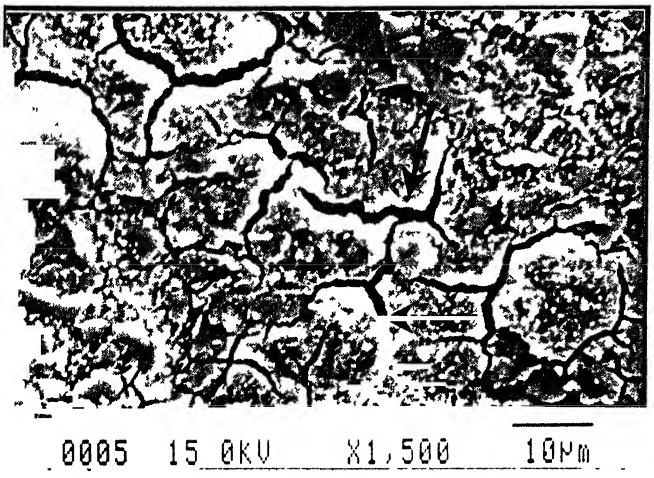

(b)

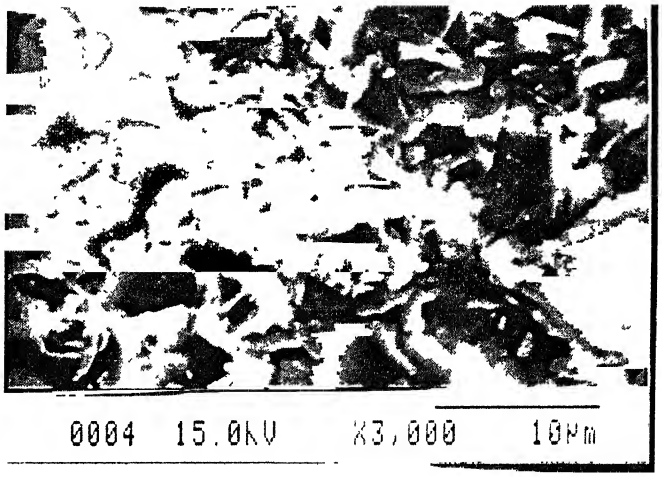

(d)

Figure 40: SEM micrograph of Ti-5Al-2.5Fe surface fretted against steel ball at 10N load, 10Hz frequency, 10000 cycles and 80µm displacement stroke. Double pointed arrows indicate the fretting direction and single pointed indicate the presence of cracks.

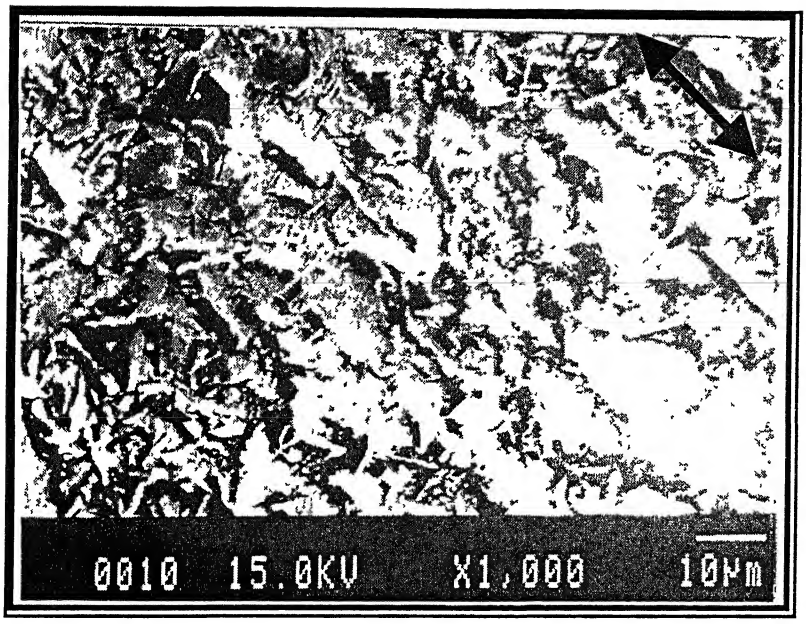

(a)

(b)

Figure 41: SEM micrograph of Co-28Cr-6Mo surface fretted against steel ball at 10N load, 10Hz frequency, 10000 cycles and 80µm displacement stroke. Double pointed arrows indicate the fretting direction and single pointed indicate the presence of cracks.

Summarizing the wear results, it is evident that all the investigated materials (with the exception of Ti-5Al-2.5Fe) have undergone severe wear under the experimental fretting conditions, in simulated body fluid environment. The wear occurs predominantly by abrasion, plastic deformation and cracking. Under the tribomechanical stress conditions Ti-based materials undergo heavy plastic deformation, which involves the formation of 'persistent slip bands'. The extensive formation of slip bands possibly leads to the observed cracking in the investigated materials. The formation of tribomechanical oxide layers (TiO_2 or a mixture of TiO_2 and Fe_2O_3) is commonly observed. Moreover the non-protective nature of the oxide tribo film leads to severe wear of the investigated materials. In case of Ti-5Al-2.5Fe the severity of the abrasion is much less compared to other Ti-based alloys investigated. Also the smooth appearance of the worn surface correlates well with the low COF obtained with this material.

Chapter 5

SUMMARY

5.1 Conclusions

The electrochemical and tribological behavior of several Ti-based alloys and 316L stainless steel was studied. The experiments were carried out in simulated body fluid solution (Hank's solution at pH-7.4 and 37°C). Scan rate used for all the electrochemical experiments was 0.166 mV/sec. All the samples exhibited active-passive polarization behavior. Corrosion rates of the investigated materials were calculated using Tafel extrapolation method. The following are the conclusions of the study:

- Al enrichment alone of the alpha-phase was found to be detrimental to the passivity of titanium alloys. Protective passive film may be affected by absence of grain boundaries (as observed in micrograph of Ti-15Al). It exhibited a low breakdown potential (750mV vs. SCE) as compared to other Ti-alloys thereby increasing the susceptibility of the alloy to crevice corrosion.

- Addition of alloying elements like aluminum, niobium, iron, zirconium and vanadium lowered i_{pass} (passive current density) to the range of 1.2 to 4.3 $\mu A/cm^2$ as compared to unalloyed CP titanium, which showed an i_{pass} of 6.8 $\mu A/cm^2$. The least value of i_{pass} was exhibited by Ti-5Al-2.5Fe (1.2 $\mu A/cm^2$).

- The highest breakdown potential (E_b) of 1290 mV (vs. SCE) was exhibited by Ti-6Al-4V. Earlier investigations have reported an E_b value of 1900 mV (vs. SCE) for this alloy [95]. Breakdown potential for

Ti-5Al-2.5Fe (1240mV vs. SCE) and CP titanium (1250mV vs. SCE) were comparable with that for Ti-6Al-4V.

- The highest passive range of 1898mV (vs. SCE) was shown by commercial pure titanium. The equiaxed-recrystallized grains of alpha in microstructure of CP titanium may be the reason for this. Ti-5Al-2.5Fe and Ti-13Nb-13Zr are close to this value at 1802 mV (vs. SCE) and 1700mV (vs. SCE) respectively. Addition of aluminum apparently decreased the passive range considerably (for Ti-15Al, E_b - ZCP is 1298mV).

- Ti-13Nb-13Zr alloy exhibited the least corrosion current density (i_{corr}) and corrosion rate (0.0045 mpy) as compared to other Ti-alloys investigated which exhibited a corrosion rate in the range of 0.02 to 0.05 mils per year. Owing to two-phase equiaxed microstructure (as observed in the micrograph of the alloy), Ti-6Al-4V is more susceptible to corrosion as the compositional difference across the grain boundaries increases. The improved corrosion resistance of Ti-13Nb-13Zr may be attributed to modification in passive layer and higher volume fraction of beta phase as compared to other titanium alloys tested.

- Micrograph of Ti-13Nb-13Zr reveals a fibrous structure with extremely elongated primary alpha in beta matrix. This structure resembles with that of bone as reported in the literature [104].

- Corrosion rate of Ti-6Al-4Nb is low as compared to other alpha beta alloys due to increase in grain size (826μm) with niobium addition.

- 316L steel exhibited the maximum corrosion rate of 0.16 mpy (for Ti-alloys it was 0.02 to 0.05 mpy, except for Ti-13Nb-13Zr which exhibited a corrosion rate of 0.0045 mpy) and minimum breakdown potential of 37mV (E_b for titanium alloys was in the range of 1300mV

to 1900mV). Corrosion current density for 316L steel is 0.421 $\mu A/cm^2$ as compared to that of Ti-alloys, which were in the range of 0.01 to 0.2 $\mu A/cm^2$.

- The tribological testing in SBF solution (Hank's solution) revealed that the steady state COF of the investigated Ti-alloys, with the exception of Ti-5Al-2.5Fe lies around 0.46-0.50 while fretting against bearing steel. The measured COF in SBF solution is found to be lower as compared to the reported COF (0.6) of the CP titanium and Ti-6Al-4V under unlubricated sliding condition.

- The COF of Ti-5Al-2.5Fe/Steel couple is lowest and at around 0.3. This value is even lower than that of Co-28Cr-6Mo/steel couple (0.4) under identical fretting conditions.

- Detailed microstructural investigation of the worn surface using SEM suggests that the major wear mechanism of the Titanium alloys is tribomechanical abrasion, transfer layer formation and cracking.

- The smooth and polished appearance along with the absence of cracking and deep abrasive grooves on the worn surface of Ti-5Al-2.5Fe is indicative of low COF.

- For CP titanium, Ti-6Al-4V and Ti-13Nb-13Zr, the material removal occurs via formation of non-protective tribochemical oxide layer. The cracking and spalling of the tribolayer leads to severe wear of these materials.

- The observation of cracking on the worn surface can be related to the heavy deformation and formation of 'persistent slip bands'.

Based on the current research results, the following materials exhibited the optimum electrochemical and tribological behavior, which can be exploited in the use as an orthopedic implant material.

Table 12: Summary of important experimental results obtained.

Material	Corrosion Rate mils per year (mm/year)	Passivity Range (mV vs. SCE)	Steady State Coefficient of Friction (COF)
CP Titanium	0.036 (0.0009)	1898	0.5
Ti-13Nb-13Zr	0.0045 (0.0001)	1700	0.48
Ti-6Al-4V	0.0550 (0.0013)	1690	0.46
Ti-5Al-2.5Fe	0.0300 (0.0007)	1802	0.3

5.2 Suggestions for Future work

- Study of stabilization of free corrosion potential and subsequent polarization behavior of Ti-13Nb-13Zr can be undertaken. An in depth morphological analysis of passive oxide layer formed on the surface of this alloy can be made, which might provide the reason for superior corrosion resistance exhibited by this alloy as compared to other commercially used orthopedic materials.

- Ability of these materials to repassivate in biological environments can be studied by conducting cyclic anodic polarization experiments.

- Studies on the nature of oxide film formed on the surface of 316L and Ti-based biomedical materials can be conducted so as to know the real mechanism working behind the breakdown of passive film formed on these materials in human body conditions.

- Effect of heat treatment on localized corrosion resistance and passivity of these candidate biomaterials can be investigated.

- The tribological parameters selected in the current research are based on the intention to simulate severe fretting conditions i.e. the highest normal load. However, to better assess the tribological behavior of Ti-alloys further research needs to be carried out in the following directions:

    - To perform wear tests under varying normal load (1-10N).
    - To carry out wear test for different testing duration (100,000 cycles and more).
    - To perform wear test under different linear sliding speed condition.

- To understand the detailed wear mechanism in the above mentioned testing conditions.
- Identify the 'mild' and 'severe' wear regime of titanium alloys and to develop a 'wear map'.

- Wide ranges of biomaterials are used in blood contacting applications. A key challenge for such materials is the ability to resist thrombus formation. Ti and its alloys are widely used in the fabrication of orthopedic and dental implants; hence an attempt can be made for chemical modification of the surface by biocompatible coatings (like hydroxyapatite) on such metallic implants which may allow the attachment of bioactive biomolecules and enhance their osseointegration.

- The corrosion behavior of several existing materials used today is not ideal in all respects. Although a small number of biomaterials have been in use, post-healing surgery is essential in order to remove the implanted material. Further, the implant is obviously an item for which complete resistance of the metal should be aimed at throughout the period of use. Therefore, it is essential to develop a material that can satisfy all the required properties over the stipulated period and then start degrading in the body itself without further surgery. In fact, it is real challenge to scientists and surgeons and has tremendous potential for future research. This will direct the attention to the development of an excellent 'biocompatible and biodegradable polymeric material', which will certainly be a smart material and thereby eliminate costly post-healing operations.

GLOSSARY OF MEDICAL TERMS

Cerclage: The use of a ring or a loop to bind together the ends of an obliquely fractured bone.

Defibrillators: Apparatus used to control heart fibrillation (irregular spontaneous contraction in the individual fibers of a muscle especially in heart).

Distal: Away from the body or origin, e.g. the free end of the limb.

Endoprosthesis: A permanent prosthesis used wholly within the body, e.g. as a replacement for a bone, a joint, a tendon or a ligament.

Extracellular: Outside of a cell or cells.

Femur: The thigh bone in vertebrates.

Haematoma: The collection of blood in tissues due to haermorrhage.

Haermorrhage: An escape of blood from blood vessels; bleeding.

Histological: Structure and composition of organic tissues on microscopic scale.

Intramedullary nail: An implant for introduction into the marrow cavity of long bones forming an internal splint. The nail may be straight or curved and of V, clover-leaf (e.g. Kuntscher nail) or circular cross-section.

Intra-vascular: Situated or occurring within a vessel especially blood vessel.

In-vitro: Literally, 'in glass', e.g. in laboratory.

In-vivo: In a living organism, e.g. a human being.

Lateral: Away from median plane of the body.

Lymph: Away from median plane of the body.

Medial: Towards the median plane of the body.

Median: The longitudinal anteroposterior plane dividing the body into apparently similar halves.

Orthotic: An artificial external device, as a brace or splint, serving to prevent or assist relative movement in the limbs or the spine.

Patella: A small-flattened convex bone covering the front of the knee joint; the kneecap.

Pathology: The study of disease.

Phospholipids: A lipid containing phosphorous which on hydrolysis yields fatty acids, glycerin, and a nitrogenous compound. Lecithin cephalin and sphingomyelin are the best-known examples.

Physiological Environment: The study of the function of the body.

Plasma: Anything formed or molded. The fluid portion of the blood in which corpuscles are suspended.

Prosthesis: Any device that replaces an anatomical part or deficiency.

Proximal: Nearer to the body or origin, e.g. the root of a limb.

Resorption: The loss of substance through physiological or pathological means, such as loss of dentin and cementum of a tooth.

Telemetric: The making of measurements at a distance from the subject, the measurable evidence of the phenomena under investigation being transmitted by radio signals.

Tibia: Inner and larger of the two bones of lower leg, between the knee and the ankle.

Total joint replacement: The replacement of a joint by an endoprosthesis.

Trauma: A wound or injury.

BIBLIOGRAPHY

1. Galante J.O., Laing P.G., Lautenschloger E., *BIOMATERIALS AAOS Instr. Course Lect.*, 24:1, (1975).

2. Friedman R.J., Black J., Galante J.O., Jacobs J.C., Skinner H.B., Correct Concepts in Orthopedic BIOMATERIALS and Implant fixation, *J Bone Joint Surg. (Am)*, 75A, 1086-1090, (1993).

3. William D.F., Critical Reviews in BIOCOMPATIBILITY CRC Press Inc.; Boca Raton, FL, USA; (1996).

4. Mathieson E.B., Ahlbohm A., Berman, Linggrn J.O., Total Hip Replacement and Cancer, (Br) 77B, 345-350, (1992).

5. Wickstrom J.K., Surgical Implants-The Mechanical and Environmental Problems, *Journal of Materials*, 1,366-372, (1966).

6. Bardos D.I., Stainless Steels in Medical Devices, in *Handbook of Stainless Steels,* (Eds) D. Peckner and I.M. Bernstein, 42.1-42.10. McGraw-Hill, New York (1977).

7. Luckey H.A., Kubli Jr. F., Editors Introduction in, Titanium Alloys in Surgical Implants, *ASTM Publication* STP 796-800,1-3,Phiadelphia (1983).

8. Lemons J.E., Venugopalan R. and Lucas L.C.: Corrosion and Biodegradation, In: *Handbook of Biomaterials Evaluation*, Ed: A. Von Recum, Taylor Francis, Inc., 2,155-170, (1999).

9. ASTM G5: Standard reference test method for making Potentiostatic and Potentiodynamic anodic polarization measurements. In: Metals, Test Methods and Analytical Procedures, PA: *American Society for Testing and Materials*, 03.02.Philadelphia, 48-58, (1995).

10. Brown S.A. and Meritt K., Electrochemical Corrosion in Saline and Serum, *Journal of Biomedical Materials Research*, 14,173-175, (1980).

11. Kruger, Jerome, Fundamental Aspects of the Corrosion of Metallic Implants, Corrosion and Degradation of Implant Materials, B.C. Syrett and A. Acharya, Eds, *American Society for Testing and Materials, ASTM* STP 684,107-127, (1979).

12. Litsky A.S., Spector M., Biomaterials-Orthopaedic basic science, American academy of orthopaedic surgeons, Simon SR (ed), 470–473, (1994).

13. Jacobs J.J., Gilbert J.L., Urban R.M., Corrosion of metal orthopaedic implants. *Journal of Bone and Joint Surgery*, 80A, 268 – 282, (1998).

14. Atkinson J.R., Jobbins B. Properties of Engineering materials for use in the body, In Dowson D., Wright V. (eds). Introduction to the Biomechanics of Joints and Joint Replacement, London, Mechanical Engineering Publications Ltd, (1981).

15. Williams D.F., The Deterioration of Materials in used in Implants in Surgery, (Eds) D.F. Williams and R. Roaf, W.B. Saunders, Philadelphia, 137-183, (1973).

16. Pourbaix M., Electrochemical Corrosion of Metallic Biomaterials, *Biomaterials*, 5, 122-134 (1984).

17. Bardos D.I., Stainless Steels in Medical Devices, in *Handbook of Stainless Steels*, (Eds) D. Peckner and I. M. Bernstein, 42.1-42.10 McGraw-Hill, New York (1977).

18. Zapffe C.A., Human Body fluids affect Stainless Steel, Metal Progress, 67, 95-98, (1965).

19. Hughes A.N., Jordan B.A. and Orman S., The Corrosion Fatigue Properties of Surgical Implant Materials. Third Progress Report-May 1973, *Engineering in Medicine*, 7, 135-141 (1978).

20. Walker G.D., *Journal of Biomedical Materials Research* (Symposium), 5, 11-26 (1974).

21. Jacobson B., and Webster J.B., Chapter 10. Surgery in Medicine and Clinical Engineering, (Eds) Jacobson and Webster Prentice-Hall Inc., New Jersey, 525-532, (1977).

22. Guyton A.C., Chapter 33, Partition of the Body Fluids Osmotic Equilibria between Extracellular and Intracellular Fluids, in Textbook of Medical Physiology (5th Edition), (Ed.) Guyton A.C., W.B. Saunders, Philadelphia, 424-437, (1976).

23. Greene N.D., Corrosion of surgical implant alloys: A few basic ideas, in Corrosion and Degradation of Implant materials, Second Symposium, (Eds) A.C. Fraker and C.D. Griffin, ASTM Publication STP 859, Philadelphia (1985).

24. Laing P.G., Compatibility of Biomaterials, Orthopaedic Clinics of North America, 4, 249-273 (1973).

25. Pazzaglia U.E., Minola C., Gualtieri G., Gualtieri, Riccardi C., Cecillani L., Metal ions in body fluids after arthroplasty. *Acta Orthop Scand*, 57, 415 – 418, (1986).

26. Dorr L.D., Bloebaum R., Emmanual J., Meldrum R., Histologic, Biochemical, and ion analysis of tissue and fluids retrieved during Total Hip Arthroplasty. *Clin Orthop*, 261, 82 – 95, (1990).

27. Urban R.M., Jacobs J.J., Gilbert J.L., Galante J.O., Migration of corrosion products, from modular hip prostheses. Particle microanalysis and histopathological findings. *Journal of Bone and Joint Surgery*, 76A, 1345–1359, (1994).

28. Park J.B., Lakes R.S., Metallic Implant Materials, In Biomaterials-an Introduction, and ed, New York, Plenum Press, 75-115, (1992).

29. Black J., Metallic Ion Release and its relationship to Oncogenesis, In Fitzgerald RH Jr (ed): The Hip, St. Louis, Mosby, 199-213, (1985).

30. Hoar T.P., and Mears D.C., Corrosion Resistant Alloys in Chloride Solutions, *Proceedings of Royal Society*-Series A, 294, 486-510 (1966).

31. Lucas L.C., Buchanan R.A., Lemons J.E., and Griffin C.D., Susceptibility of Surgical Cobalt-base Alloy to Pitting Corrosion, *Journal of Biomedical Materials Research*, 1, 405-414 (1967).

32. Svare C.W., Belton G., and Korostoffe E., The Role of Organics in Metallic Passivation, *Journal of Biomedical Materials Research,* 457-467 (1970).

33. Revie R. and Greene N.D., Comparison of the In-Vivo and In-Vitro Corrosion of 18-8 Stainless Steel and Titanium, *Journal of Biomedical Materials Research*, 3,465-470 (1969).

34. Colangelo V.T., Greene N.D., Kettelkamp D.B., Alexander H., and Campbell, C.J., Corrosion Rate Measurement In-Vivo, *Journal of Biomedical Materials Research*, 1, 405-414 (1967).

35. Steinemann S.G., Corrosion of Surgical Implants- In-Vivo and In-Vitro Tests, in Evaluation of Biomaterials, (Eds) G.D. Winter, J.L. Leray and K. deGroot, *Advanced Biomaterials*, 1,1-34 (1980).

36. Buchanan R.A. and Lemons J.E., In-Vivo Corrosion-Polarization Behaviour of Titanium-Base and Cobalt-Base Surgical Alloys, Transactions of the 8th Annual Meeting of the Society of Biomaterials, 5,110 (1982).

37. Brown S.A. and Merritt K., Fretting Corrosion in Saline and Serum, *Journal of Biomedical Materials Research*, 15, 867-878 (1981).

38. Thull R. and Schaldach M., Corrosion of Highly Stressed Orthopaedic Joint Replacements, in Engineering Medicine: Advances in Artificial Hip and Knee Joint Technology, (Eds) M. Schaldach and D. Hohmann, Springer Verlag, Berlin, Heidelberg, New York, 242-256, (1976).

39. Bundy K.J., Vogelbaum M.A. and Desai V.H., The influence of Static Stress on the Corrosion Behaviour of 316L Stainless Steel in Ringer's Solution, *Journal of Biomedical Material's Research*, 20,493-505, (1986).

40. Semlitsch M., and Willert H.G., Properties of Implant alloys for artificial Hip Joints, *Medical and Biological Engineering and Computing*, 18, 511-520 (1980).

41. Revie R.W., Greene N.D., Corrosion Behaviour of Surgical Implant Materials1: Effect of Sterilisation, *Corrosion Science*, 9,755-761, (1969).

42. Revie R.W., Greene N.D., Corrosion Behaviour of Surgical Implant Materials 2: Effect of Surface Preparation, *Corrosion Science*, 9, 763-770 (1969).

43. Mueller H.J. and Greener E.H., Polarization Studies of Surgical Materials in Ringer's Solution, *Journal of Biomedical Materials research*, 4, 29-41 (1970).

44. Ogundele G.I., and White W.E., Polarization Studies on Surgical- Grade Stainless Steels in Hank's Physiological Solution, in Corrosion and Degradation of Implant Materials, second symposium, (Eds) Fraker A.C. and Griffin C.D., *ASTM Publication STP* 859, Philadelphia 117-135, (1985).

45. White W.E., Postlethwaite J. and LeMay I., in Microstructural Science, *American Elsevier*, New York, 4,145-157 (1976).

46. Black J., Corrosion and degradation in Orthopaedic biomaterials in research and practice, New York, Churchill, Livingstone, 235-266, (1988).

47. Griffin C.D., Buchanan R.A., Lemons J.E., In vivo electrochemical corrosion study of coupled surgical implant materials. *Journal of Biomedical Materials Research*, 17,489–500, (1983).

48. Syrett B.C. and Wing S.S., Pitting Resistance of New and Conventional Orthopaedic Implant Materials-Effect of Metallurgical Condition, *Corrosion*, 34A, 138-145, (1978).

49. Syrett B.C., and Davis E.E., Crevice Corrosion of Implant Alloys-A comparison In-Vitro and In-Vivo Studies, Presented at Spring Meeting of ASTM, Kansas City, MO. (1978).

50. Sury P., Corrosion Behaviour of Case and Forged Implant Materials for Artificial Joints, Particularly with Respect to Compound Designs. Research and Development Department, Sulzer Brothers Ltd., CH-8401, Winterthur, Switzerland.

51. Cohen J., Clinical failure Caused by Corrosion of a Vitalium Plate, *Journal of Bone and Joint Surgery*, 54A, 617-628 (1972).

52. Rose R.M., Schiller A.L. and Radin E.L., Corrosion-Accelerated Mechanical Failure of Vitalium Nail-Plate, *Journal of Bone and Joint Surgery*, 54A, 854-862 (1972).

53. Cahoon J.R., Bandyopadhya R. and Tennese L., The Concept of Protection Potential Applied to the Corrosion of Metallic Orthopaedic Implants, *Journal of Biomedical Materials Research*, 9, 259-264, (1975).

54. Morral F.R., Crevice Corrosion of Cobalt Based Surgical Alloys, *Journal of Materials*, 1, 384 (1966).

55. Rostoker W., Pretzel C.W. and Galante J.O., Couple Corrosion Among Alloys for skeletal Prostheses, *Journal of Biomedical Materials Research*, 8, 407-419 (1974).

56. Syrett B.C., and Wing S.S., An Electrochemical Investigation of Fretting Corrosion of Surgical Implant Materials, *Corrosion*, 34, 379-386 (1978).

57. Cohen J., Corrosion Testing of Orthopaedic Implants, *Journal of Bone and Joint Surgery*, 44A, 307-316 (1962).

58. Lucas L.C., Buchanan R.A., Lemons J.E., and Griffin C.D., Susceptibility of Surgical Cobalt-base Alloy to Pitting Corrosion, *Journal of Biomedical Materials Research*, 16, 799-810 (1982).

59. Bowden F.P., Williamson J.B.P., Laing P.G., The Significance of Metal Transfer Orthopaedic Surgery, *Journal of Bone and Joint Surgery*, 37B, 676-690, (1955).

60. Gilbert T.L., Buckley C.A., Jacobs J.J., In vivo Corrosion of Modular Hip Prosthesis components in mixed and similar combinations. The effect of crevice, stress, motion and stress coupling, *Journal of Biomedical Materials Research*, 27,1533 - 1544, (1993).

61. Pugh J., Dee R., Properties of Musculosk-eletal tissues and Biomaterials, In Dee R, Mango E, Hurst LC (eds); *Principles of Orthopaedic Practice*, New York, McGraw Hill, (1988).

62. Greener E., Lauten Schlager E., Materials for Bioengineering Applications, In: Brown JHV, Jacobs JE and Stuart L (eds): *Biomedical Engineering*, Philadelphia, FA Davis, (1971).

63. Colangelo V.J., and Greene N.D., Corrosion and Fracture of Type 316 SMO Orthopaedic Implants, *Journal of Biomedical Materials Research*, 3, 247-265, (1969).

64. Cahoon J.R., and Paxton H.W., Metallurgical Analyses of Failed Orthopaedic Implants, *Journal of Biomedical Materials Research*, 2, 1-22, (1968).

65. Sheehan J.P., Morin C.R. and Packer K.F., Study of Stress Corrosion Cracking Susceptibility of Type 316L Stainless Steel In-Vitro, in Corrosion and Degradation of Implant Materials, Second Symposium, (Eds) A.C. Fraker and C.D. Griffin, *ASTM Publication STP 859*, 57-72, Philadelphia (1985).

66. Bundy K.J., and Desai V.H., Studies of Stress-Corrosion Cracking Behaviour of Surgical Implant Materials Using a Fracture Mechanics Approach, in Corrosion and Degradation of Implant Materials, Second Symposium, (Eds) A.C. Fraker and C.D. Griffin, *ASTM Publication STP 859*, 73-90, Philadelphia (1985).

67. Leclerc M.F., A Review of the Factors Influencing the Mechanical Failure of the Femoral Component used in Total Hip Replacement, Proceedings: *Engineering in Orthopaedic Surgery and Rehabilitation*, published by Bioengineering Unit, Princess Margaret Rose Hospital, 36-48, Edinburgh (1982).

68. Bechtol C.O., Failure of Femoral Implant Components in Total Hip Replacement Operations, *Orthopaedic Review*, 4, 23-29, (1975).

69. Hughes A.N., Jordan B.A. and Orman S., The Corrosion Fatigue Properties of Surgical Implant Materials, Third Progress Report-May 1973, *Engineering in Medicine*, 7, 135-141 (1978).

70. Rollins V., Arnold B. and Lardner E., Corrosion Fatigue in High Carbon Steel, *British Corrosion Journal*, 5,33 (1970).

71. Piehler H.R., Portnoff M.A., Sloter L.E., Vegdahl E.J., Gilbert J.L. and Weber M.J., Corrosion-Fatigue Performance of Hip Nails: The Influence of Materials Selection and Design, in Corrosion and Degradation of Implant Materials, Second Symposium, (Eds) Fraker A.C. and Griffin C.D., *ASTM Publication STP 859*, 93-104, Philadelphia (1985).

72. Hille G.H., *Journal of Materials*, 1:2, 373, (1966).

73. McMaster J.A., Titanium for Prosthetic Devices, presented at IMD Dental-Medical Committee, *American Institute of Mechanical Engineers*, Cleveland, 21 Oct. (1974).

74. Greene N.D., Onkelinx C., Richelle L.J., Ritland G.D. and Ward P.A., Biomaterials: Improved Implant Alloys, presented in Brighton Implant Meeting, Brighton, Utah, 8-9 Nov. (1972).

75. Hochman R. and Mark M., In-Vivo Evaluation of Mechanical and Corrosion Characteristics of Ti and Ti-6Al-4V ELI, presented at MATCON ' 74, *ASM/TMS-AIME*, Detroit, 22 Oct. (1974).

76. Titanium Alloys Handbook MCIC-HB02, MCIC (1972).

77. ASTM: Standard specification for unalloyed and alloyed titanium for surgical implant applications. In: Medical Devices and Services, Philadelphia, PA: *American Society for Testing and Materials*, 13.01, 1-20, (1998).

78. Farthing T.W., The Development of Titanium and its Alloys, *Clinical Materials*, 1-2, Feb. (1987).

79. Agins H.J., Alcock N.W. Metallic Wear in Failed Titanium - Alloy Total Hip Replacements. Arthrological and Quantative Analysis, *Journal of Bone and Joint Surgery. (Am)*, 70A, 347–356, (1988).

80. Titanium as a metal for implantation – Part 2: Biological properties and Clinical applications. *Journal of Medical Engineering Technology*, 1, 266-270, (1977).

81. Bluementhal N.C., Cosma V. Inhibition of Apatite formation by Titanium and Vanadium ions. *Journal of Biomedical Materials Research*, 23, 13-22, (1989).

82. Torgerson S., Gjerdet N.R., Retrieval study of Stainless Steel and Titanium miniplates and screws used in Maxillofacial Surgery, *Journal of Material Science*: Mater Med, 5, 256-262, (1994).

83. Scales J.T., Black J., Staining around Titanium alloy Prosthesis–an orthopaedic enigma. *Journal of Bone and Joint Surgery*, 73B, 534-536, (1991).

84. Mirza Rosca J.C., Gonzalez S., Llorente M.L., Popa M.V., Vasilescu E. and Drob P. In: 7th European Conference on Applications of Surface and Interface Analysis Wiley, New York, 377-380, (1997).

85. Popa M.V., Vasilescu E., Mirza Rosca J.C., Rodrigues J.J.S., Gonzalez S., Drob P. in: M. Andritschky (Ed.), *Advances in Materials and Processing Technologies*, 2-AMPT'97, 737, (1997).

86. Popa M.V., Radovici O., Vasilescu E., Mirza Rosca J.C., Gonzalez S., Drob P., *9th Proceedings of the International Metallurgy and Materials Congress*, 1, p.209, (1997).

87. Yu S.Y. and Scully J.R., *Corrosion*, 12, 965, (1997).

88. Bandyopadhya R. and Cahoon J.R., Effect of composition on the Electrochemical behaviour of Austenitic Stainless Steel in Ringer's solution, Corrosion, 33, 204-208, (1977).

89. Cahoon J.R., Chaturvedi M.C., and Tennese L., Corrosion studies on metallic implant materials, JAAMI 7, 131-135, (1973).

90. Donachie M.J., Titanium-a technical guide. OH, USA: *ASM International*, (1988).

91. Steinemann S.G. et al., Beta Titanium Alloy for Surgical Implants, *Titanium 92 Science and Technology*, 3, 2689-2696, TMS, (1993).

92. Hoar T.P. and Mears D.C., Corrosion-resistant alloys in chloride solutions: materials for surgical implants, Pro Royal Soc 294A, 486-510, (1966).

93. Kovacs P., Davidson J.A., The electrochemical behaviour of a new titanium alloy, Ti-13Nb-13Zr. Presented at the 19th Annual meeting of the Society for Biomaterials. Davidson JA, Mishra AK, Kovacs P, Poggie RA. New surfacehardened, low modulus, corrosion resistant Ti-13Nb-13Zr alloy for total hip arthroplasty. *Biomedical Materials Engineering*, 4, 231-243, (1994).

94. Sousa S.R., Barbosa M.A., Corrosion resistance of titanium CP in saline physiological solutions with calcium phosphate and proteins. *Clinical Materials*, 12, 1-4, (1993).

95. Gurappa I., Characterization of Different Materials for Corrosion Resistance under Simulated Body Fluid Conditions, *Materials Characterization*, 49, 73-79, (2002).

96. Kovacs P., Davidson J.A., The electrochemical behaviour of a new titanium alloy, Ti-13Nb-13Zr. Presented at the 19th Annual meeting of the Society for Biomaterials, (1993-88).

97. Williams D.F., Physiological and Microbiological Corrosion, *Critical Reviews on Biocompatibility*, 1, 1-24, (1985).

98. Khan M.A. et al., The Corrosion behaviour of Ti-6Al-4V, Ti-6Al-7Nb and Ti-13Nb-13Zr in Protein Solutions, *Biomaterials*, 20, 631-637, (1999).

99. Andreeva V. and Kazarin V., *Proceedings of third International Congress on Metallic Corrosion*, Mir Publications, Moscow, 1, 464, (1969).

100. Fraker A.C., Ruff A.W., and Yeager M.P., Proceedings, Second International Titanium Conference, Plenum, New York, (1976) (preprint).

101. Tomashov N.D., *Corrosion*, 20, 7t, (1964).

102. Bomberger H.B., Alloying to Improve Crevice Corrosion Resistance of Titanium, *presented at MATCON '74, ASM/TMS-AIME*, Detroit, 22 Oct. (1974).

103. Sousa S.R., Barbosa M.A. Corrosion Resistance of Titanium CP in saline physiological solutions with calcium phosphate and proteins, *Clinical Materials*, 12, 1-4, (1993).

104. Davidson J., Kovacs P., Biocompatible Low-Modulus Titanium Alloy for Medical Implants, U.S. Patent No. 5169597 (1992).

105. Brown B.F., Fujii C.T., Dahlberg E.F., Methods for studying solution chemistry within stress corrosion cracks, *Journal of Electrochemical Society*, 116, 218, (1969).

106. Schutz R., An Overview of Beta Titanium Alloy Environmental Behaviour, In Beta Titanium Alloys in the 1990's eds. D. Eylon, R. Boyer, 75, D. Koss (Warrendale, PA: TMS, 1993), 75.

107. Stern M., Wissenberg H., Influence of Noble metal alloying additions on Electrochemical and Corrosion behavior of Titanium, *Journal of Electrochemical Society*, 106.9, 755, (1959).

108. Kolman D.G., Scully J., Electrochemistry and passivity of Ti-15V-3Al-3Sn beta Titanium alloy in ambient chloride solutions, *Journal of Electrochemical Society*, 141, 10, 2.633, (1994).

109. Silverman D., Derivation and Application of EMF-pH Diagrams, in Electrochemical Techniques for Corrosion Engineering, ed. R. Baboian (Houston, TX: NACE), 117, (1986).

110. Beck T.R., Pitting of Titanium, Electrochim. *Acta 18*, 807, (1973).

111. Baes C., Mesmer R., The Hydrolysis of Cations, 147, New York, NY: Jhon Wiley and Sons, (1976).

112. Beck T.R., in Localized Corrosion, ed. B.F. Brown, Houston, TX: NACE, 644, (1974).

113. Dugdale I., Cotton J., *Corrosion Science*, 4, 397, (1964).

114. Yu S.Y. and Scully J.R., Corrosion and Passivity of Ti-13Nb-13Zr in Comparison to Other Biomedical Implant Alloys, *Corrosion*, 53-12, 965-976, (1997).

115. Simpson J., Electrochemical behavior of titanium and titanium alloys with respect to their use as Surgical Implant materials in Biological and and Biomedical performance of Biomaterials. Eds. P. Christel A. Meunier A. Lee, p.63, Amsterdam, The Netherlands: Elseveir Science Publishers, (1986).

116. Jones D.A., Principles and Prevention of Corrosion, Maxwell Macmillan, New York (1992).

117. Bockris J.O'M., Modern Aspects of Electrochemistry, Butterworths, (1954).

118. Tomashov N.D., Theory of Corrosion and protection of Metals, Macmillan, (1966).

119. Baboian R., Ed., Electrochemical Techniques for Corrosion, *National Association of Corrosion Engineers*, (1977).

120. Bertocci U. and Mansfield F., Ed., Electrochemical Corrosion Testing, STP 727, *American Society for Testing and Materials*, (1979).

121. Bard A.J. and Faulker L.R., Electrochemical methods: Fundamentals and Applications, p.19, John Wiley and Sons, Inc., (1980).

122. Hoare J.P., Passivity of Metals, Frankenthal R.P. and Kruger J., editors, Electrochemical Society monograph series, Princeton, NJ, p. 505, (1978).

123. Martin R.L., Application of Electrochemical Polarization to Corrosion Problems, Petrolite Corp., St. Louis, MO (1977).

124. Hack H. and Scully J.R., Crevice Corrosion behavior of 45 molybdenum containing Steels in sea water, *Corrosion*, 42, 79, (1986).

125. Mansfeld F., Electrochemical Methods, edited by Baboian R., *National Association of Corrosion Engineers*, Houston, TX, 67-71, (1996).

126. Anand R. R., *21st Annual Conference of NACE*, St. Louis, MO (1965).

127. Kaesche H., Metallic Corrosion, *National Association Corrosion Engineers*, Houston TX, p. 92, (1985).

128. Martin R.L., Application of Electrochemical Polarization to Corrosion Problems, Petrolite Corp., St. Louis, MO (1977).

129. Metals Test Methods and Analytical Procedures, *Annual Book of ASTM Standards*, 3.02, Section 3, Philadelphia, USA, (1987).

130. Klaffke D., *Tribology International*, 22, 89, (1989).

131. Solar R.J., Corrosion Resistance of Titanium surgical implant Alloys, A Review, Corrosion and Degradation of Implant Materials, *American Society for Testing of Materials*, STP 684, 259-273, (1979).

132. Brown S.A and Simpson J.P., Crevice and Fretting Corrosion of Stainless Steel plates and screws, *Journal of Biomedical materials research*, 15, p 867-878, (1988).

133. Collings E.W., Physical Metallurgy of Titanium Alloys, Materials Properties Handbook: Titanium Alloys, *ASM International*,1-22, (1994).

134. Margolin H. and Farrar P., The physical Metallurgy of Titanium Alloys, Ocean Engineering, 1, 329-343, (1969).

135. Murakami Y., Critical Review: Phase Transformations and Heat Treatment, *Titanium 80*, The Metallurgical Society of AIME, Warrendale, PA, 153-167, (1981).

136. Bundinski K.G., Tribological Properties of Titanium alloys, *Wear*, 151, 203-217, (1991).

137. Mathew Donachie J., Jr., Titanium a Technical Guide, *ASM International*, 2nd Edition, 143-282, (2000).

138. Black J., Biological Performance of Materials: Fundamentals of Biocompatibility, Marcel Decker Inc., New York, NY, 2nd Edition, 38-59, (1992).

139. Hutchings I.M. and Mercer A.P., The influence of atmosphere composition on the abrasive wear of titanium and Ti-6Al-4V, *Wear*, 124, 165-176, (1988).

Appendix (A)

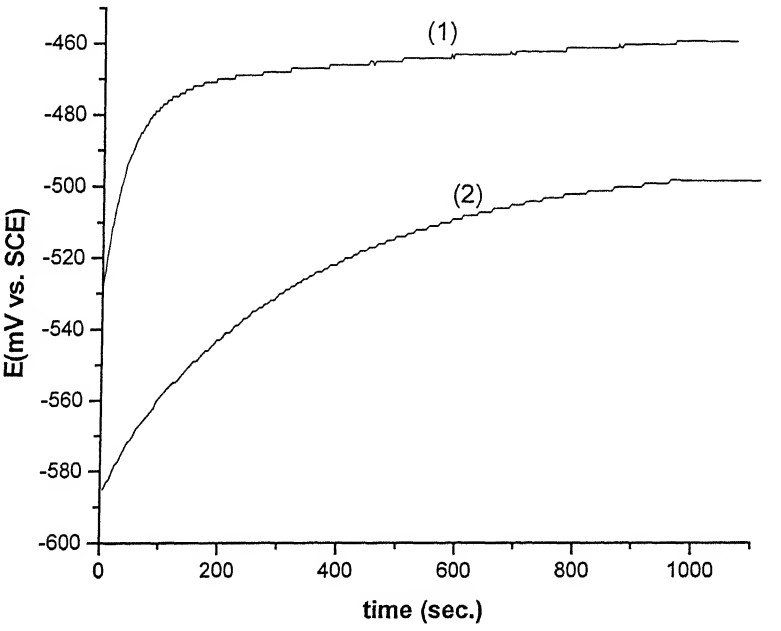

Figure 1: Open circuit potential as function of time for CP Titanium in Hank's Solution at 37°C temperature and 7.4 pH.

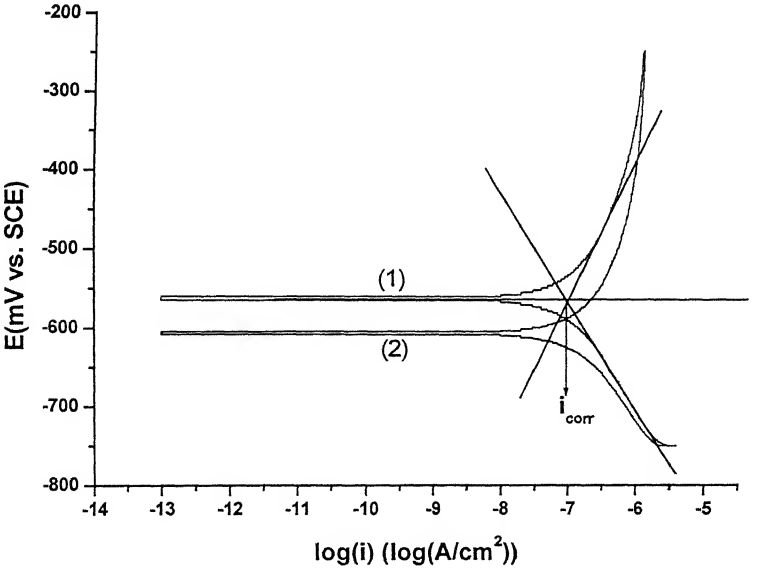

Figure 2: Tafel extrapolation curve for CP Titanium in Hank's Solution at 37°C temperature and 7.4 pH.

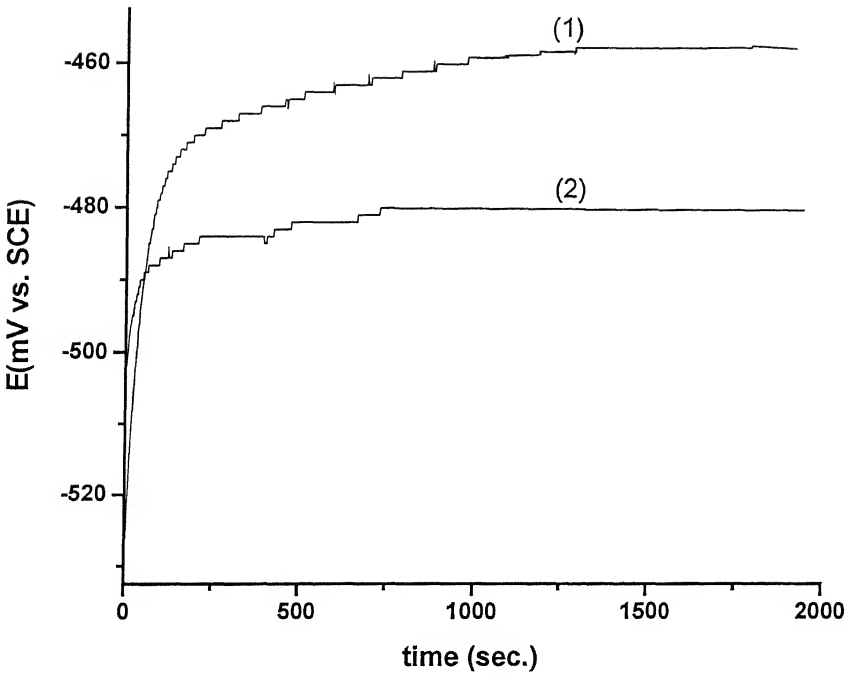

Figure 3: Open circuit potential as function of time for CP Titanium in Hank's Solution at 37°C temperature and 7.4 pH.

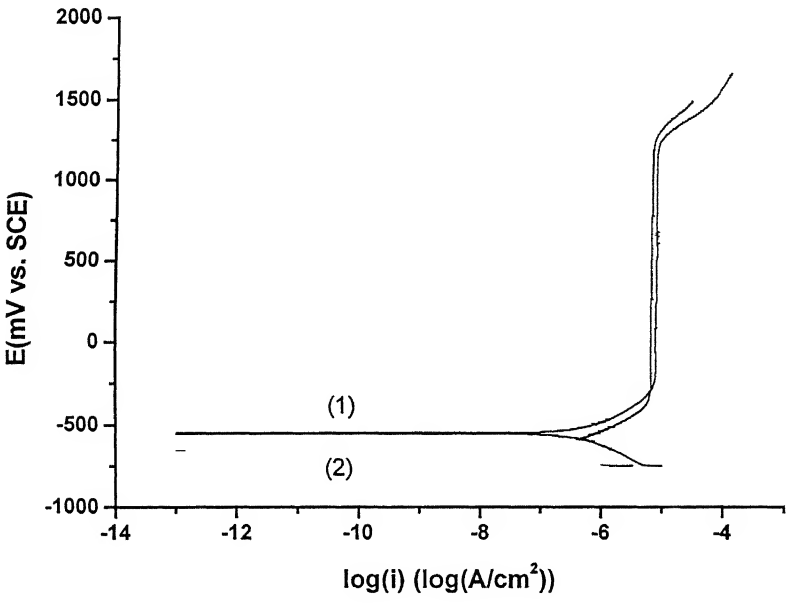

Figure 4: Potentiodynamic polarization curve for CP Titanium in Hank's Solution at 37°C temperature and 7.4 pH.

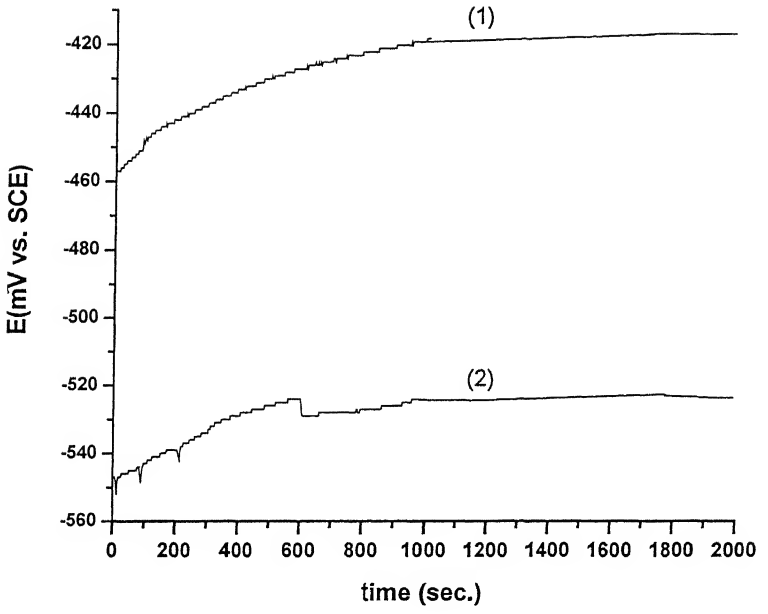

Figure 5: Open circuit potential as function of time for Ti-15Al in Hank's Solution at 37°C temperature and 7.4 pH.

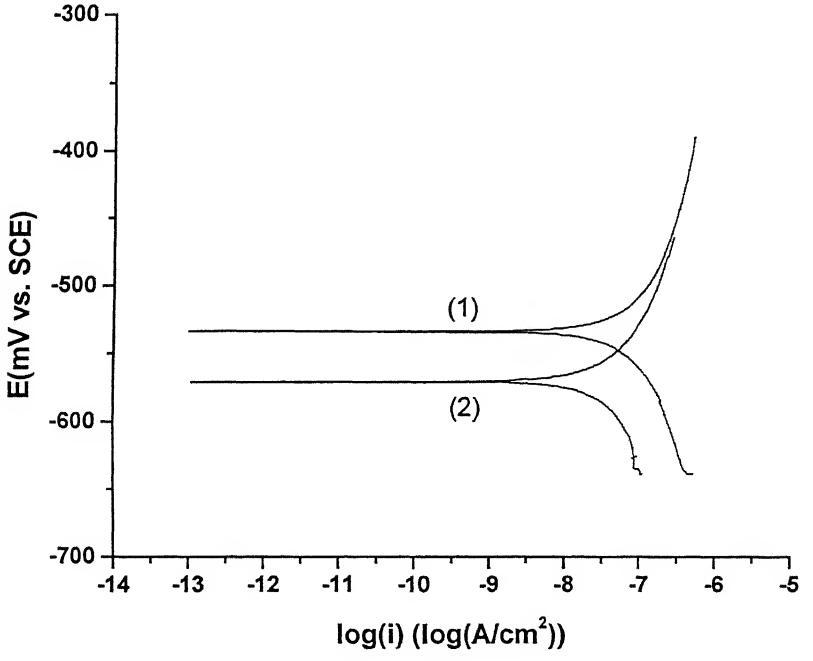

Figure 6: Tafel extrapolation curve for Ti-15Al in Hank's Solution at 37°C temperature and 7.4 pH.

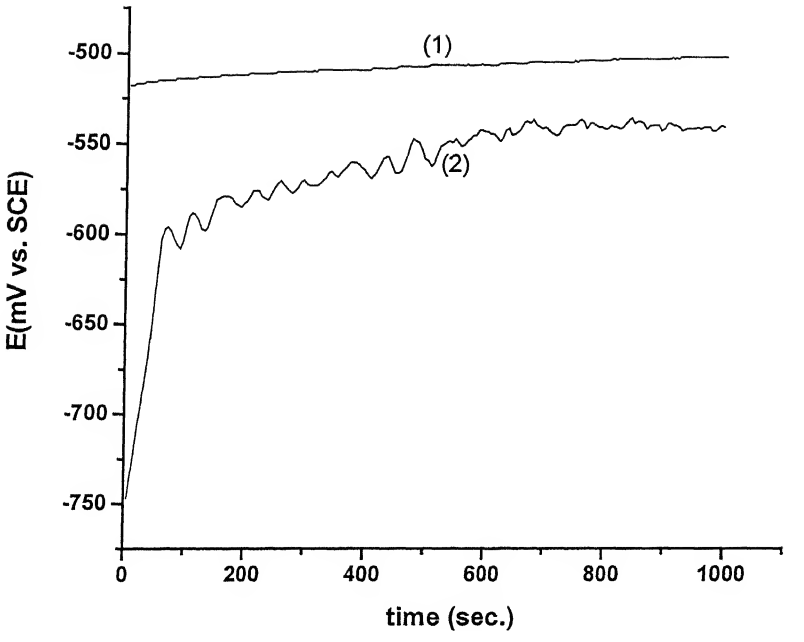

Figure 7: Open circuit potential as function of time for Ti-15Al in Hank's Solution at 37°C temperature and 7.4 pH.

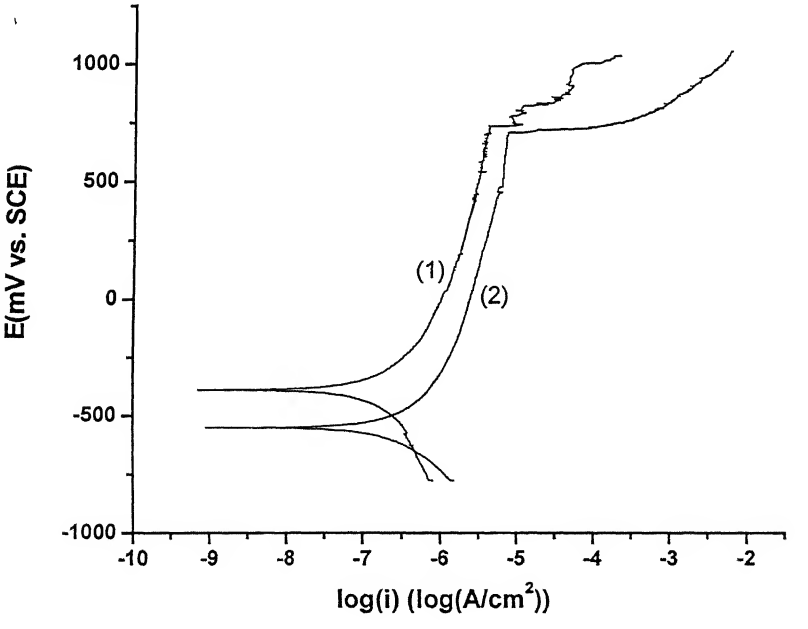

Figure 8: Potentiodynamic polarization curve for Ti-15Al in Hank's Solution at 37°C temperature and 7.4 pH.

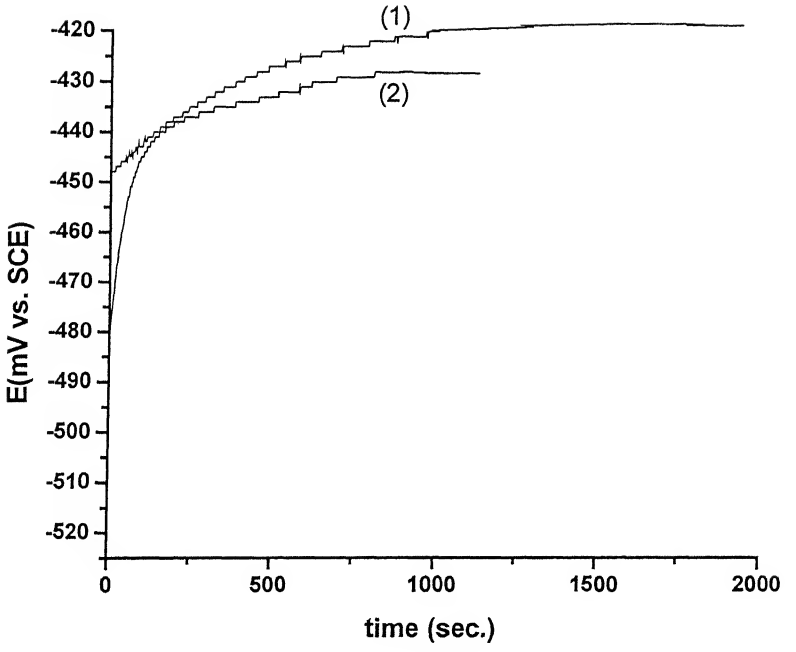

Figure 9: Open circuit potential as function of time for Ti-5Al-2.5Fe in Hank's Solution at 37°C temperature and 7.4 pH.

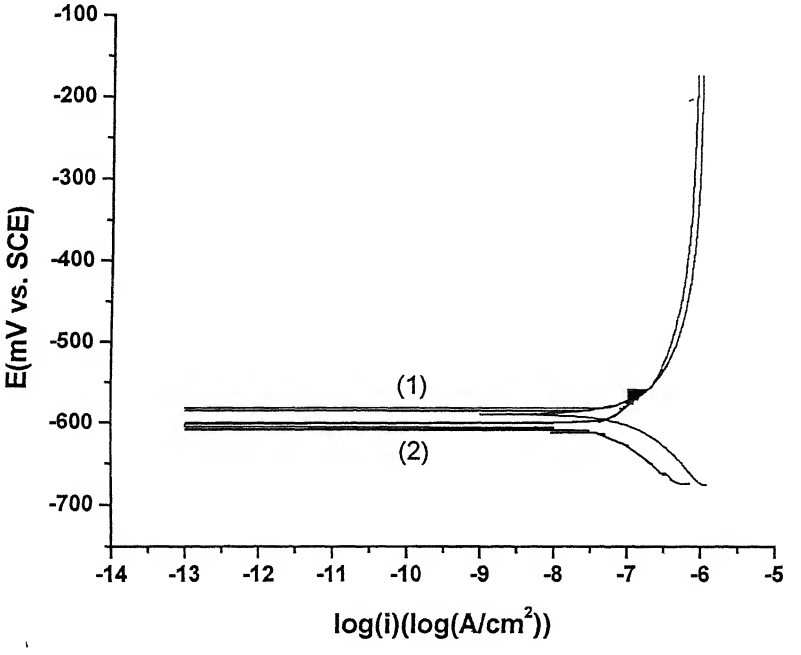

Figure 10: Tafel extrapolation curve for Ti-5Al-2.5Fe in Hank's Solution at 37°C temperature and 7.4 pH.

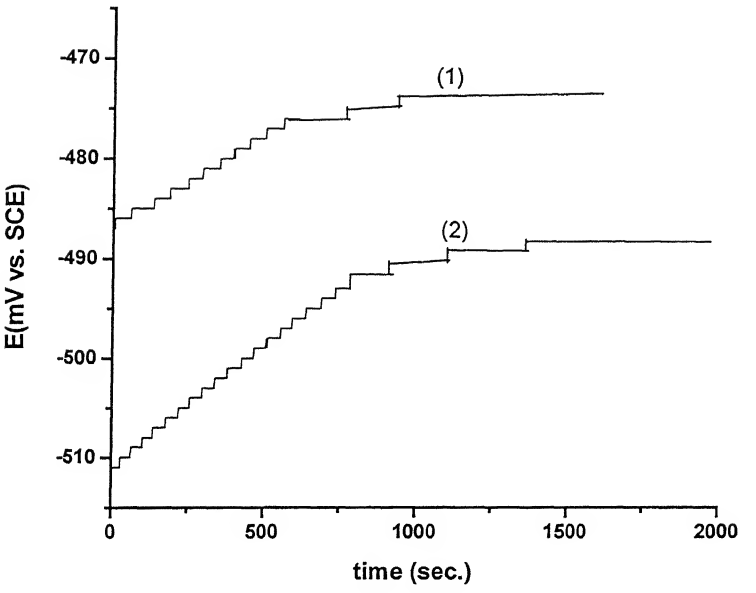

Figure 11: Open circuit potential as function of time for Ti-5Al-2.5Fe in Hank's Solution at 37°C temperature and 7.4 pH.

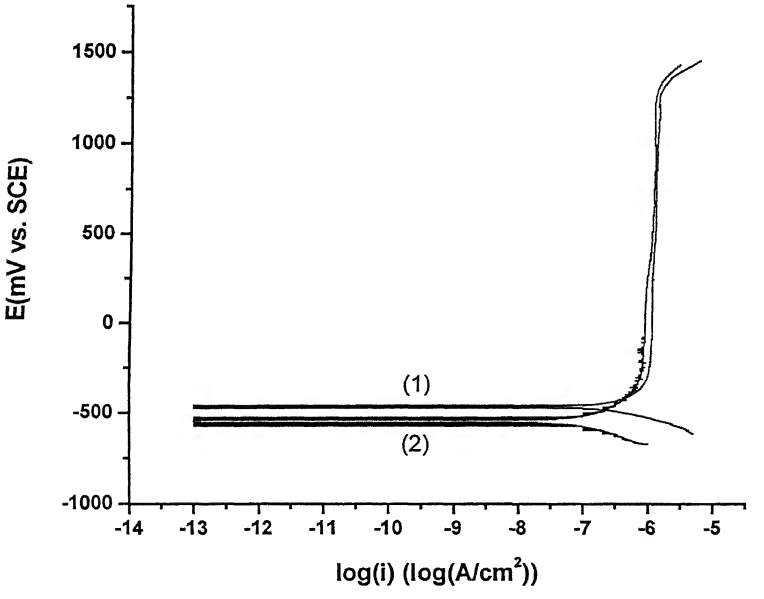

Figure 12: Potentiodynamic polarization curve for Ti-5Al-2.5Fe in Hank's Solution at 37°C temperature and 7.4 pH.

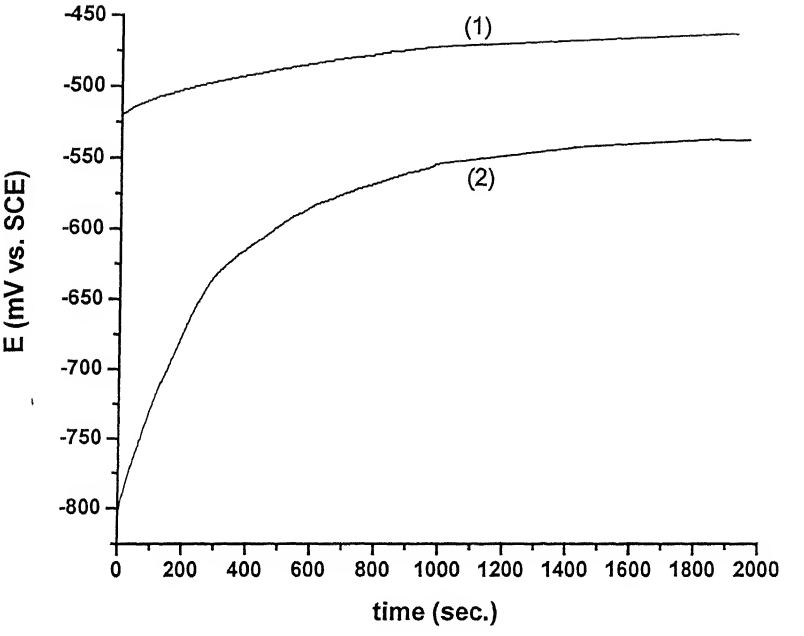

Figure 13: Open circuit potential as function of time for Ti-13.4Al-29Nb in Hank's Solution at 37°C temperature and 7.4 pH.

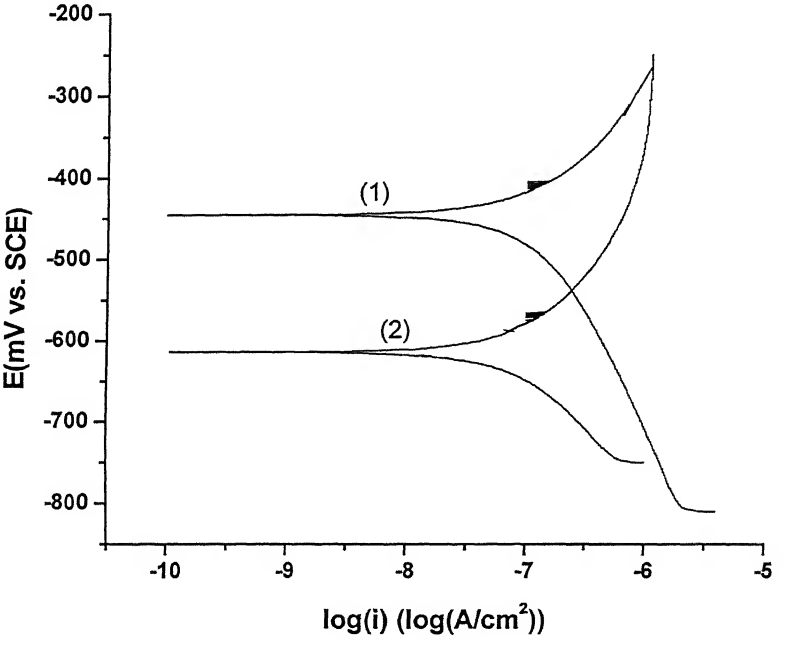

Figure 14: Tafel extrapolation curve for Ti-13.4Al-29Nb in Hank's Solution at 37°C temperature and 7.4 pH.

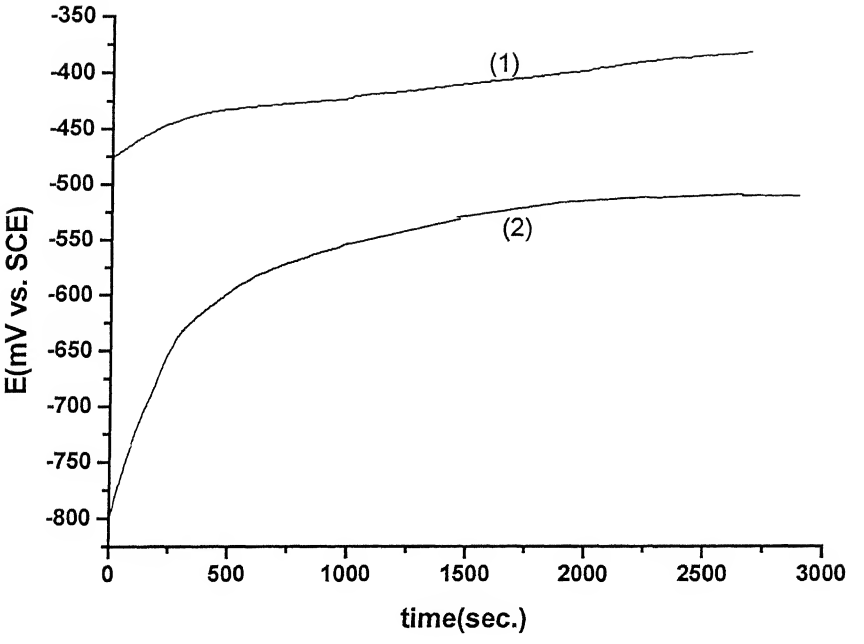

Figure 15: Open circuit potential as function of time for Ti-13.4Al-29Nb in Hank's Solution at 37°C temperature and 7.4 pH.

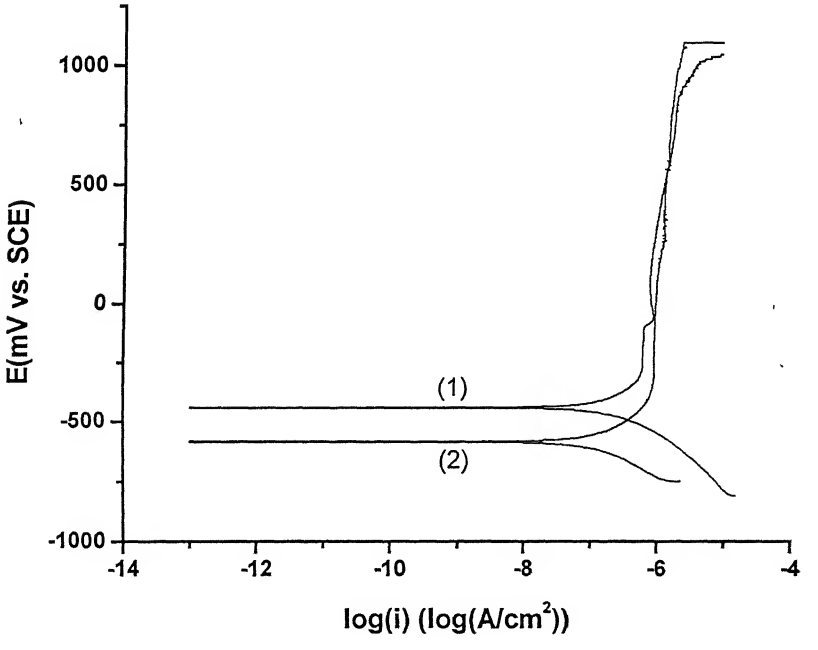

Figure 16: Potentiodynamic polarization curve for Ti-13.4Al-29Nb in Hank's Solution at 37°C temperature and 7.4 pH.

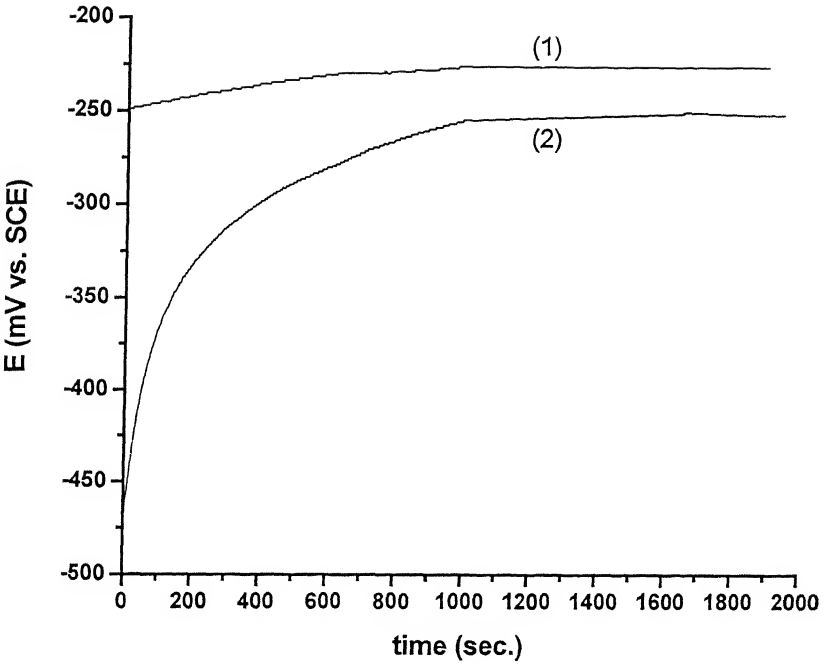

Figure 17: Open circuit potential as function of time for Ti-6Al-4V in Hank's Solution at 37°C temperature and 7.4 pH.

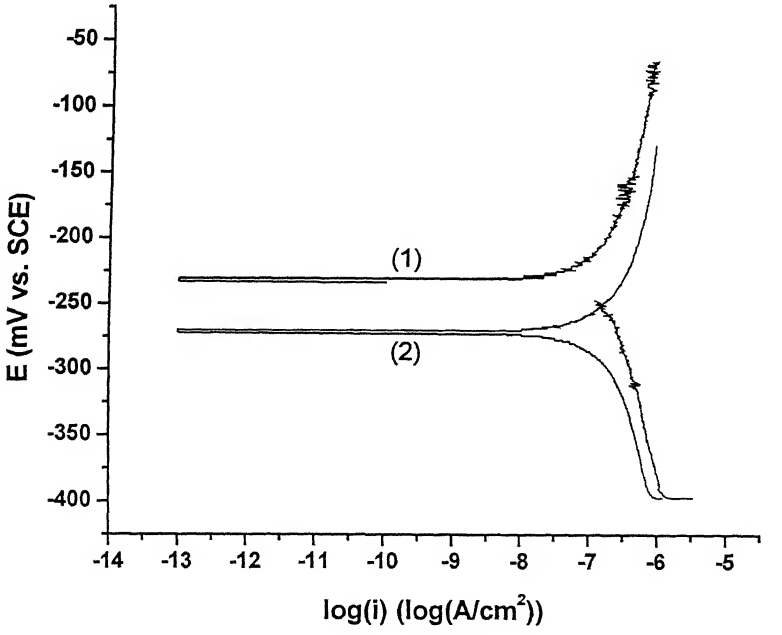

Figure 18: Tafel extrapolation curve for Ti-6Al-4V in Hank's Solution at 37°C temperature and 7.4 pH.

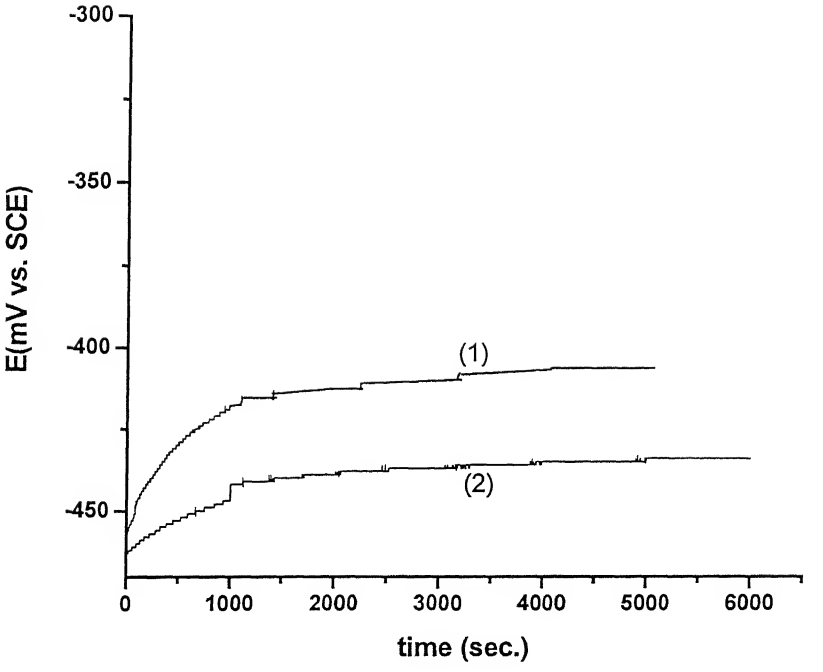

Figure 19: Open circuit potential as function of time for Ti-6Al-4V in Hank's Solution at 37°C temperature and 7.4 pH.

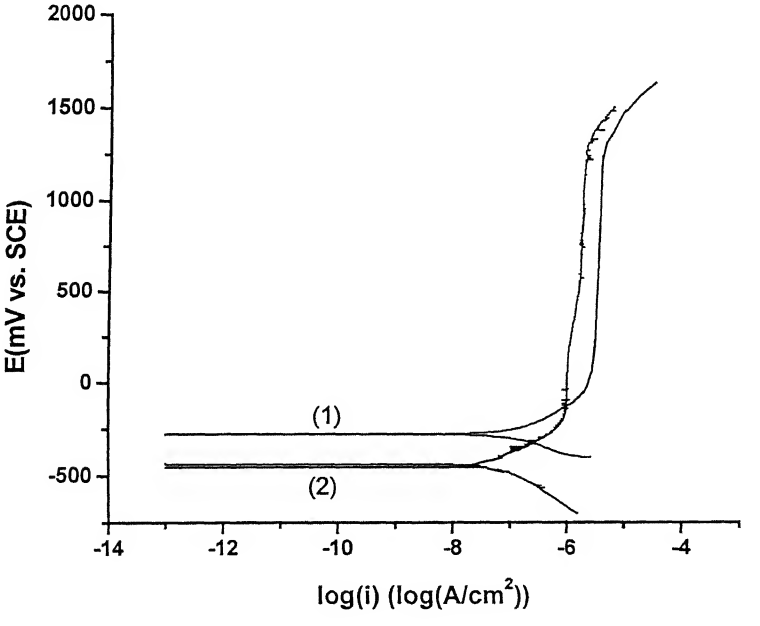

Figure 20: Potentiodynamic polarization curve for Ti-6Al-4V in Hank's Solution at 37°C temperature and 7.4 pH.

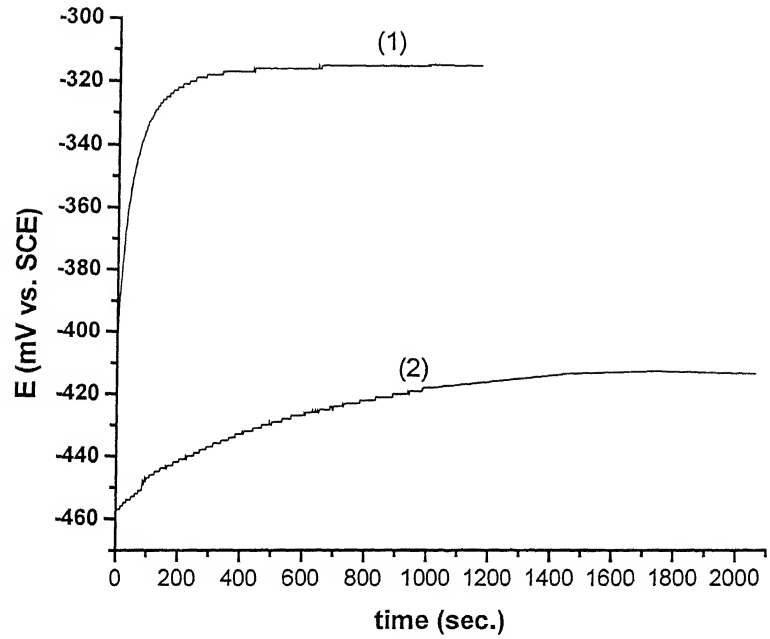

Figure 21: Open circuit potential as function of time for Ti-6Al-4Fe in Hank's Solution at 37°C temperature and 7.4 pH.

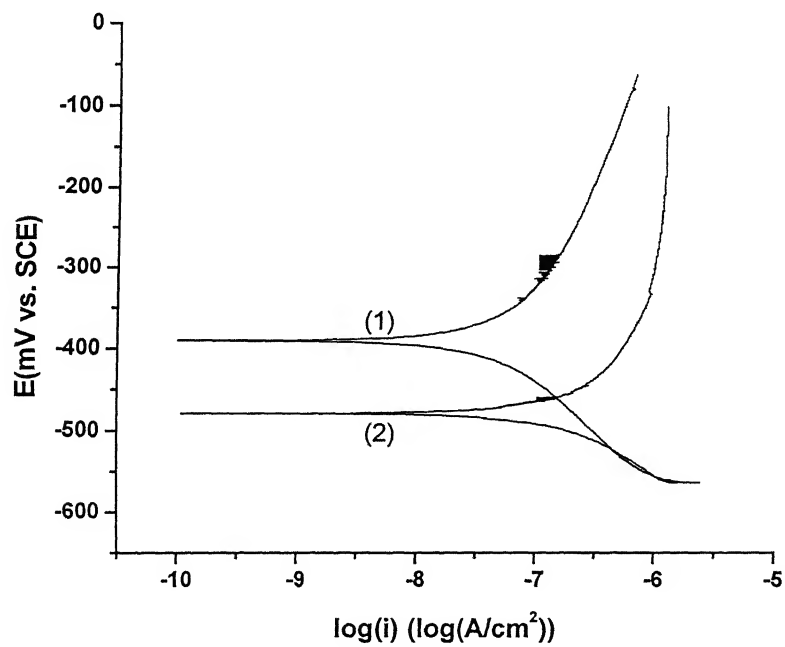

Figure 22: Tafel extrapolation curve for Ti-6Al-4Fe in Hank's Solution at 37°C temperature and 7.4 pH.

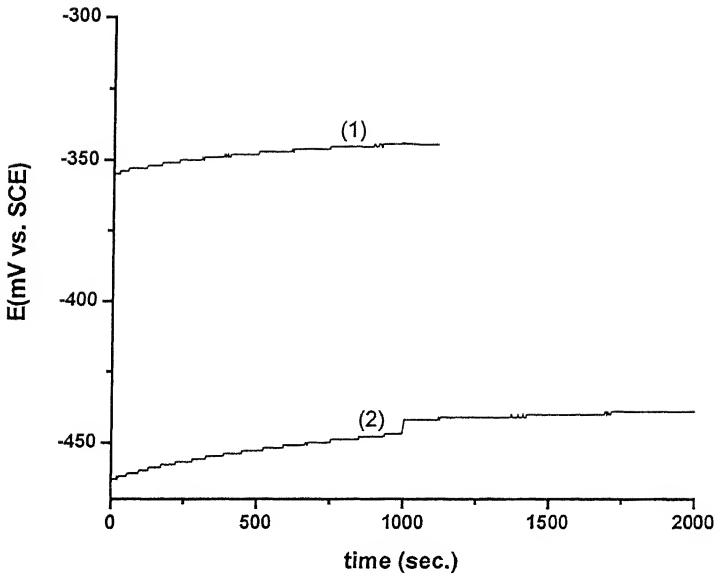

Figure 23: Open circuit potential as function of time for Ti-6Al-4Fe in Hank's Solution at 37°C temperature and 7.4 pH.

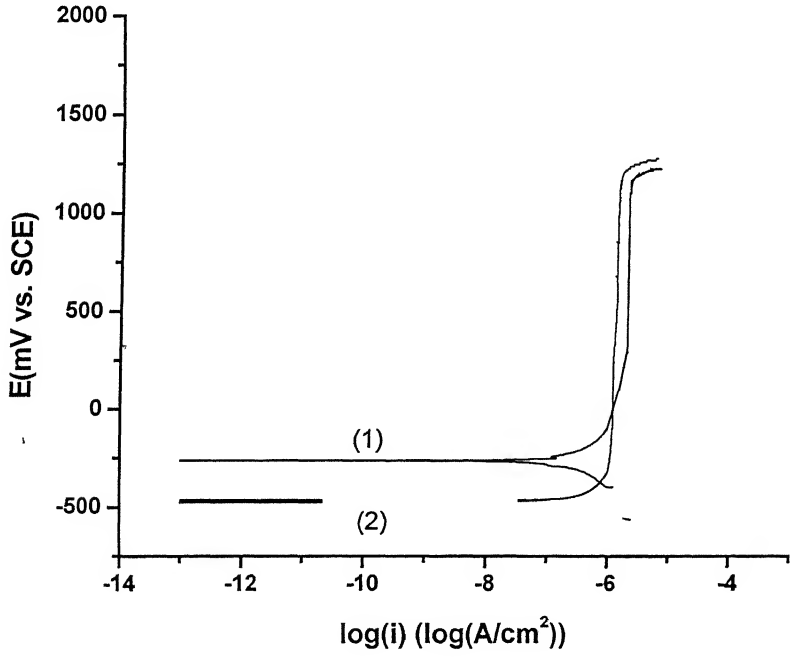

Figure 24: Potentiodynamic polarization curve for Ti-6Al-4Fe in Hank's Solution at 37°C temperature and 7.4 pH.

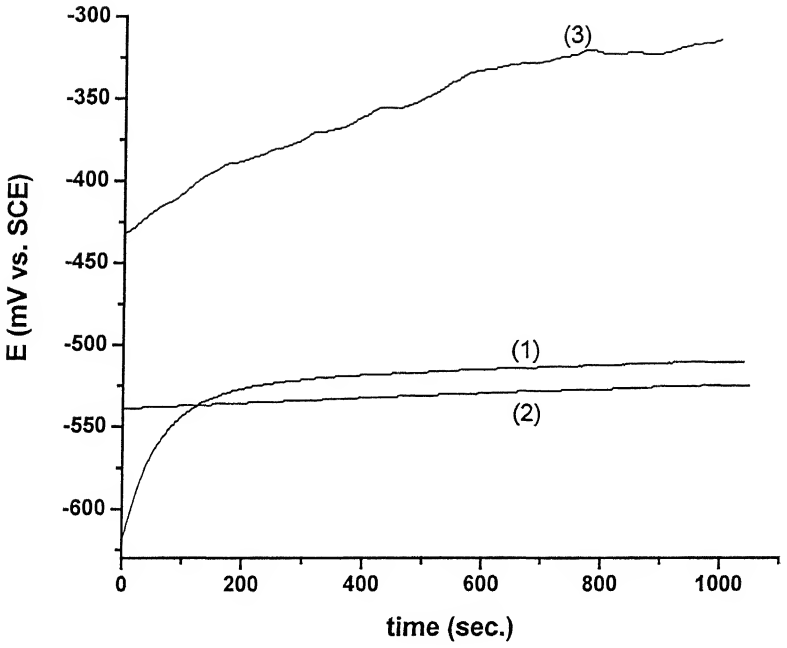

Figure 25: Open circuit potential as function of time for Ti-6Al-4Nb in Hank's Solution at 37°C temperature and 7.4 pH.

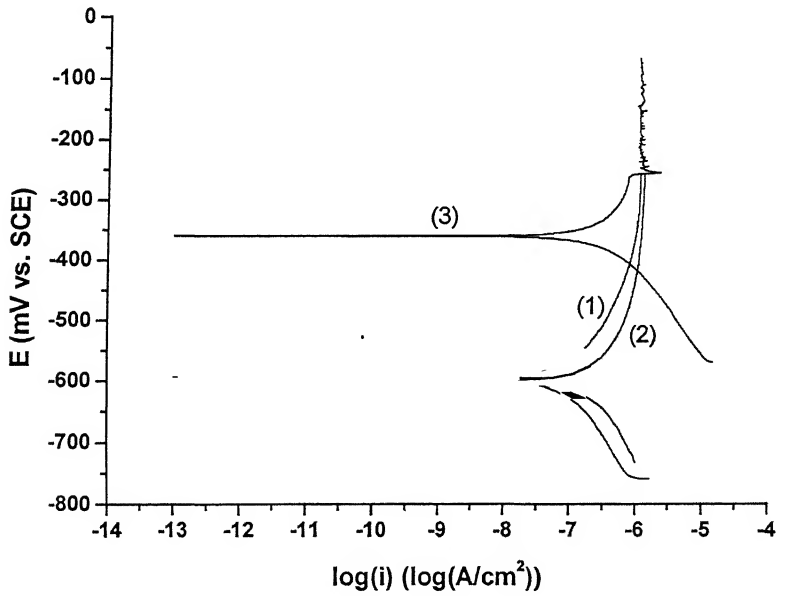

Figure 26: Tafel extrapolation curve for Ti-6Al-4Nb in Hank's Solution at 37°C temperature and 7.4 pH.

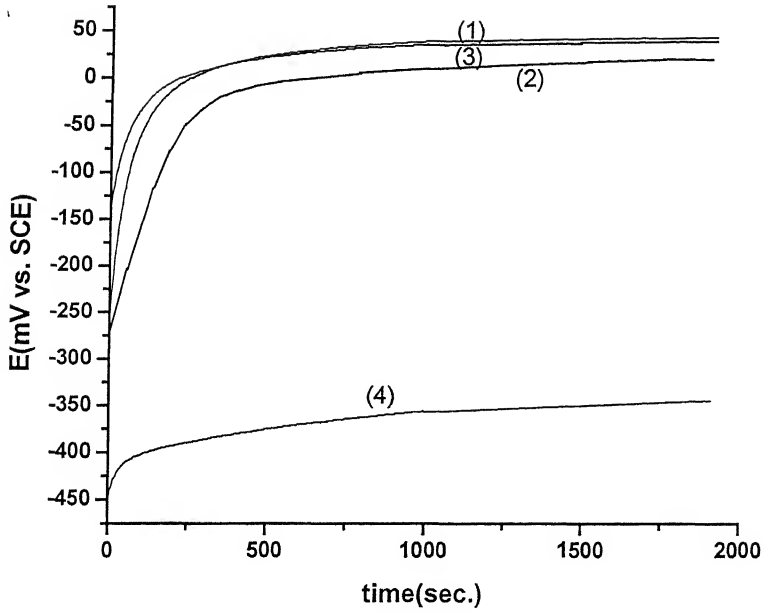

Figure 27: Open circuit potential as function of time for Ti-6Al-4Nb in Hank's Solution at 37°C temperature and 7.4 pH.

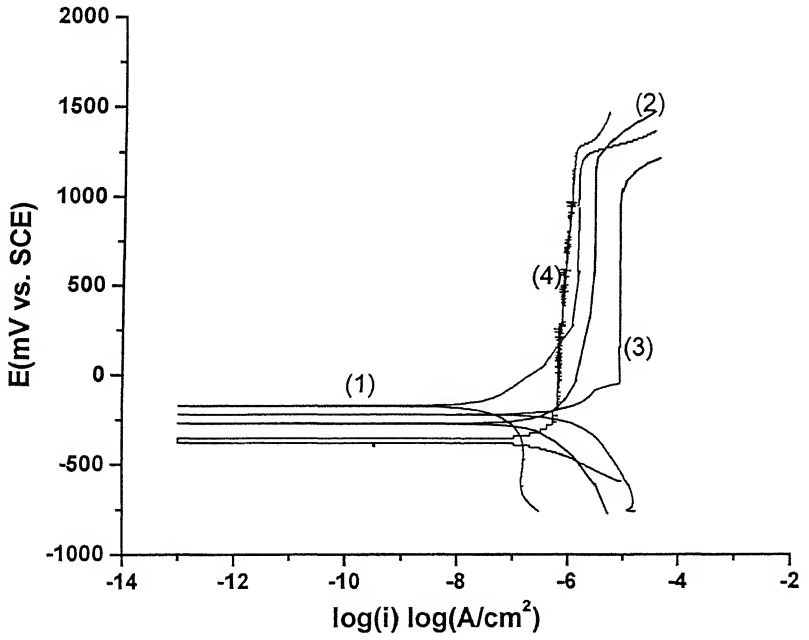

Figure 28: Potentiodynamic polarization curve for Ti-6Al-4Nb in Hank's Solution at 37°C temperature and 7.4 pH.

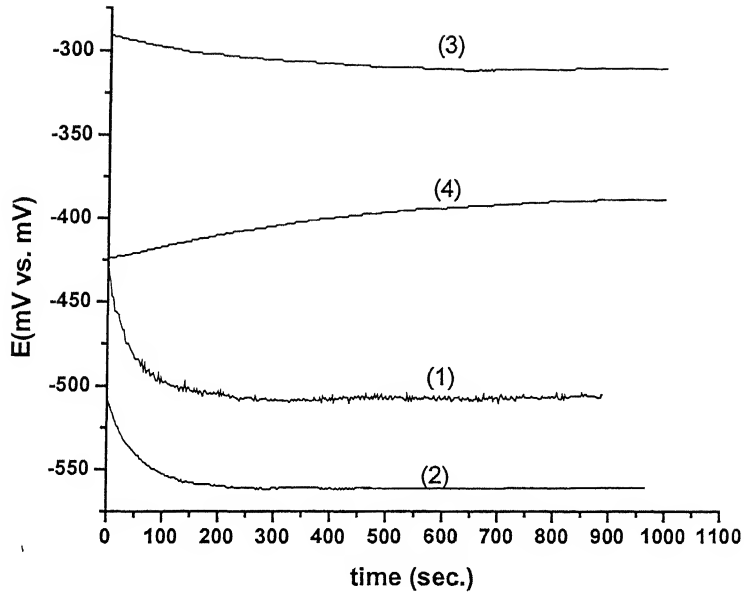

Figure 29: Open circuit potential as function of time for Ti-13Nb-13Zr in Hank's Solution at 37°C temperature and 7.4 pH.

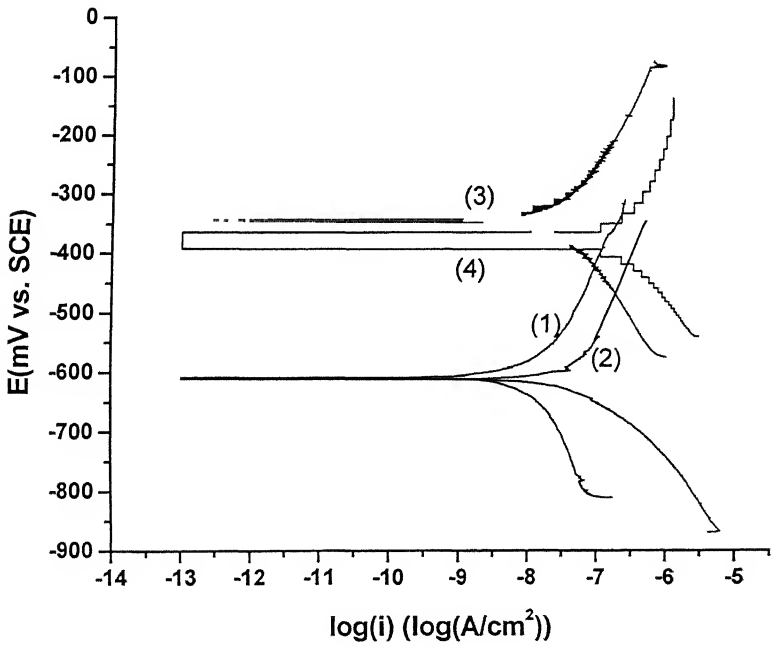

Figure 30: Tafel extrapolation curve for Ti-13Nb-13Zr in Hank's Solution at 37°C temperature and 7.4 pH.

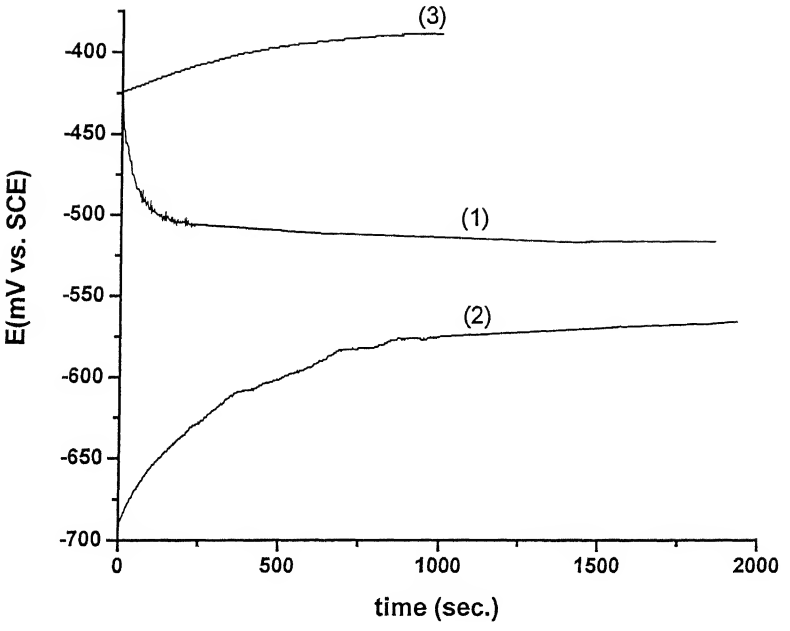

Figure 31: Open circuit potential as function of time for Ti-13Nb-13Zr in Hank's Solution at 37°C temperature and 7.4 pH.

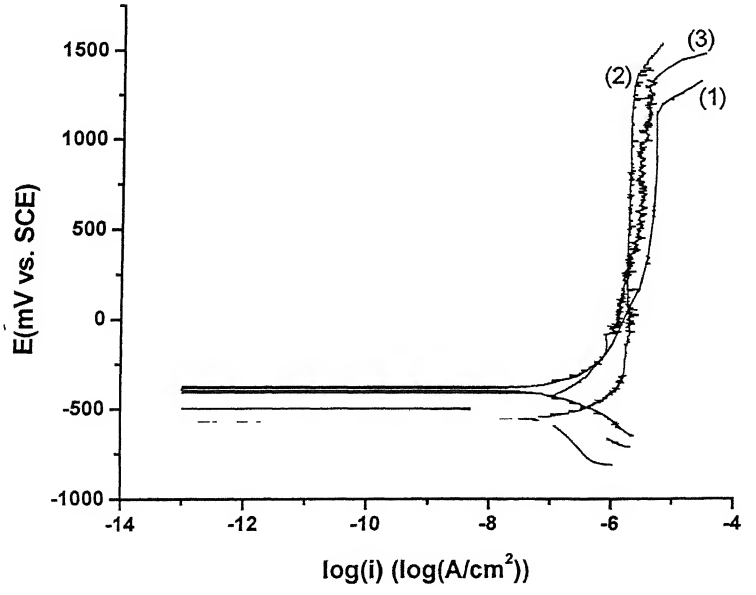

Figure 32: Potentiodynamic polarization curve for Ti-13Nb-13Zr in Hank's Solution at 37°C temperature and 7.4 pH.

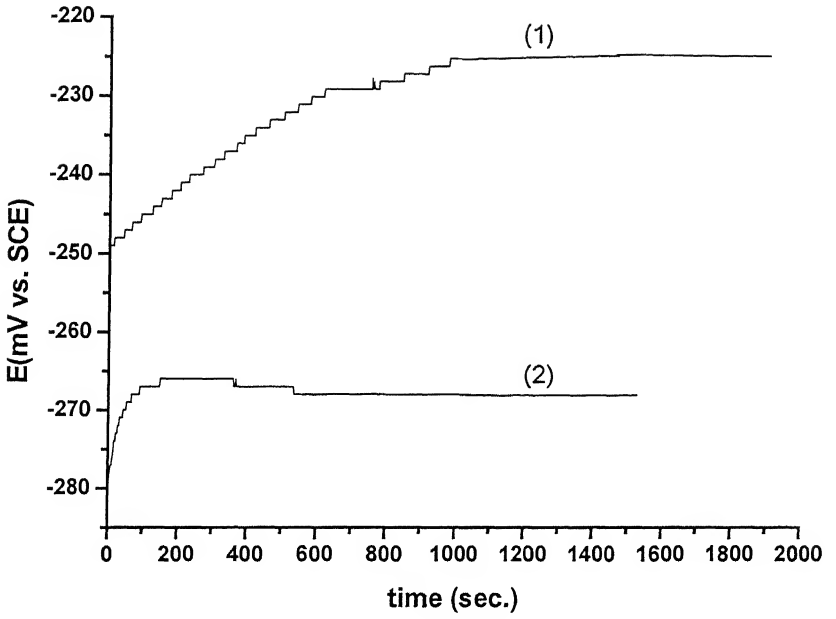

Figure 33: Open circuit potential as function of time for 316L stainless steel in Hank's Solution at 37°C temperature and 7.4 pH.

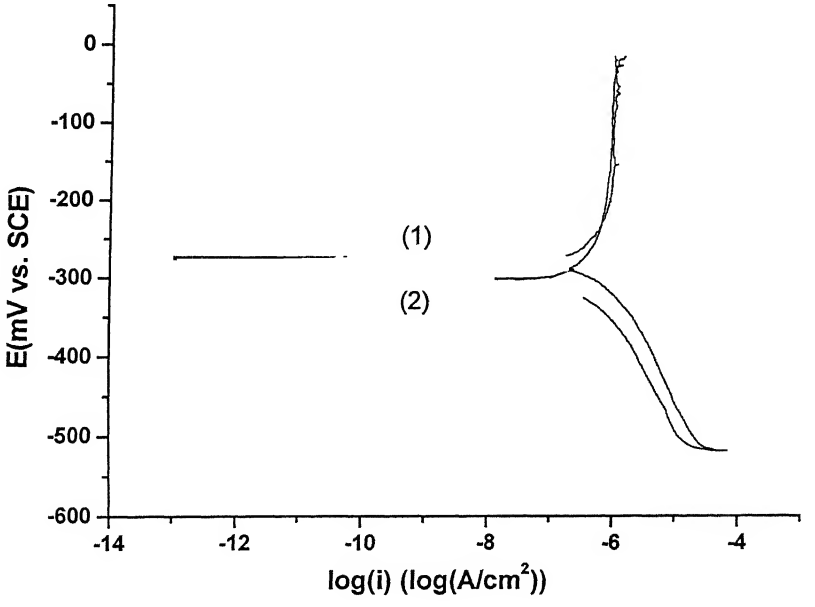

Figure 34: Tafel extrapolation curve for 316L stainless steel in Hank's Solution at 37°C temperature and 7.4 pH.

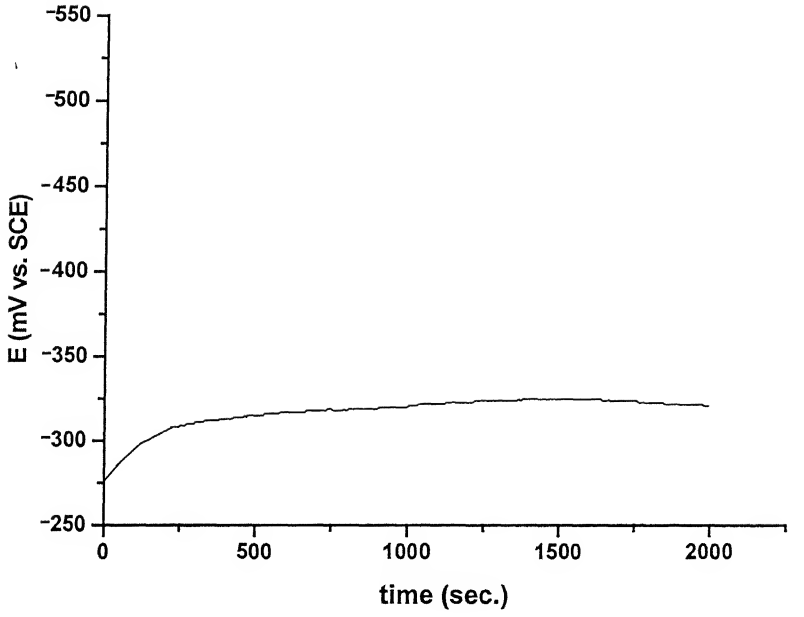

Figure 35: Open circuit potential as function of time for 316L stainless steel in Hank's Solution at 37°C temperature and 7.4 pH.

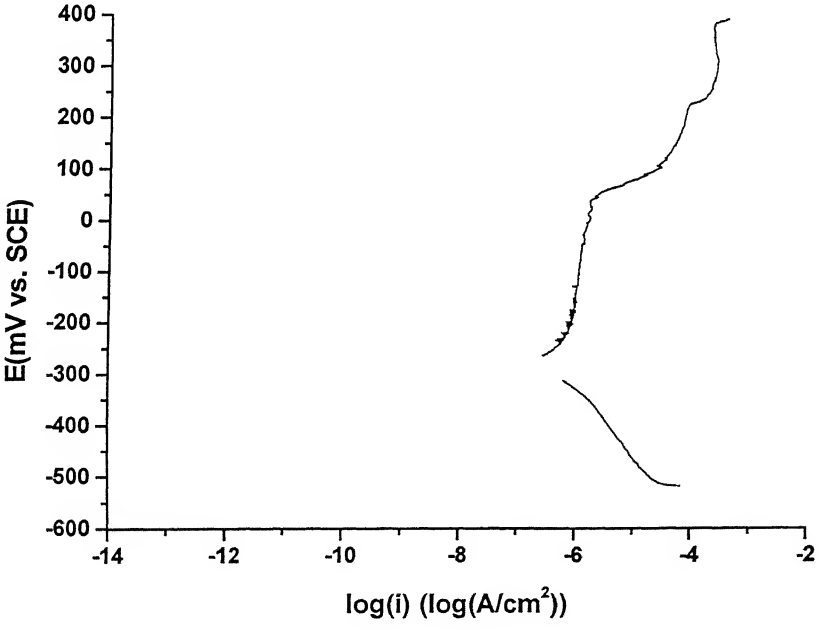

Figure 36: Potentiodynamic polarization curve for 316L stainless steel in Hank's Solution at 37°C temperature and 7.4 pH.

Appendix (B)

Table 1:Duplicate test results of passivation parameters of the samples in Hank's solution at pH 7.4 and 37°C temperature. All the potentials are with respect to SCE.

Sample	Z_{cp} (mV vs SCE)		E_b (mV vs SCE)		i_{pass} ($\mu A/cm^2$)		i_{corr} ($\mu A/cm^2$)		β_c (mV/dec)		β_a (mV/dec)	
	(1), (3)	(2), (4)	(1), (3)	(2), (4)	(1), (3)	(2), (4)	(1), (3)	(2), (4)	(1), (3)	(2), (4)	(1), (3)	(2), (4)
C.P. Titanium	-540	**-648**	1250	**1250**	8.5	**6.8**	0.63	**0.22**	-181	**-126**	208	**180**
Ti-15Al	-389	**-548**	750	**750**	1.6	**2.5**	0.19	**0.22**	-610	**-266**	527	**348**
Ti-5Al-2.5Fe	-461	**-562**	1244	**1240**	1.2	**1.2**	0.27	**0.15**	-100	**-171**	166	**301**
Ti-6Al-4V	-276	**-400**	1277	**1290**	3.0	**1.5**	0.13	**0.06**	-111	**-181**	164	**183**
Ti-6Al-4Fe	-257	**-470**	1152	**1170**	1 3	**1.3**	0.16	**0.24**	-161	**-86**	192	**215**
Ti-6Al-4Nb	**-170** -219	-276 -370	**1182** 1153	1179 1248	**1.4** 7.9	2.6 0.7	**0.072** 1.6	0.69 0.3	**-531** -406	-593 -153	**380** -	- 489
Ti-13.4Al-29Nb	-441	**-585**	1097	**979**	1.0	**1.3**	0.134	**0.16**	-174	**-177**	192	**195**
Ti-13Nb-13Zr	**-500** -396	-546	**1200** 1307	1334	**4.3** 2.6	1.9	**0.063** 0.17	0.12	**-349** -222	-127	**296** 321	191
316L Steel	**-281**	-	**37**	-	**1.0**	-	**0.54**	-	**-144**	-	**590**	-

Table 2: Passivation range of the samples in Hank's solution at pH 7.4 and 37°C temperature. All the potentials are with respect to SCE.

Sample	**E_b - Z_{cp} (mV vs SCE)**	**E_b - Z_{cp} (mV vs SCE)**
	(1), (3)	(2), (4)
C.P. Titanium	1790	**1898**
Ti-15Al	1139	**1298**
Ti-5Al- 2.5Fe	1705	**1802**
Ti-6Al-4V	1553	**1690**
Ti-6Al-4Fe	1409	**1640**
Ti-6Al-4Nb	**1352** 1372	1455 1618
Ti-13.4Al-29Nb	1538	**1564**
Ti-13Nb-13Zr	**1700** 1703	1880
316L Steel	**319**	-

Table 3: Duplicate test results of corrosion rates determined by Tafel extrapolation method of the samples, in Hank's solution at pH 7.4 and 37°C temperature. All the potentials are with respect to SCE.

.

Sample	ZCP (mV vs SCE)		β_c (mV/dec)		β_a (mV/dec)		i_{corr} ($\mu A/cm^2$)		Corrosion rate mils per year (mm/year)	
	(1), (3)	(2), (4)	(1), (3)	(2), (4)	(1), (3)	(2), (4)	(1), (3)	(2), (4)	(1), (3)	(2), (4)
C.P. Titanium	**-563**	-606	**-137**	-123	**145**	151	**0.08**	0 125	**0.036** (0.0009)	0 057 (0.0014)
Ti-15Al	**-534**	-571	**-155**	-188	**160**	124	**0.08**	0.04	**0.028** (0.0007)	0 014 (0.0003)
Ti-5Al-2.5Fe	-588	**-604**	-102	**-121**	175	**170**	0.134	**0.121**	0.047 (0.0012)	**0.042** (0.0010)
Ti-13.4Al-29Nb	-447	**-616**	-318	**-138**	203	**134**	0.147	**0.067**	0.054 (0.0013)	**0.024** (0.0006)
Ti-6Al-4V	-231	**-271**	-176	**-181**	168	**106**	0.16	**0.16**	0.055 (0.0013)	**0.055** (0.0013)
Ti-6Al-4Fe	-390	**-478**	-122	**-120**	181	**120**	0.039	**0.199**	0.013 (0.0003)	**0.041** (0.0010)
Ti-6Al-4Nb	**-596** -360	-590	**-158** -149	-155	**185** 448	182	**0.1** 0.48	0.199	**0.029** (0.0007) 0.16 (0.0040)	0.071 (0.0018)
Ti-13Nb-13Zr	**-607** -343	-606 -379	**-249** -176	-138 -141	**202** 211	195 184	**0.0125** 0.03	0.12 0.16	**0.0046** (0.0001) 0.01 (0.0002)	0.043 (0.0010) 0.05 (0.0012)
316L Steel	-279	**-303**	-144	**-145**	383	**382**	0.407	**0.421**	0.15 (0.0038)	**0.16** (0.0040)

Appendix (C)

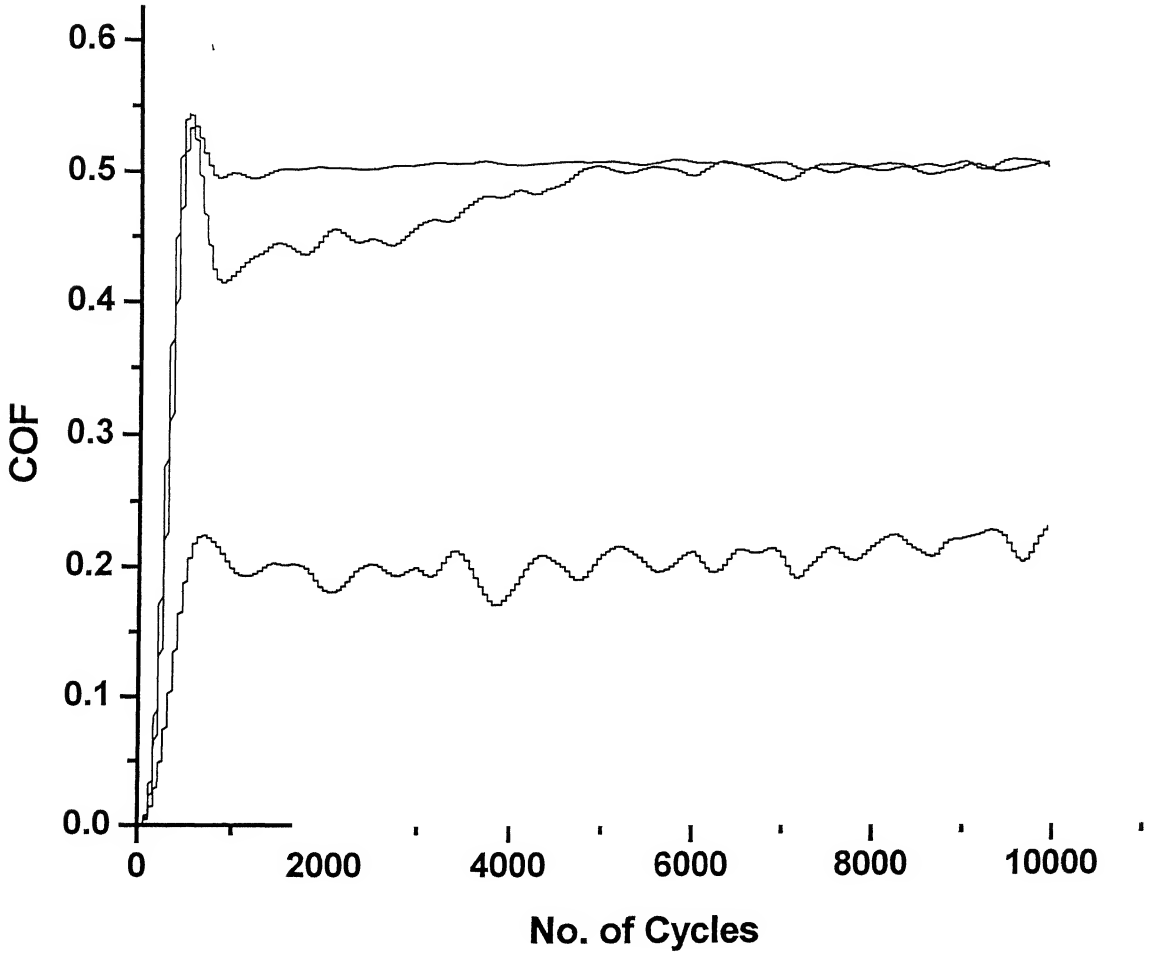

Figure 1: Plot for coefficient of friction (COF) versus number of cycles for commercial pure titanium at 10N load, 10000 cycles, 10Hz frequency and 80μm displacement stroke.

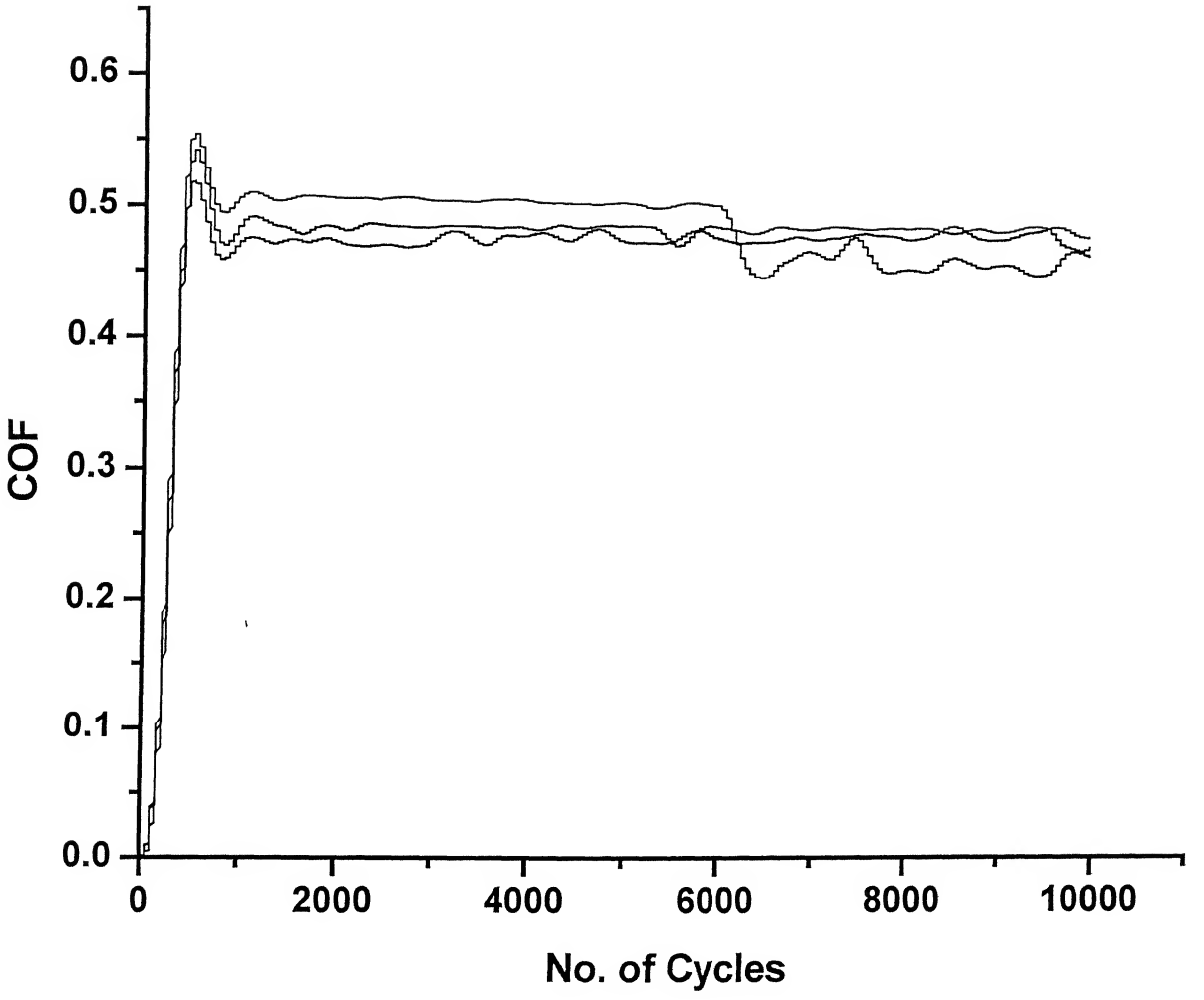

Figure 2: Plot for coefficient of friction (COF) versus number of cycles for Ti-13Nb-13Zr at 10N load, 10000 cycles, 10Hz frequency and 80μm displacement stroke.

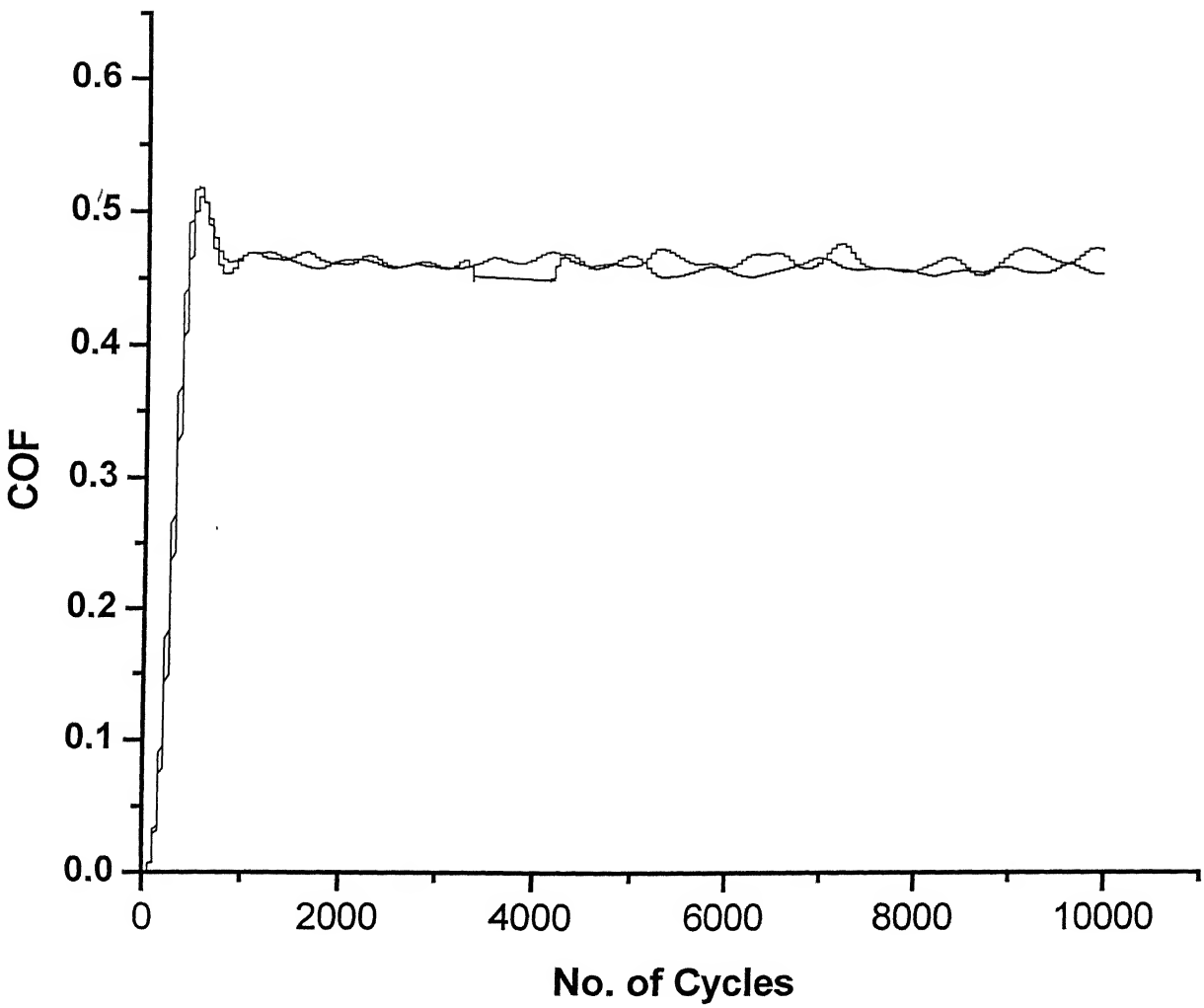

Figure 3: Plot for coefficient of friction (COF) versus number of cycles for Ti-6Al-4V at 10N load, 10000 cycles, 10Hz frequency and 80μm displacement stroke.

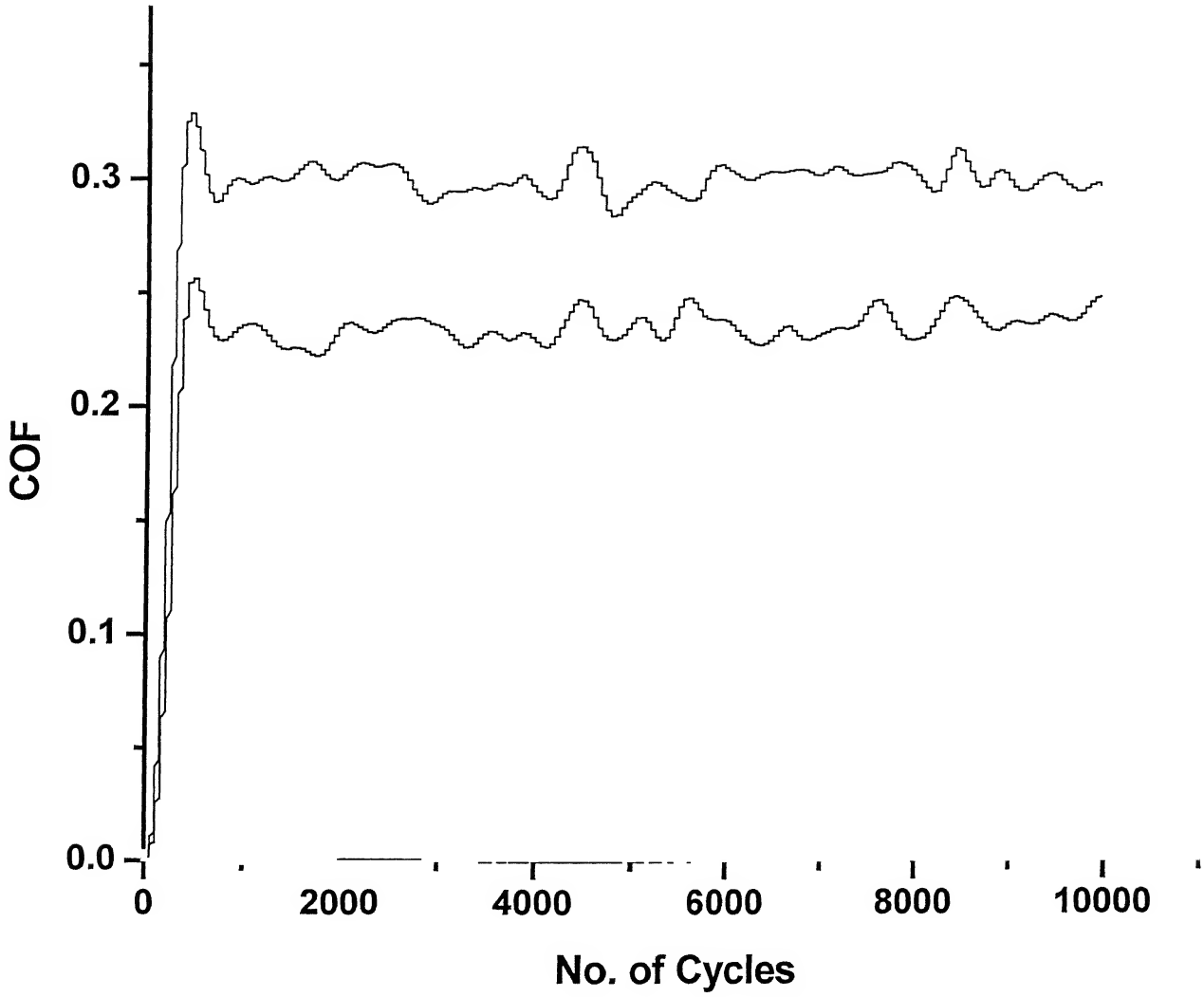

Figure 4: Plot for coefficient of friction (COF) versus number of cycles for Ti-5Al-2.5Fe at 10N load, 10000 cycles, 10Hz frequency and 80μm displacement stroke.

Appendix (D)

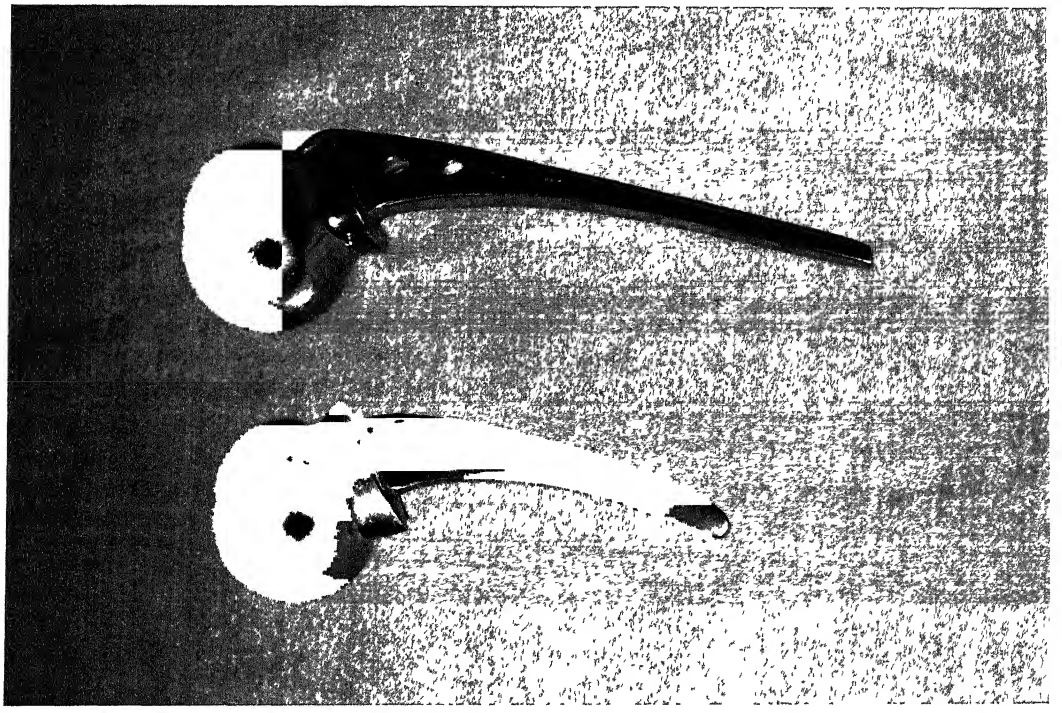

Figure 1: 316L Partial Hip joint replacement (permanent implant) removed after the death of the patient. Surface roughening of the material can be observed. (Scale 1cm=1.5cm)

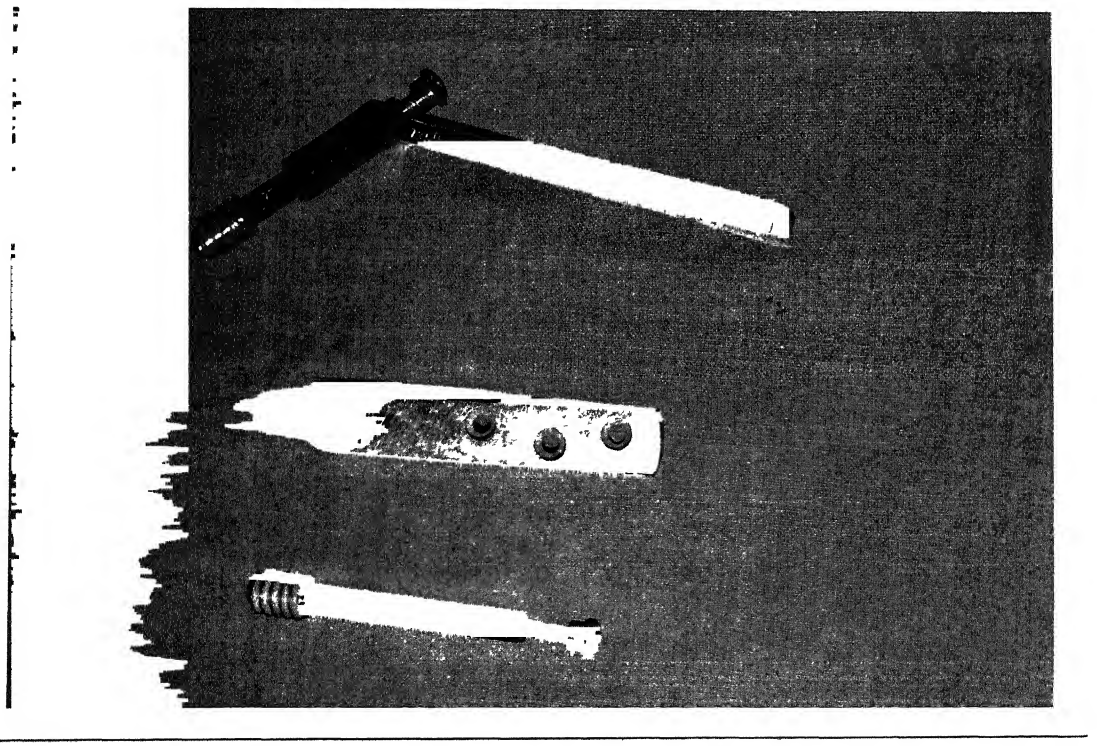

Figure 2: 316L Dynamic Hip screws (temporary implant) removed by post healing surgery. Used for joining of fracture near the femur, that helps in fast union of the bone. (Scale 1cm=1.8cm)

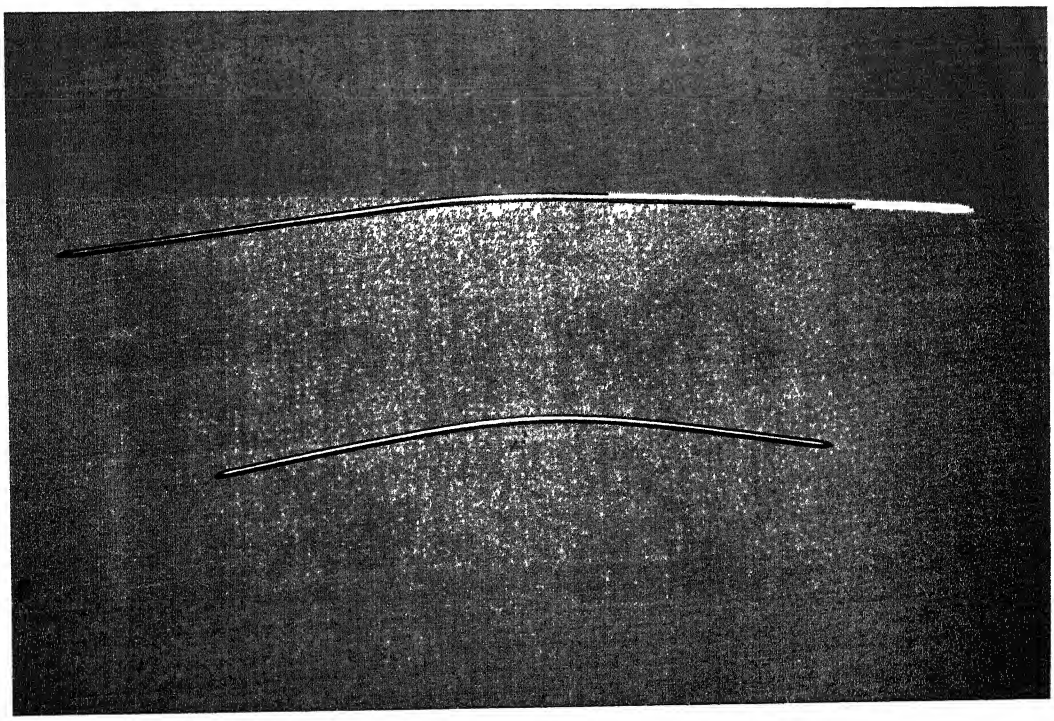

Figure 3: 316L Kirschner's wire (K-wire) removed by post healing surgery. Used for treatment for fractured Patella. It can be used as a permanent or temporary implant device. (Scale 1cm=2cm)

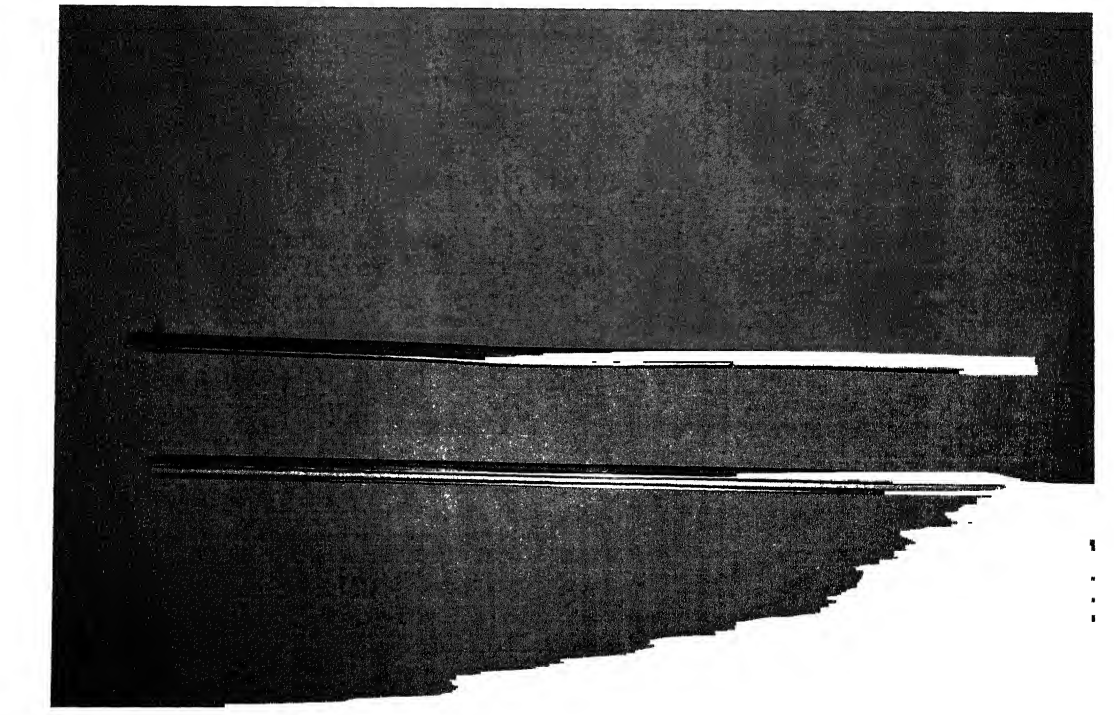

Figure 4: 316L Tibial Intramedullary Nail (permanent implant) removed after the death of the patient. Used for joining shaft of Tibia. (Scale 1cm=2.8cm)

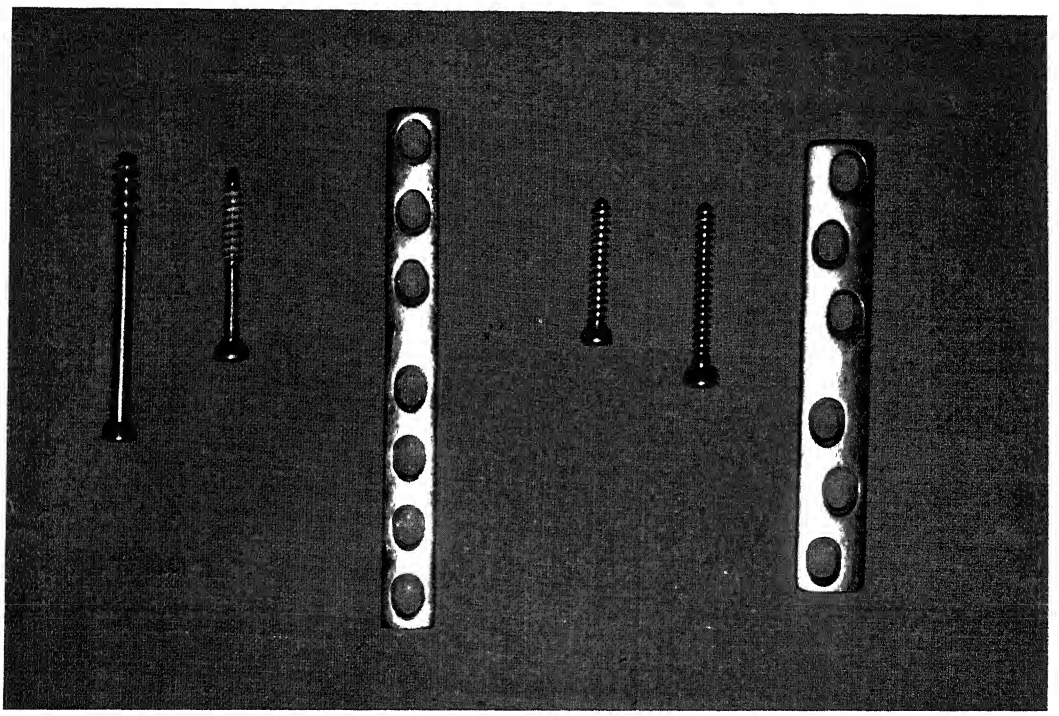

Figure 5: 316L Dynamic Compression Plate with Cancellous and Corteal screws (temporary implant) removed by post healing surgery. Used for internal fixation of fractures of long bone. (Scale 1cm=2cm)

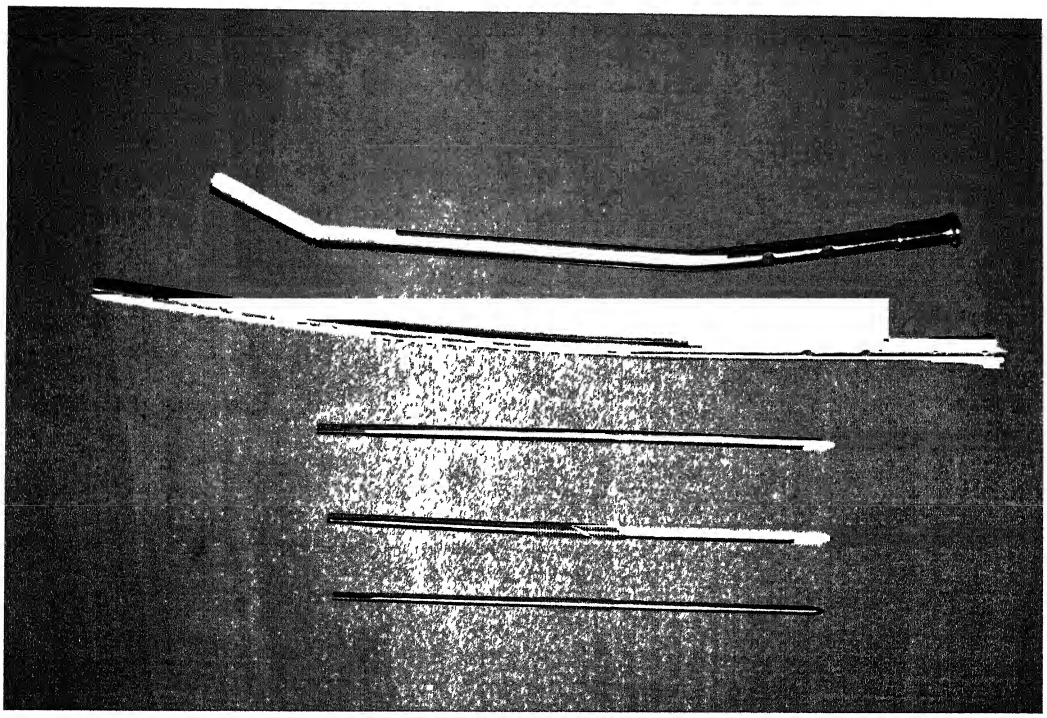

Figure 6: 316L Radial Intramedullary Nail (permanent implant) and Steinemann Pins removed by post healing surgery. Used for internal fixation of fractures of long bone. (Scale 1cm=3cm)